REPORT DOCUMENTATION PAGE

Form Approved
OMB No. 0704-0188

1. AGENCY USE ONLY (Leave Blank)	2. REPORT DATE	3. REPORT TYPE AND DATES COVERED
	April 1996	Final

4. TITLE AND SUBTITLE
Stability of Sodium Electrodeposited From a Series of Room Temperature Chloroaluminate Molten Salts

5. FUNDING NUMBERS

6. AUTHORS
Gary Edward Gray

AFRL-SR-BL-TR-98-
0367

7. PERFORMING ORGANIZATION NAME(S) AND ADDRESS(ES)
Georgia Institute of Technology

9. SPONSORING/MONITORING AGENCY NAME(S) AND ADDRESS(ES)
AFOSR/NI
110 Duncan Avenue, Room B-115
Bolling Air Force Base, DC 20332-8080

10. SPONSORING/MONITORING AGENCY REPORT NUMBER

11. SUPPLEMENTARY NOTES

12a. DISTRIBUTION AVAILABILITY STATEMENT
Approved for Public Release

12b. DISTRIBUTION CODE

13. ABSTRACT *(Maximum 200 words)*
See attached.

14. SUBJECT TERMS

15. NUMBER OF PAGES

16. PRICE CODE

17. SECURITY CLASSIFICATION OF REPORT	18. SECURITY CLASSIFICATION OF THIS PAGE	19. SECURITY CLASSIFICATION OF ABSTRACT	20. LIMITATION OF ABSTRACT
Unclassified	Unclassified	Unclassified	UL

Stability of Sodium Electrodeposited From a Series of Room Temperature Chloroaluminate Molten Salts

A Thesis
Presented to
The Academic Faculty

by

Gary Edward Gray

In Partial Fulfillment
of the Requirements for the Degree
Doctor of Philosophy in Chemical Engineering

Georgia Institute of Technology
April 1996

To Laura, whose love and support have helped me achieve my goals.

ACKNOWLEDGEMENT

I am grateful for the guidance and wisdom provided by my advisors, Jack Winnick and Paul A. Kohl. Also instrumental in this work are the members of my research group for their technical contributions as well as making my work here a pleasure.

TABLE OF CONTENTS

LIST OF TABLES

LIST OF FIGURES

Summary

An urgent need exists for a high energy density secondary battery for applications such as electric vehicles and load leveling. This work involved the synthesis of room temperature molten salts and the examination of the electrochemical and transport properties of these salts with the goal of developing a room temperature molten salt electrolyte for the sodium / nickel(II) chloride battery. The high temperature design of the sodium / nickel(II) chloride battery is commonly referred to as the "Zebra Cell" and operates at 250 °C. The Zebra Cell consists of a liquid sodium anode, a β"-alumina ceramic electrolyte, sodium aluminum chloride liquid electrolyte, and an iron cathode. An ambient temperature electrolyte would eliminate the need for the ceramic separator and allow the use of a solid sodium anode. The compatibility of the molten salts with the anode material (sodium) has been investigated using electroanalytical techniques such as cyclic voltammetry, chronoamperometry, and chronopotentiometry. Three organic salts have been investigated: 1-methyl-2-ethylimidazolium chloride (MEIC), 1,2-dimethyl-3-propylimidazolium chloride (DMPIC), and 1-methyl-2-propylimidazolium chloride (MPIC). Work has focused on the use of sodium as an anode and the conditions which provide the greatest coulombic efficiency on reduction / oxidation cycles.

CHAPTER 1

INTRODUCTION AND BACKGROUND

Concerns about automobile emissions (NO_X, CO, particulates, hydrocarbons) have accelerated the search for lightweight, energetic secondary batteries. According to B. D. McNicol and D. A. J. Rand, "The major factor inhibiting the development of traffic compatible electric road vehicles is the lack of a commercially available, effective, and economical electrochemical power source.[1] " In response to this need, the U.S. Department of Energy and the United States Advanced Battery Consortium (USABC) set forth goals for the development of secondary battery technology. Parameters such as specific energy, a measure of a battery's energy storage ability per unit weight; specific power, a measure of a battery's power output per unit weight; energy density, a measure of a battery's energy storage ablity per unit volume; power density, a measure of a battery's power output per unit volume; and others relating to cycle life and costs were included in these goals. These goals are summarized in Table 1. Presently, the lead acid battery is the only battery system that has reasonable performance as well as a combination of reliability, commercial availability, and low cost. Other systems the

Table 1.1. Goals of the USABC[2]

	Mid-Term	Long Term	Na/ $FeCl_2$*
Specific Energy (Wh/kg) (C/3 discharge rate)	80	200	193
Energy Density (Wh/L) (C/3 discharge rate)	135	300	386
Specific Power (W/kg) (80% Depth of Discharge per 30 seconds)	150	400	Depends on Full Cell Geometry
Power Density (W/L)	250	600	
Life (yrs)	5	10	
Life Cycles (80% DOD)	600	1000	
Ultimate Cost ($/kWh)	<150	<100	
Operating Environment	-30°C to 65°C	-40°C to 85°C	10°C to 80°C
Recharge Time (hrs)	<6	3-6	
Continuous discharge in one hour (no failure)	75% of rated capacity		
Power and Capacity degradation	20% of rated specification		

* Projected from Theoretical Values

USABC believes have promise in the mid-term are sodium / sulfur, zinc / air, nickel / metal hydride, and lithium / iron monosulfide.

1.1 High- Temperature Na / $NiCl_2$ Cell

Another candidate system is the sodium / nickel(II) chloride ("Zebra") cell. This cell design is pictured in Figure 1.1 and, for comparison, some projected performance data is included in Table 1.1. This cell operates at approximately 250°C, utilizes a molten sodium anode, an iron(II) chloride cathode, molten $AlCl_3$-NaCl electrolyte, and a β"-alumina separator.[3] During discharge, two electrochemical reactions take place. At the anode, metallic sodium is oxidized to sodium ions. At the cathode, iron(II) chloride is reduced to metallic iron and chloride ions. The overall reactions $Na/FeCl_2$ cell are:

Charge		Discharge
$2Na$	$\Leftrightarrow$	$2Na^+ + 2e^-$
$FeCl_2(s) + 2e^-$	$\Leftrightarrow$	$Fe(s) + 2\ Cl^-$

The $Na/FeCl_2$ cell is promising because it utilizes materials that are very abundant and easily recyclable. This configuration produces 2.35 V at 250°C but, at present, this

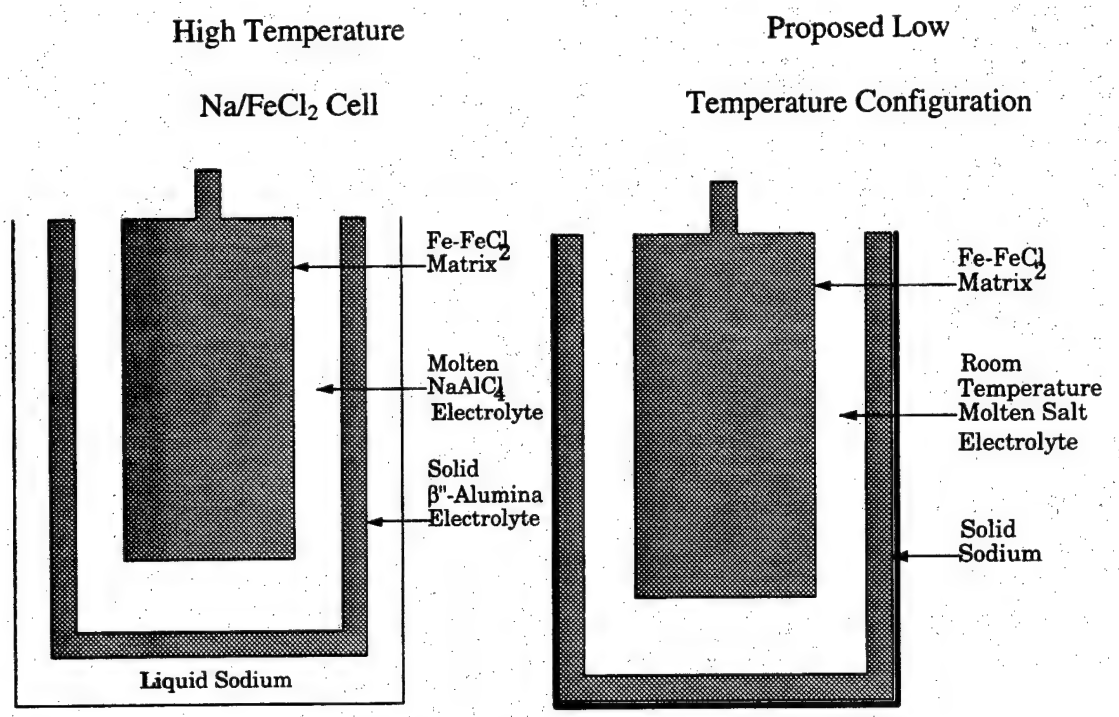

Figure 1.1. Present configuration of the Na / $FeCl_2$ battery (Adapted from 3).

battery is not among one of the three prime candidates for electric vehicle applications in the U.S., but is being vigorously tested in Europe.

1.2 Ambient Temperature Na / $MeCl_2$ Cell

The high operating temperature is a severe handicap toward the sodium / nickel(II) chloride battery's widespread use. Reduction of the operating temperature below the melting point of sodium (98°C), would not only eliminate the need for a solid separator, but also eliminate the hazards and inconveniences associated with high temperature devices. By utilizing a solid sodium anode, many safety and materials selection problems are eliminated.

One requirement for lowering the operating temperature is to utilize an electrolyte which can function at this lower temperature. The properties of such an electrolyte would be: reasonable conductivity ($>10^{-3}$ S/cm) at temperatures below 98°C, stability in the presence of sodium, solubility of sodium ions, and stability in the presence of the cathode metal. Electrolytes which show promise are room temperature molten salt mixtures made from organic salts, such as 1-methyl-3-ethylimidazolium chloride (MEIC), 1,2-dimethyl-3-propylimidazolium chloride (DMPIC), or 1-methyl-3-propylimidazolium chloride (MPIC), and aluminum chloride ($AlCl_3$). The structures of these organic chlorides are shown in Figure 1.2. A comparison of the melting point versus composition curves for

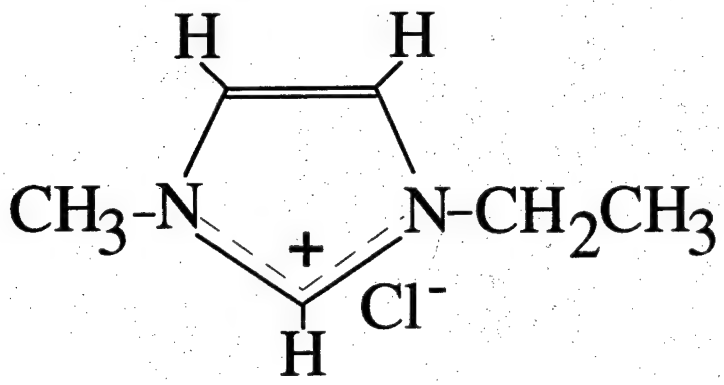

A

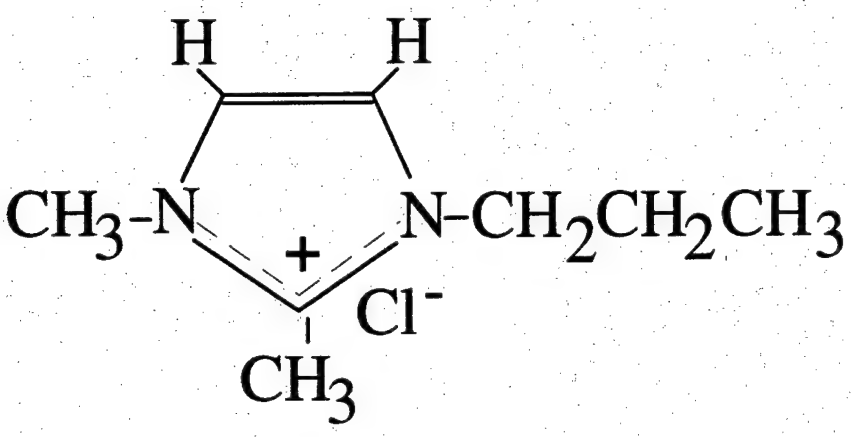

B

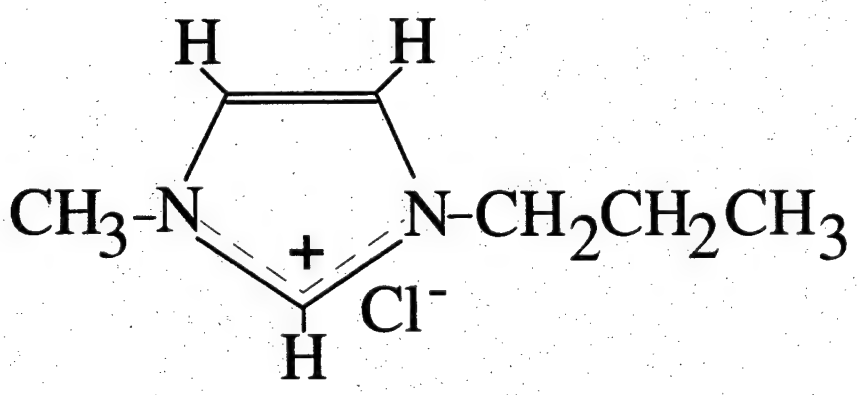

C

Figure 1.2. Structures of Organics Chlorides Studied. A:MEIC, B:DMPIC, C:MPIC

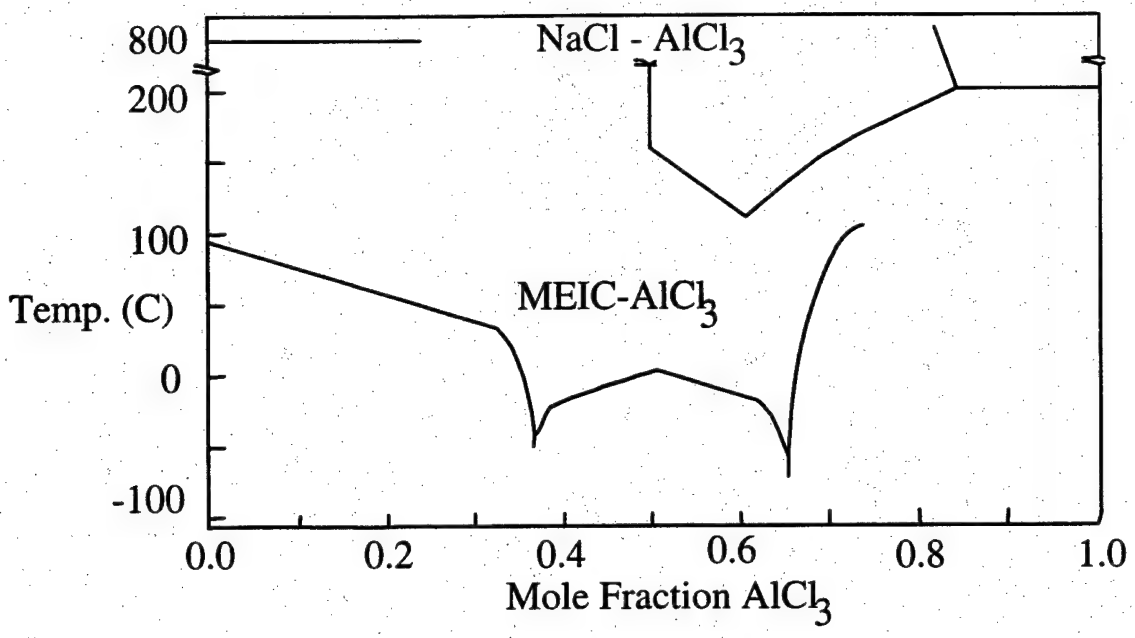

Figure 1.3. Phase Diagram of $AlCl_3$-NaCl and MEIC-$AlCl_3$ Systems

the electrolyte used in the high temperature sodium / iron chloride cell and the MEIC aluminum chloride system is shown Figure 1.3.

1.2.1 Melt Equilibrium

Although both the organic chlorides and aluminum chloride are solid at room temperature, when combined in the proper stoichiometry, the salts form a salt mixture with a melting point below room temperature. The room temperature molten salt is similar to a high temperature molten salt. It has ionic species which can move freely in the liquid, thus giving it a relatively high conductivity (~3.25×10^{-2} S/cm). The types of ions present depend on the stoichiometry of the original mixture. Two reactions that govern the melt equilibrium at room temperature are:[4]

$$Cl^- + AlCl_3(s) \Leftrightarrow AlCl_4^- \qquad K=1.6*10^{19}$$

$$AlCl_4^- + AlCl_3(s) \Leftrightarrow Al_2Cl_7^- \qquad K=1.6*10^{3}$$

When the mole fraction of $AlCl_3$ in the melt is less than 0.5 ($N<0.5$), the two chloroaluminate species that dominate are Cl^- and $AlCl_4^-$. Such a melt is termed basic, due to the presence of the Lewis base, Cl^-. When $N>0.5$ the two chloroaluminate species that dominate are $Al_2Cl_7^-$ and $AlCl_4^-$, such a melt is termed acidic. When $N=0.5$ the dominant species is $AlCl_4^-$ and the melt is termed neutral.

At neutrality the electrochemical behavior of the melt is governed by the reduction of the organic cation (MEI^+)[5,6] and the oxidation of the tetrachloroaluminate ion ($AlCl_4$-). These two reactions occur nearly 4.6 V apart; this wide range of electrochemical inactivity is referred to as an electrochemical "window". Because this extremely wide electrochemical window is observed only when the melt is exactly neutral, it can be somewhat elusive.

One method for producing a more facile neutral melt is to add to the melt a substance that can react with excess $Al_2Cl_7^-$ in an acidic melt or Cl^- in a basic melt, in effect, a buffer. Conveniently, alkali metal chlorides meet these criteria. When added to a slightly acidic (N=0.55) melt, alkali metal chlorides react with $Al_2Cl_7^-$ according to the following reaction.

$$MCl(s) + Al_2Cl_7^- \Leftrightarrow M+ + 2\ AlCl_4^-$$

$$M=(Li, Na, K)$$

This serves to consume any $Al_2Cl_7^-$ present and also produces dissolved alkali metal ions. The dissolved alkali metal ions react with excess chloride ions by the following reaction.

$$M^+ + Cl^- \Leftrightarrow MCl(s)$$

Thus alkali metal chlorides can serve to buffer a melt and help maintain its neutrality.

Previous work by Yu[7] has shown that a properly treated melt of MEIC, $AlCl_3$, and NaCl can produce a sodium plating / stripping couple at mercury. Carlin, Fuller, and Wilkes[8] have reported the reduction of lithium at tungsten, and the reduction of lithium, sodium, and potassium at mercury. Riechel and Wilkes[9] have reported the reduction of sodium at tungsten from a buffered, neutral melt treated with an HCl source. Riechel and Wilkes extended the negative limit of the electrochemical window of the melt by the addition of HCl. The addition of HCl in the form of 1-methyl-3-ethylimidazolium hydrogen dichloride ($MEIHCl_2$) appears to force the potential at which the MEI^+ ion is reduced to a more negative value. Other melt additives have been shown to produce a similar effect. This allows the reduction and oxidation of sodium to occur within the melt window.

1.2.2 Electrode Reactions

A successful electrolyte will allow reversible electrochemical reactions at both the anode and cathode. Anode and cathode can be studied independently using an electrochemical half-cell.

1.2.2.1 Anode

Riechel and Wilkes[9] reported the reversible plating and stripping of sodium at tungsten in a buffered neutral $AlCl_3$ / MEIC melt treated with $MEIHCl_2$. Two techniques for evaluating the practicality of the sodium anode are cyclic voltammetry and chronopotentiometry. Using cyclic voltammetry and integrating the area under the oxidation and reduction peaks, the number of coulombs used by each process can be determined. The ratio of coulombs used for oxidation to the number used for reduction is called the coulombic efficiency of the couple. Similarly, the efficiency of the couple may be measured by chronopotentiometry. The current is constant in this technique, so the efficiency of the couple can be calculated by measuring the amount of time reactions occur at potentials on either side of the formal potential of the couple.

Recent work has demonstrated that the efficiency of the plating / stripping couple has a strong dependence on the amount of HCl in the melt or, equivalently, the partial pressure of hydrogen chloride above the melt. One of the difficulties in producing an efficient plating / stripping couple in a buffered neutral $AlCl_3$ / MEIC melt is the fact that the sodium couple is located near the edge of the electrochemical window. In an HCl free melt, the potential for sodium reduction is outside the melt window, thus the organic ion in the melt is reduced before the reduction of sodium. The addition HCl appears to shift the potential for the reduction of the MEI^+ ion farther negative, thus allowing the reversible reduction and reoxidation of sodium. By the addition of HCl to the melt and

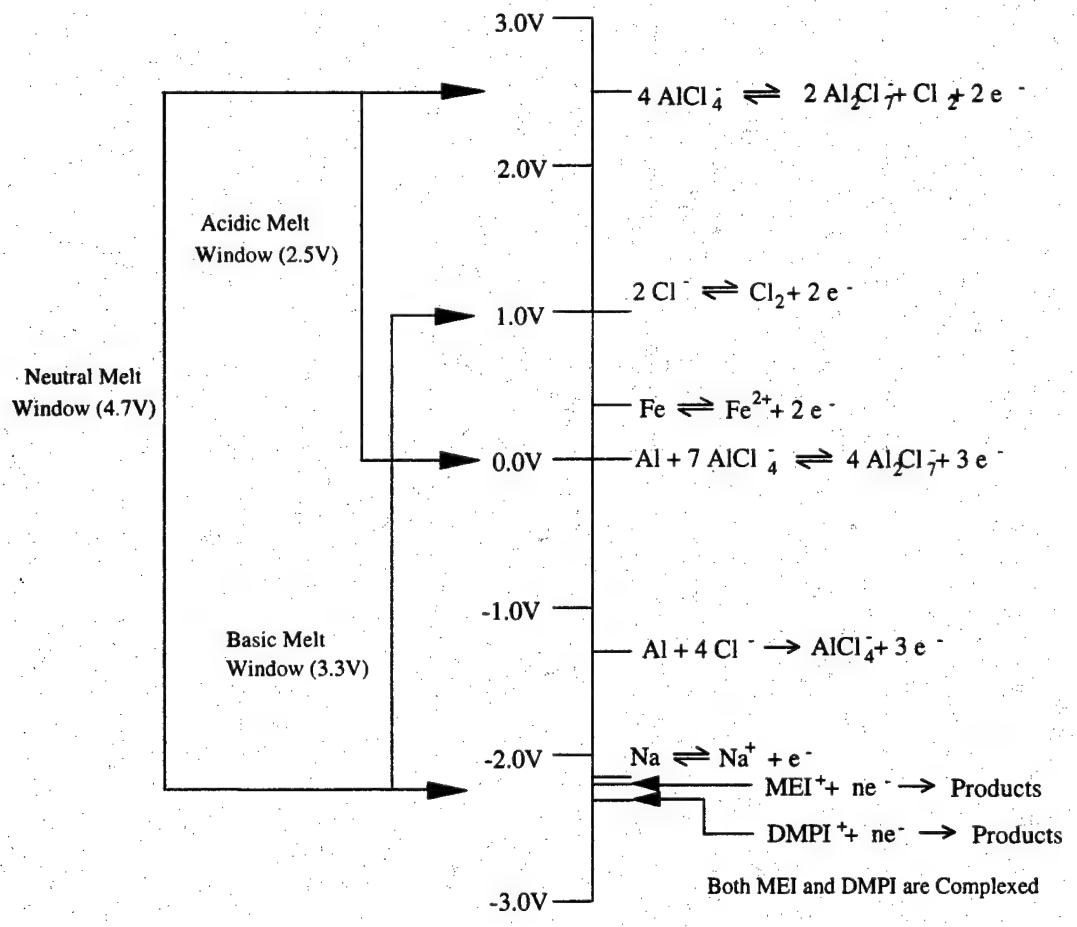

Figure 1.4. Electrochemical Window of two Room Temperature Molten Salt Systems

maintaining a constant partial pressure of HCl above the melt, efficiencies above 80% have routinely been obtained.

Work by Gifford[10] first suggested that a second organic salt, 1,2-dimethyl-3-propylimidazolium chloride (DMPIC), may have a reduction potential more negative than MEIC. Gifford compared the electrochemical window of MEIC and DMPIC and concluded that melts made from $AlCl_3$ and DMPIC possess a wider electrochemical window. Recently, Scordilis-Kelley calculated the standard reduction potential of sodium in a protonated buffered neutral $AlCl_3$ / DMPIC melt.[11] Scordilis-Kelley found that sodium couple was more reversible in the HCl treated DMPIC melts. The approximate reduction potentials and the electrochemical windows of both the MEIC and the DMPIC melts are shown in Figure 1.4.

1.2.2.2 Cathode

The ideal cathode material would be one that can be oxidized to an insoluble chloride near the positive edge of the melt window. In early Zebra cells, iron was used; reversible redox behavior was observed. More recently, nickel has replaced iron in this high temperature cell.

In the ambient temperature version, iron and nickel are both candidates, despite the fact that their formal potentials are quite negative of the melt window, not utilizing its full capabilities. The cathode selection is the subject of a separate study. The

development of a reversible anode and cathode would allow the assembly of a complete full cell.

1.2.3 Full Cell Electrochemistry

A schematic of a full cell is shown in Figure 1.5. The theoretical potential of the cell (E_{cell}) is given by the Nernst equation shown below[12]:

$$E_{cell} = E^{\circ}_{cell} + \frac{RT}{nF} \ln \frac{a^2_{Na} a_{Fe^{+2}}}{a^2_{Na^+} a_{Fe}}$$

Where:

$E^{\circ}_{cell} = E^{\circ}_{Red} - E^{\circ}_{Ox} = -0.409 - (-2.7109) = 2.302\,V$

Potentials are versus the Standard Hydrogen Electrode (SHE)

R=8.314 J/mol K^{-1}

T = Temperature in K

n = Number of electrons = 2

F = 96485 C/equiv.

a = Activity of reactant

An important factor is the internal cell resistance and is a function of cell geometry and the electrolyte conductivity. The internal cell resistance was of particular

concern in this work because of the organic component in the molten salt electrolyte, The simplicity of the cell design should allow a compact cell geometry and help minimize the cell resistance.

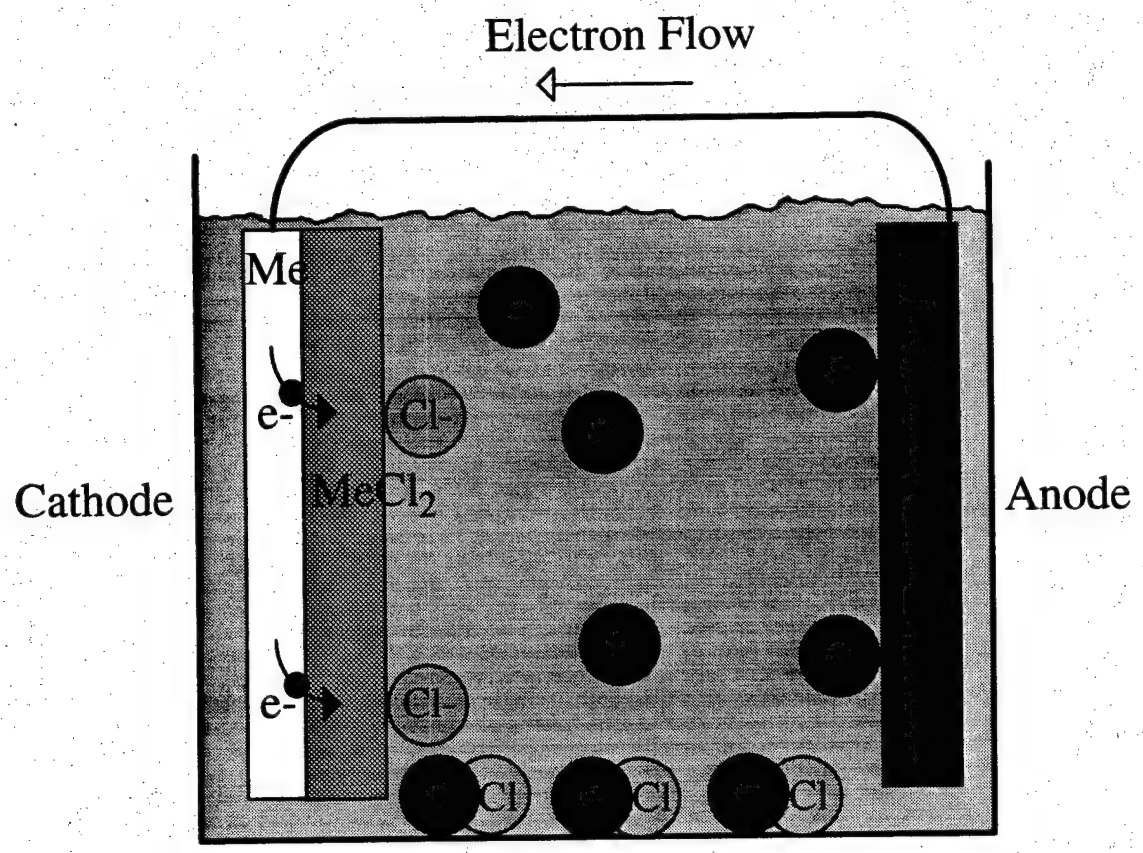

Figure 1.5 A full cell.

CHAPTER 2

EXPERIMENTAL METHODS AND EQUIPMENT

Sodium was appealing as an anode because of its light weight and reactivity. This reactivity also required more careful attention to preparation and handling of the electrolyte and other battery components. A primary requirement was that the electrolyte be water and oxygen free. Both water and oxygen react very quickly with sodium, thus reducing the amount of electroactive material available. For this reason, all electrolyte preparation was performed under a controlled atmosphere. When possible, handling of the room temperature molten salts and their precursors was carried out in a dry box (Vacuum Atmospheres) with a combined oxygen and water level below 10ppm. For operations which could not safely or conveniently be performed in the dry box, distillation and sublimation for example, apparatus was constructed for use outside the dry box. These operations were performed under nitrogen or vacuum in order to minimize water and oxygen contamination.

The dry box is a hermetically sealed nitrogen filled box. Items in the dry box are manipulated via butyl rubber gloves attached to ports in a Lexan® window. Materials and equipment were transferred in and out of the box through an antechamber. This

antechamber can be evacuated and refilled with nitrogen to prevent water and oxygen infiltration. The atmosphere inside the dry box is circulated through a bed of copper catalyst and molecular sieves which remove oxygen and water which diffuse into the box through seals, gloves, etc. Regeneration of this bed is performed periodically, eliminating oxygen bound to the copper catalyst and water absorbed by the molecular sieves. The use of chemicals in the dry box which can irreversibly react with either the copper catalyst or the molecular sieves must be avoided in order to maintain a water and oxygen free environment.

2.1 Organic Chloride Synthesis

Synthesis of the organic chlorides used in preparation of the room temperature molten salts was a multi-step procedure involving the purification of the reactants by distillation, and the products by crystallization. The solvents used in synthesis and crystallization were also by purified by distillation. A single bench top multi purpose distillation apparatus was constructed for all distillation procedures.

2.1.1 Solvent Purification

Acetonitrile and ethyl acetate were used extensively during synthesis and purification. Acetonitrile (Aldrich) and ethyl acetate (Fisher) were refluxed over calcium hydride (Fluka) using the distillation apparatus configured as shown in Figure 2.1. The

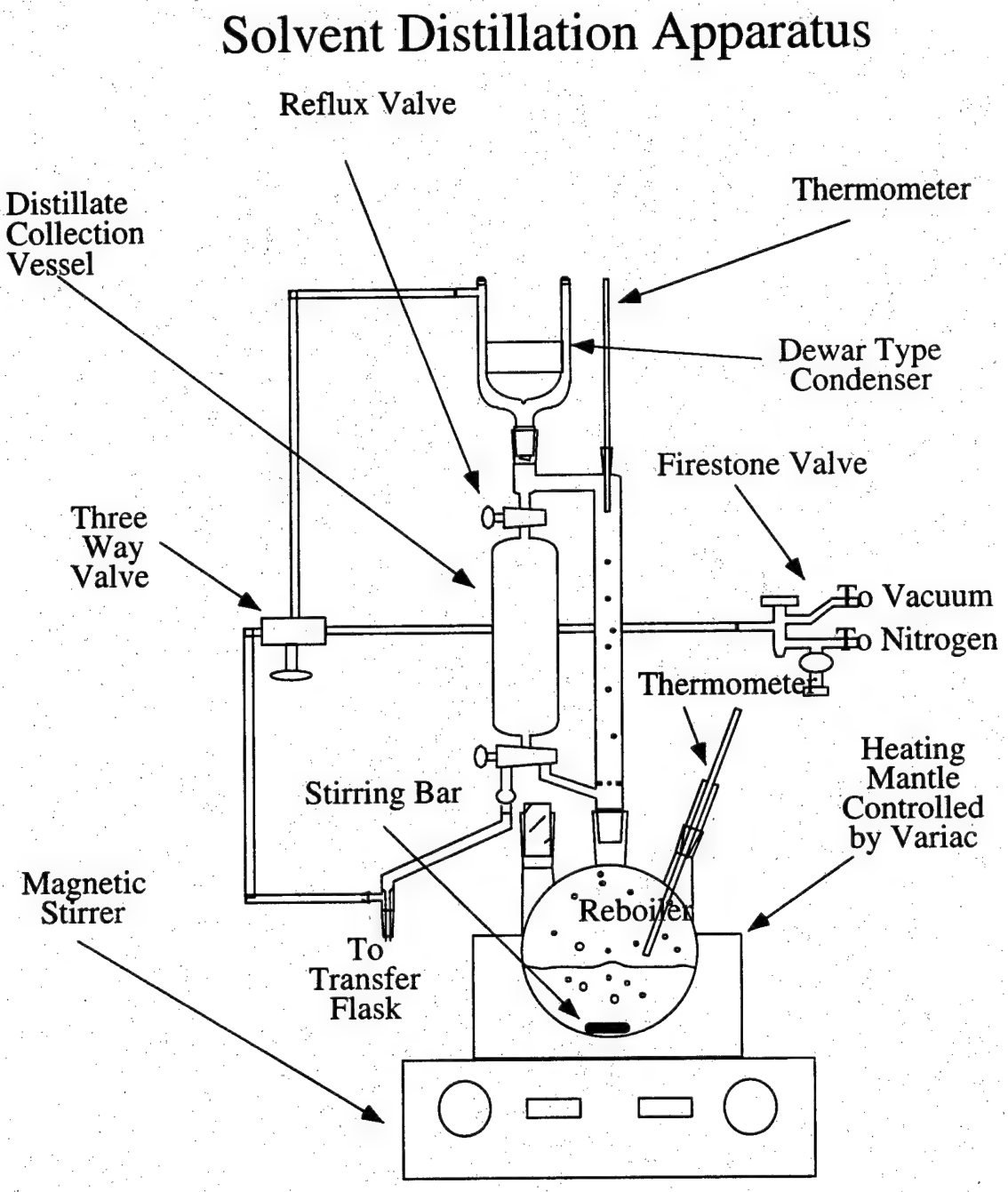

Figure 2.1. Solvent Distillation Apparatus

still was first assembled and charged with calcium hydride. The apparatus was evacuated and refilled with nitrogen several times. The solvent was introduced into the still through a port in the bottoms flask. If the amount of water in the solvent is high (>1%), the solvent must be added with great care because any water will react quickly with the calcium hydride to liberate hydrogen.

The solvent was allowed to reflux for several hours at atmospheric pressure under a nitrogen blanket. An ice / water mixture was used in the Dewar condenser. A Firestone valve (Aldrich) facilitated the evacuation and refill steps and insured that the pressure in the still remains at atmospheric pressure during distillation. This important safety device prevented pressure from building in the still. Following a period of reflux, the distillate was collected and transferred to a flask which had been evacuated. The filled flask was evacuated and chilled or completely frozen with liquid nitrogen. Flasks filled with acetonitrile fractured if completely frozen, so these flasks were only chilled to lower the vapor pressure for transfer through the antechamber. Frozen flasks of ethyl acetate were easily transferred into the dry box through the antechamber. Once thawed the solvent was transferred to different flask for storage in the drybox.

2.1.2 Reactant Purification

The reactants for the organic chloride synthesis were distilled using apparatus similar to that used for solvent distillation. The two imidazole reactants have high normal boiling points (1-methylimidazole: 198°C, 1,2-dimethylimidazole: 204°C), thus vacuum

distillation was used to prevent decomposition. The distillation was performed over calcium hydride. This consumed any water in the reactant and lessens bumping by acting as a boiling promoter.

2.1.2.1 1-Methylimidazole

The distillation apparatus used for 1-methylimidazole purification is shown in Figure 2.1. The still was purged and backfilled with nitrogen several times. Calcium hydride was transferred from the drybox to the bottoms flask. 1-methylimidazole (99+%, Aldrich) was introduced into the bottoms flask via a the access port. The 1-methylimidazole was added slowly with careful attention paid to the amount of gas evolved as the liquid contacts the calcium hydride. Since the imidazole was extremely hydroscopic, rapid hydrogen evolution could occur if the imidazole had absorbed significant amounts of water. Large amounts of hydrogen evolution could result in an explosion if the capacity of the Firestone valve to vent the excess gas is exceeded. The flask was filled to approximately half its capacity. Filling above half the capacity of the bottoms flask can result in severe bumping and calcium hydride may be carried up the column leading to distillate contamination.

Following addition of the 1-methylimidazole, the still was evacuated and refilled several times. The still was left under vacuum and the temperature of the bottoms flask was slowly raised by applying power to the heating mantle via the Variac. The still was left under vacuum for the extent of the distillation. A liquid nitrogen trap was used

between the Firestone valve and the vacuum pump. This condensed all gasses, except hydrogen, that condense at temperatures below the temperature of the Dewar condenser. Care was taken to make sure the trap did not clog due to freezing of the condensables that reach the trap. If the trap clogs, the bottoms and distillate temperatures rise as the pressure of the still increases. The operating pressure of the still was controlled by the distillate temperature and should remain constant if the condenser was at constant temperature.

The still was operated under constant reflux for several hours. An ice / water mixture was used in the Dewar condenser. The distillate was collected and transferred to a round bottoms flask for transfer to the drybox. A procedure similar to that described for the solvent transfer to the drybox was used for transfer of the imidazole distillate.

2.1.2.2 1,2-Dimethylimidazole

Vacuum distillation was also used for purification of the 1,2-dimethylimidazole. The apparatus was modified slightly due to the higher freezing point of 1,2-dimethylimidazole (~38°C). The Dewar type condenser was replaced with a coiled condenser. The apparatus is shown in Figure 2.2. This allowed circulation of water through the condenser and by using a temperature controlled circulator, careful control of the condenser temperature. If the condenser temperature was too low, formation of crystals rather than liquid condensate was observed. Following a period of reflux, the distillate was collected and transferred to a round bottoms flask for transfer into the

drybox. Special care was exercised to prevent freezing of the distillate in the transfer tubes.

2.1.2.3 Ethyl Chloride

Ethyl chloride (Matheson) was distilled over calcium hydride. The apparatus used for this procedure is shown in Figure 2.3. In this configuration the still uses a dry ice / methanol mixture in the Dewar condenser and ice water in the reboiler. The distillation was carried out at atmospheric pressure. The reboiler was charged with calcium chloride following several evacuation and refill cycles. After evacuation, ethyl chloride was introduced into the still as a gas directly from the cylinder. As the ethyl chloride entered the still, it condensed at the Dewar condenser and dripped into the reboiler. Once a suitable quantity of liquid has formed, the gas cylinder was turned off and the still brought up to atmospheric pressure with nitrogen via the Firestone valve. Reflux was commenced by slowly warming the reboiler by removing the ice. The normal boiling point of ethyl chloride is ~12°C. The amount of reflux was controlled by the temperature of the water bath. The ethyl chloride was refluxed for several hours then transferred directly to a pressure vessel charged with the other reactants and solvents.

2.1.2.4 Propyl Chloride

Propyl chloride was distilled in a manner very similar to acetonitrile and ethyl acetate. A distillation over calcium hydride was carried out at atmospheric pressure.

Very little heating was required at the reboiler due to the lower normal boiling point of propyl chloride (~46°C). An ice / water mixture was used in the dewer condenser. The propyl chloride was refluxed for several hours. Following distillate collection, the propyl chloride was transferred to a round bottom flask and taken into the dry box.

2.1.3 Synthesis

Synthesis of the three organic chlorides was carried out at room temperature. This decreased the pressure in the reactor and, thus, decreased the likelihood of an explosion.

2.1.3.1 1-Methyl-3-ethylimidazolium chloride

The reactor used for 1-methyl-3-ethylimidazolium chloride synthesis is shown in Figure 2.4. The vapor pressure of ethyl chloride is ~24 psia at 25°C. This should be the approximate operating pressure of the reactor during synthesis. The reactor was pressure tested to ~50 psia to insure some margin of safety. Several batches of MEIC were synthesized over the course of this work. A typical batch would begin with the addition of 200 ml 1-methylimidazole and 100 ml of acetonitrile to the pressure bottle. Ethyl chloride was distilled and transferred directly to the reaction vessel. This single phase solution was allowed to stir for approximately three weeks outside the dry box resulting in a single yellowish liquid. Excess ethyl chloride was removed by pulling a vacuum on the reaction vessel and condensing the resulting vapor. The liquid product was acetonitrile saturated with crude MEIC.

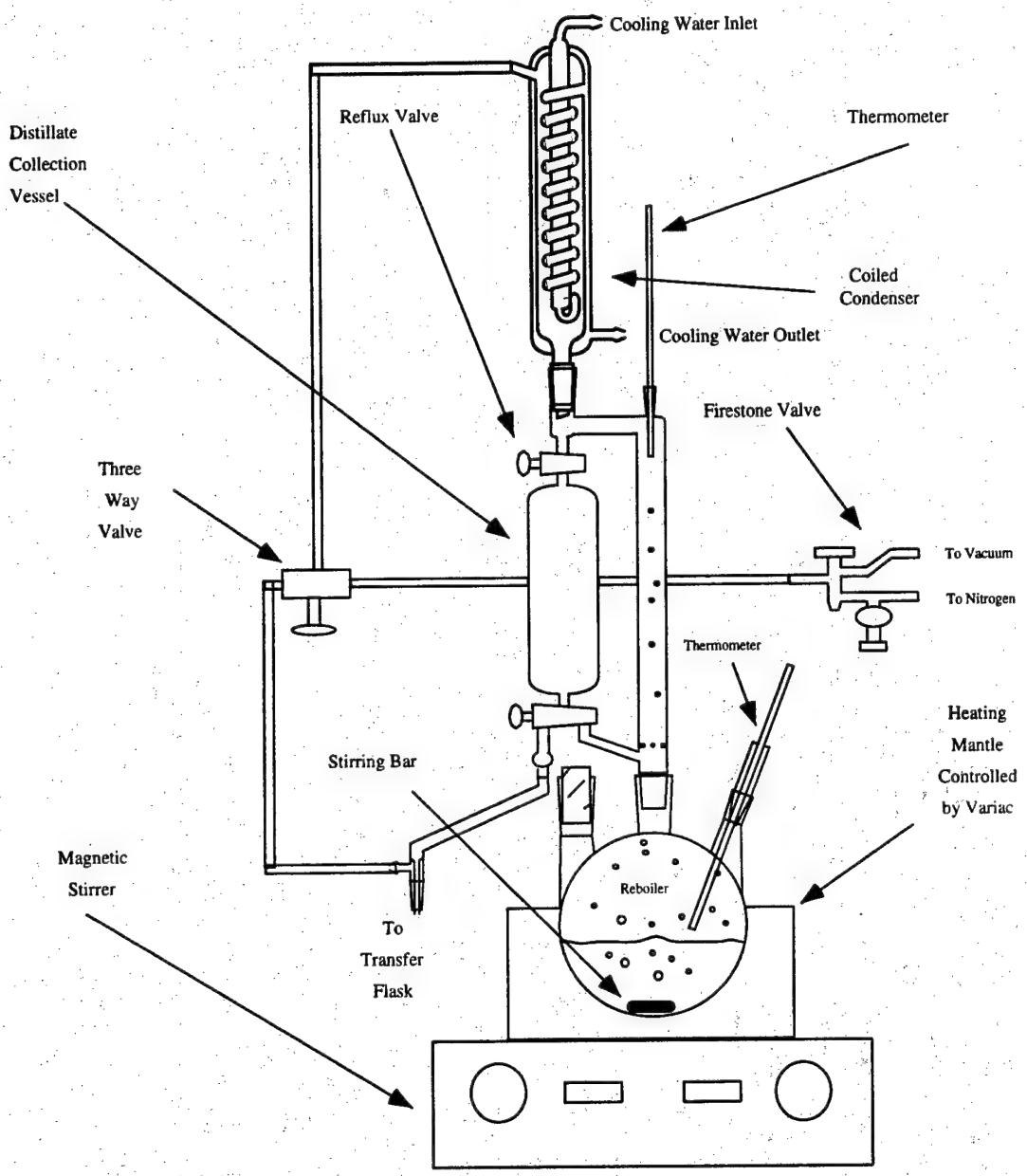

Figure 2.2. Apparatus for 1,2-Dimethylimidazole Distillation

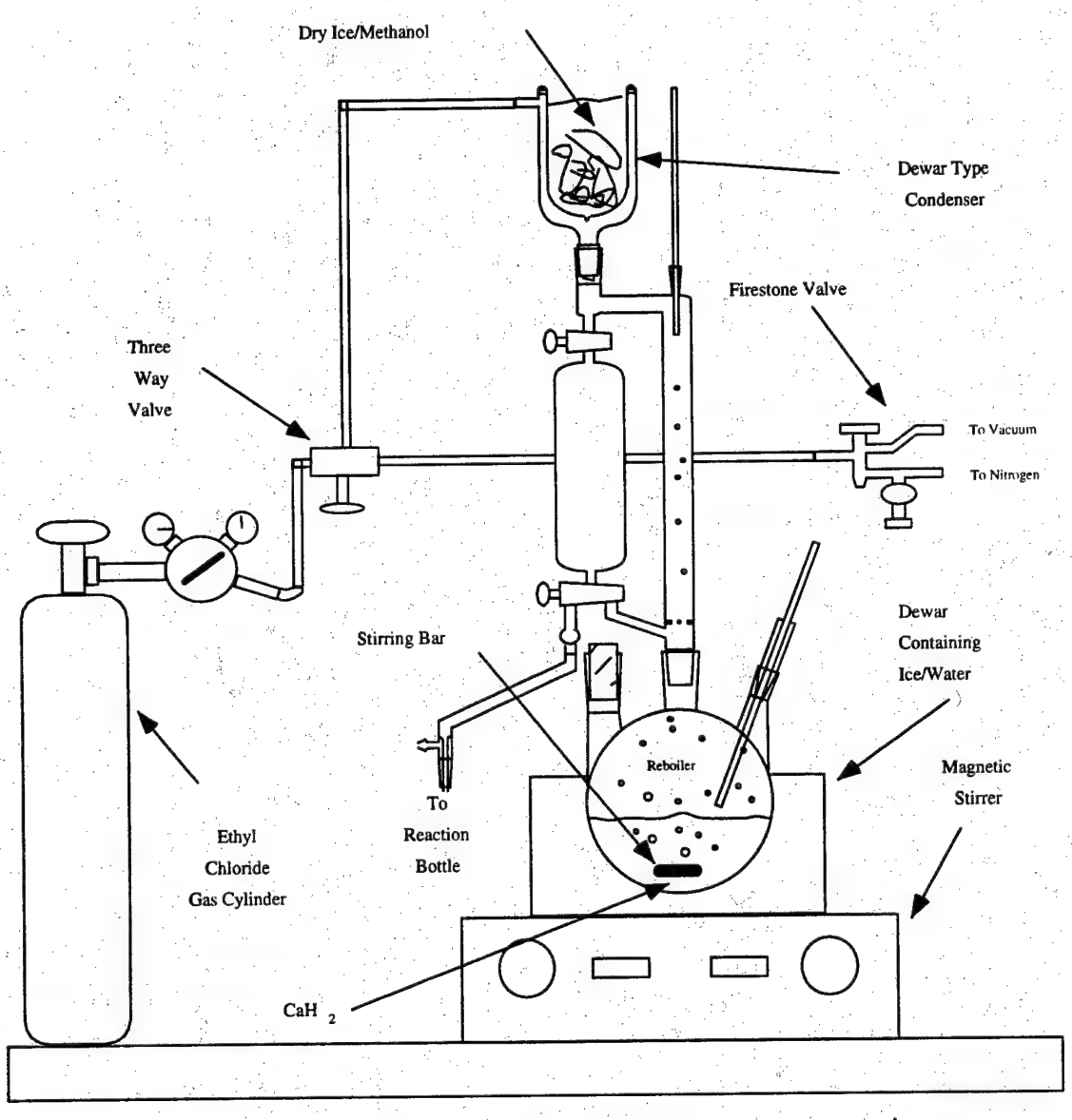

Figure 2.3. Apparatus for Ethyl Chloride Distillation

2.1.3.2 1,2-Dimethyl-3-propylimidazolium chloride

Because propyl chloride is a liquid at room temperature, the pressure requirement of the reactor was relaxed. Thus, a simple 1000 ml Erlenmeyer flask was used instead of the pressure bottle. All reactor charging was performed in the drybox thus minimizing the chance for contamination. The flask was charged with sufficient acetonitrile to dissolve approximately 200 g of 1,2-dimethylimidazole. To this a 100% excess of propyl chloride was added. The solution was allowed to sit in the dry box for several weeks at which point crystals began to form. These crystals were harvested and addition reactants added to the reactor. The crude DMPIC crystals were further purified through recrystallization.

2.1.3.3 1-Methyl-3-propylimidazolium chloride

As with the DMPIC synthesis, the 1-methyl-3-propylimidazolium chloride synthesis could be carried out at a lower pressure due to the lower vapor pressure of propyl chloride at room temperature. A 500 ml Erlenmeyer flask was used as the reaction vessel. The reactor was charged with 150 ml 1-methylimidazole and 300 ml 1-chloropropane. A single liquid phase was observed. The literature indicated some difficulty in formation of MPIC crystals so no additional solvent, i.e. acetonitrile, was added. After approximately two weeks two liquid phases were evident. The heavy phase was assumed to be the product rich phase. This heavy phase was separated from the light phase using a separatory funnel.

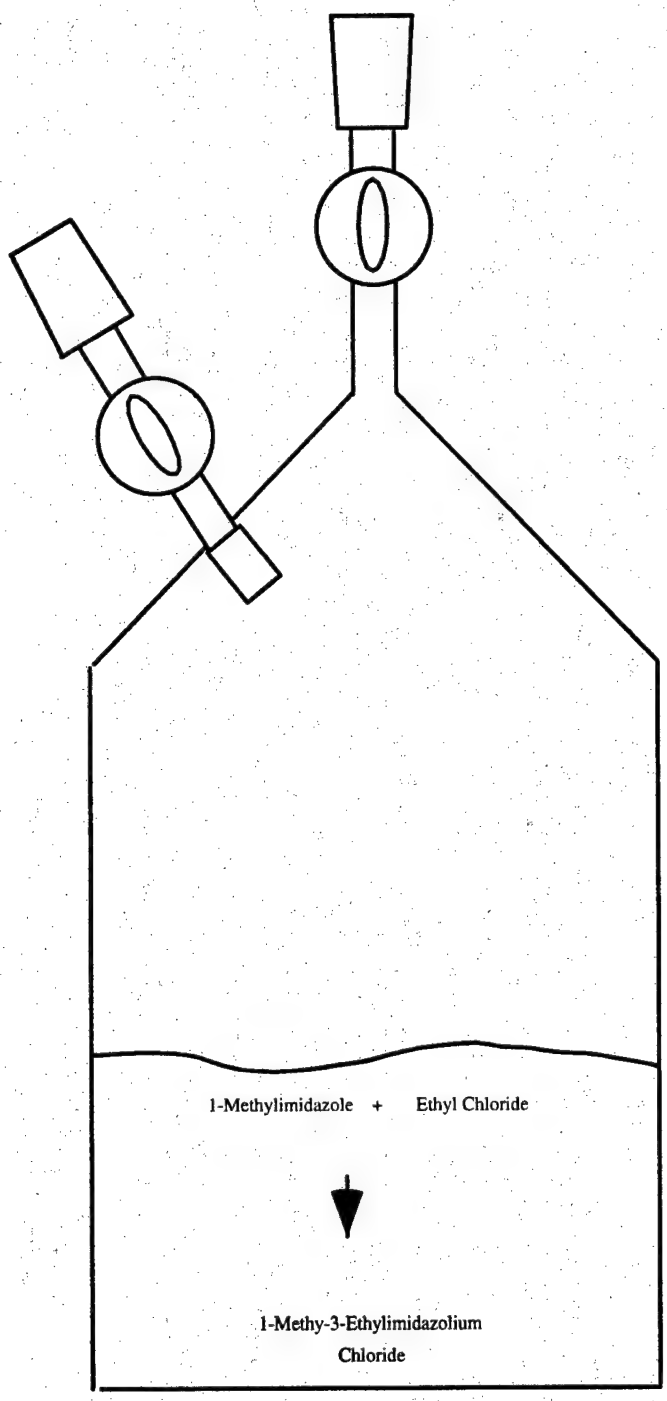

Figure 2.4. Reactor Used for MEIC Synthesis

2.1.4 Product Purification

In the case of MEIC and DMPIC, a crude, crystalline product was obtained from the synthesis. The MPIC synthesis resulted in a liquid product. These products required slightly different treatment for additional purification. The crude crystals were dissolved in a minimum amount of acetonitrile to form a single liquid phase. For the MPIC product, the formation of a seed crystal was achieved with great difficulty. A small sample of liquid product was transferred to a 50 ml flask. A few crystals of NaCl were added to the sample and the flask capped with a septum and transferred out of the dry box to a refrigerator. After several weeks, crystals formed. These seed crystals were used for further crystallization of the crude product.

Further crystallization of the crude products was essentially the same for all three products. The apparatus for this step is shown in Figure 2.5. The acetonitrile / organic chloride solution was added dropwise to a large excess of ethyl acetate. In the case of the liquid MPIC product, it was added directly to the ethyl acetate. A seed crystal was added to the ethyl acetate used for MPIC crystallization. In all cases vigorous stirring was necessary to prevent the formation of a second liquid phase. For MPIC, crystals would only form in the presence of a seed crystal; otherwise a liquid phase resulted. The crystals were separated from the ethyl acetate / acetonitrile solution by vacuum filtration.

Removal of the remaining solvent from the filtered crystals was accomplished by heating the crystals past their melting point and applying a vacuum to the molten organic salt. The apparatus for this procedure is shown in Figure 2.6. The entire apparatus was

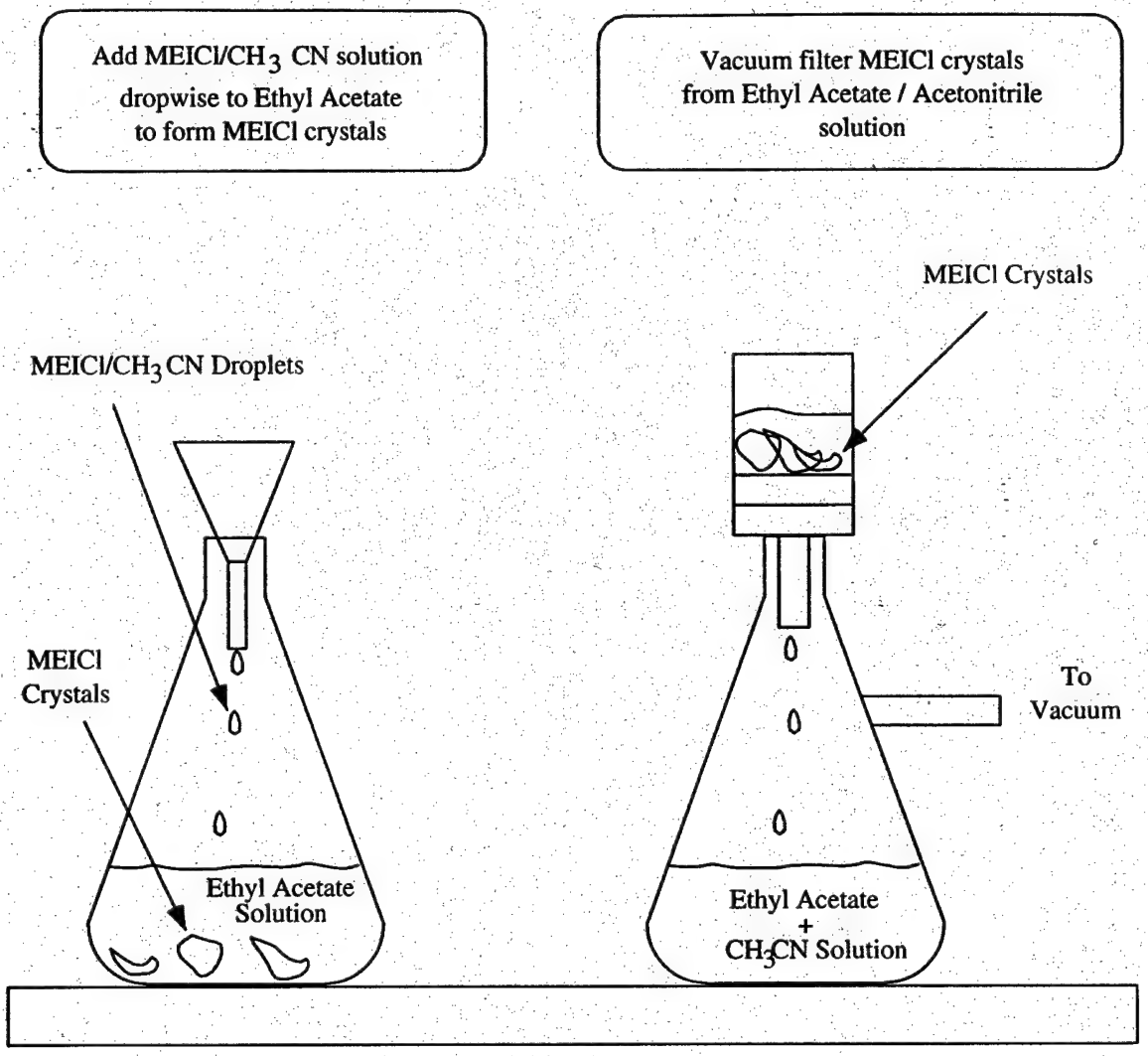

Figure 2.5. Recrystallization of the Organic Chlorides

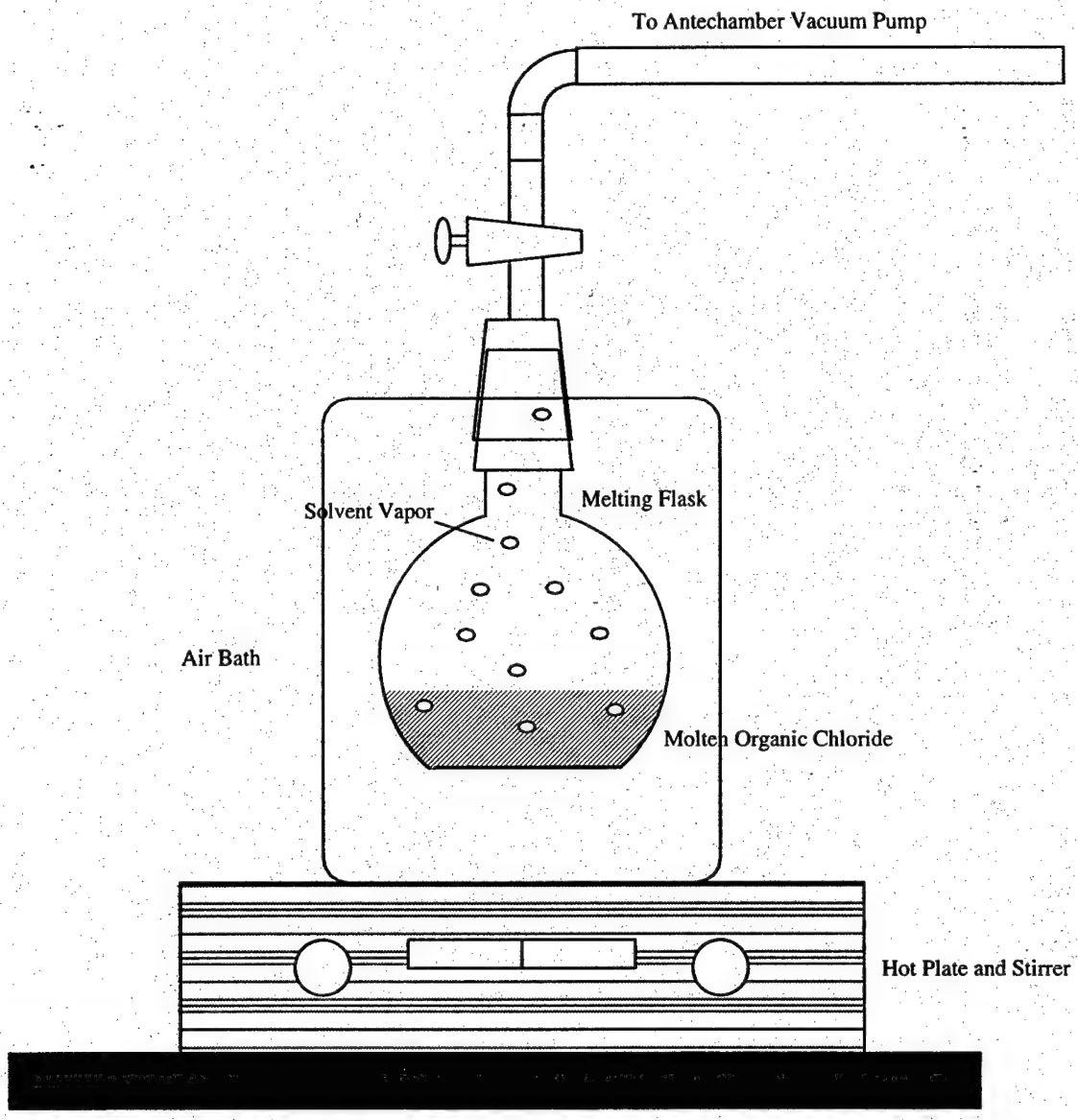

Figure 2.6. Solvent Removal from Recrystallized Organic Chloride

inside the dry box. The air bath was heated via a hot plate to slightly above the melting point of the organic chloride. The outlet of the melting flask was connected to the antechamber of the drybox and the antechamber vacuum pump was used to remove the solvent as it is released from the melting organic chloride. The vacuum was applied prior to heating the flask to minimize the risk pressure building in the flask due to heating. The solvents used have significant vapor pressures at the melting points of the organic chlorides and are easily removed leaving a pure organic chloride.

While molten, the organic chlorides were poured into small boats fashioned from aluminum foil. The organic chloride solidified as it cooled leaving a solid chunk of material. This chunk was broken into small pieces and stored in wide mouth bottles in the dry box.

2.2 Aluminum Chloride Purification

Aluminum chloride was purified using a method similar to that described by Gale and Osteryoung. Ampules were fashioned from 25 mm OD heavy walled borosilicate glass. A hi-vac stopcock was attached to one end with a ground glass joint. Each ampule was charged with 150 g of aluminum chloride (Fluka), 25 g sodium chloride (Aldrich) and several two inch lengths of 1 mm aluminum wire (Aldrich). The ampule was heated to approximately 100°C under vacuum overnight. This served to remove any gas or volatile compounds. The apparatus for this first step in the aluminum chloride

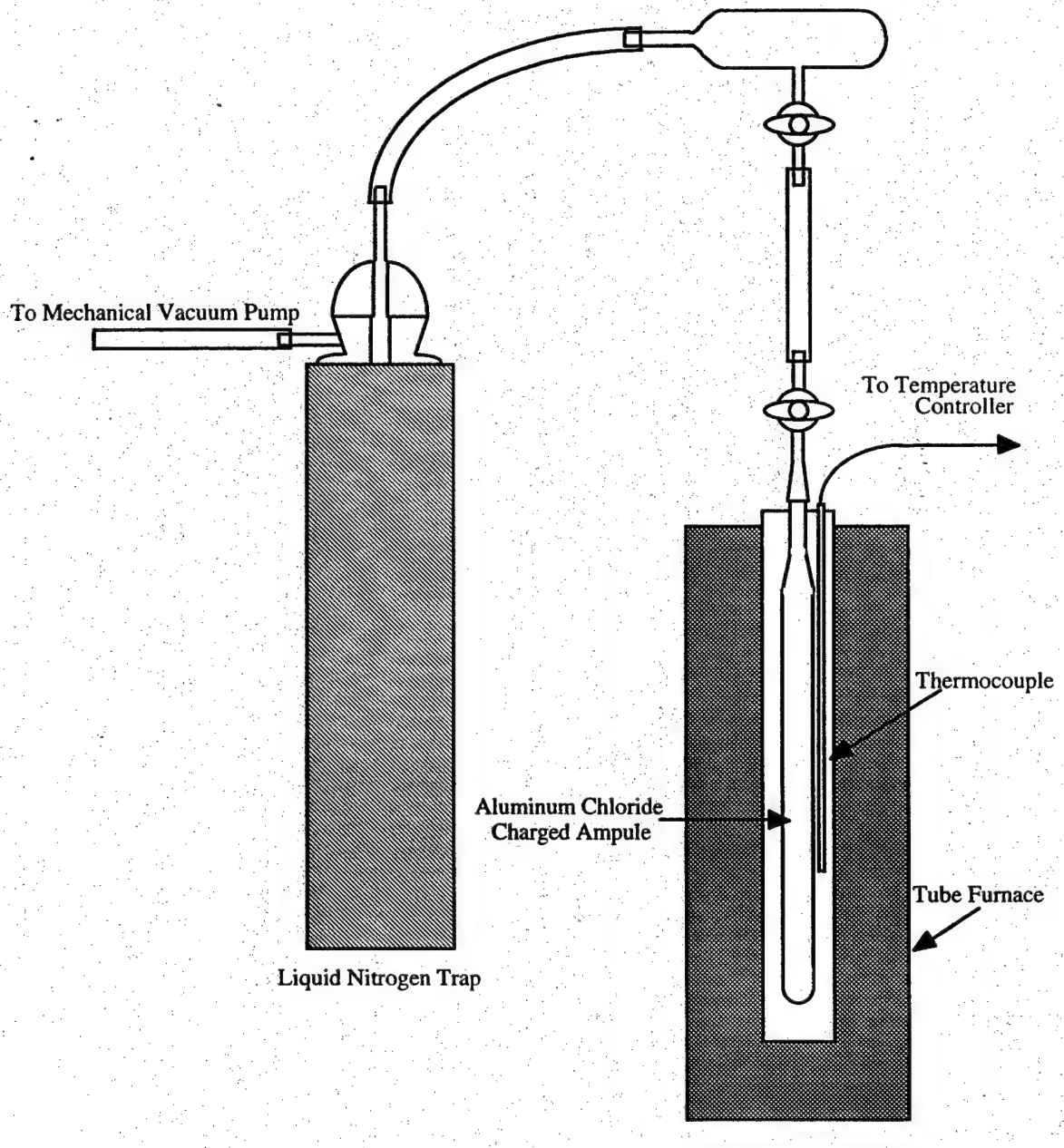

Figure 2.7. Apparatus for Low Temperature Treatment of Aluminum Chloride

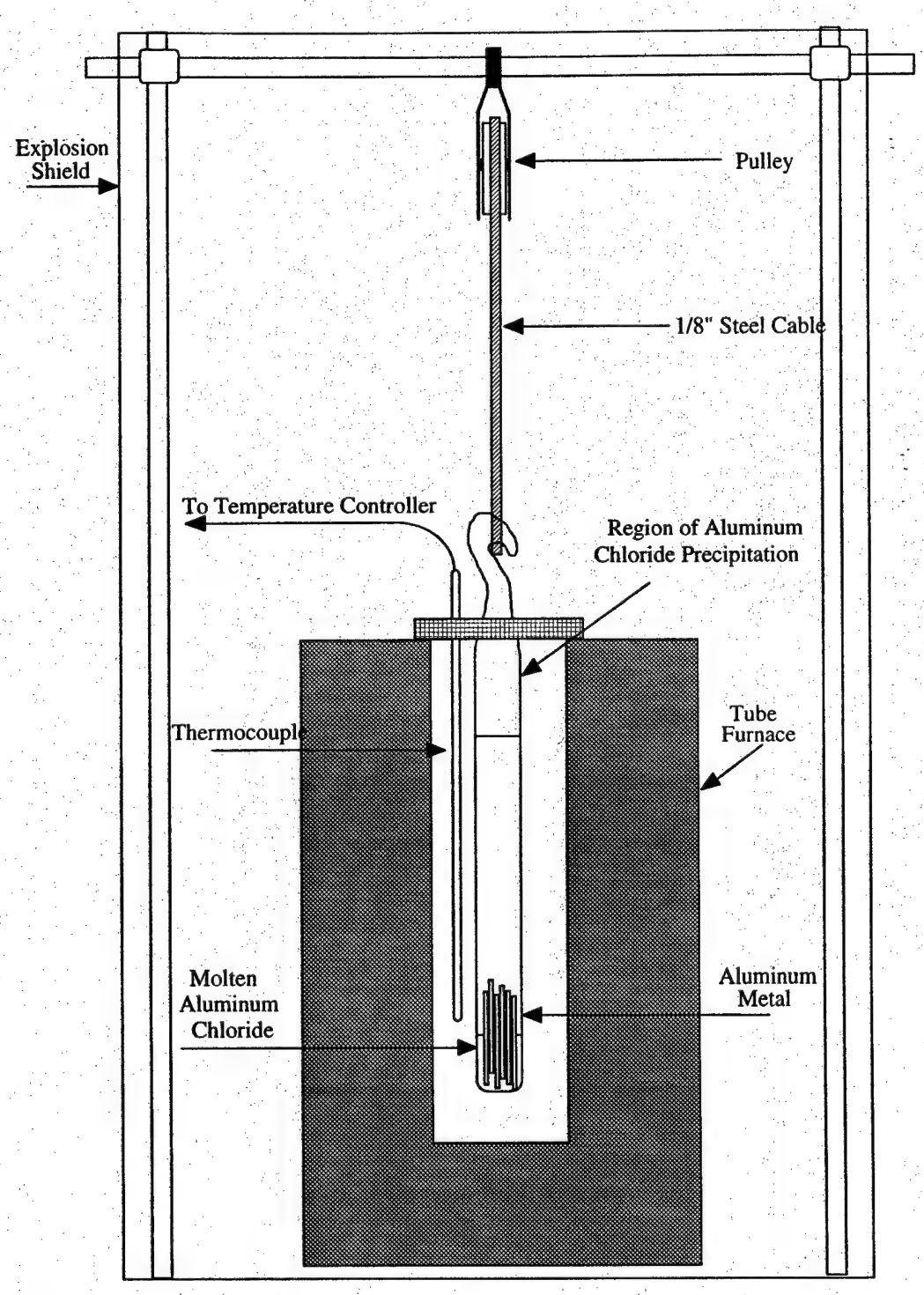

Figure 2.8. Aluminum Chloride Distillation Apparatus

purification is shown in Figure 2.7. The ampule was sealed by the glass blower and the end fashioned into a hook.

The ampule was place into a vertical tube furnace as illustrated in Figure 2.8 and heated to approximately 200°C. Care was taken to shield the apparatus in the event of any explosion. The vapor pressure of $AlCl_3$ is 295 kPa[13] at 200°C. Additionally, the exposure of $AlCl_3$ vapor to humid air results in generation of hydrogen chloride gas. As the ampule was slowly withdrawn from the oven, aluminum chloride condensed on the walls of the tube. This sublimation process continued until approximately 80% of the aluminum chloride was sublimed. The rate of sublimation was controlled by the rate of removal of the tube from the oven.

The tube was allowed to cool thus solidifying the lower liquid phase along with any impurities. The tube was transferred to the dry box. The ampule was broken and the pure aluminum chloride separated from the remnants of the tube. The chunks of aluminum chloride were stored in the dry box in small bottles.

2.3 Melt Preparation

Room temperature molten salts were formed by combining the appropriate amounts of aluminum chloride and organic chloride to form either an acidic or basic melt. The components were added as pea sized chunks to prevent fast dissolution and heat

evolution. Combining finely divided amounts of the components could result in rapid heating of the melts and decomposition of the organic component. Buffered neutral melts were formed by first preparing an acidic melt, generally N=0.55. To the acidic melt, the appropriate alkali metal chloride was added, usually in 100% excess of the amount required to completely react with the excess aluminum chloride. This melt was allowed to stir for several days to allow the undissolved sodium chloride to reach equilibrium with the free Na^+ produced during the buffering reaction.

2.4 Melt Additives

Several additives have been reported to facilitate the plating and stripping of sodium by preventing or inhibiting the electrochemical reduction of the organic cation and the direct reaction of sodium with the molten salt electrolyte.[8,9] Two of these melt additives (HCl and $SOCl_2$) are examined here. The first reports of melt additives affecting the plating and stripping of sodium from a MEIC/$AlCl_3$/NaCl molten salt indicated the addition of protons in the form of 1-methyl-3-ethylimidazolium hydrogen dichloride. This mixture is liquid at room temperatures and is a convenient method of adding protons to the melt. This mixture was formed by condensing gaseous hydrogen chloride onto solid MEIC as described by Dawodinski. As the mixture was warmed to room temperature, the MEIC dissolved and complexed with the HCl. The solubility of

HCl in this liquid was low so that a nearly equimolar mixture of HCl and MEIC is formed. The precise stoichiometry of this mixture was verified by titration with sodium hydroxide. Thionyl chloride (Aldrich) and hydrogen chloride (Matheson, Semiconductor Grade) were used as received.

2.5 Electrochemical Analysis

A variety of electrochemical methods and tools were utilized to investigate the electrochemical behavior of the molten salt electrolyte. Of specific interest was its ability to plate sodium on a solid substrate and the stability of metallic sodium in contact with the molten salt.

2.5.1 Closed Electrochemical Cell

In order to investigate the effect of hydrogen chloride gas on the electrochemical behavior of the molten salt, a gas tight electrochemical cell was constructed. This cell is pictured in Figure 2.9. The cell allows HCl to be bubbled through the molten salt in order to maintain a constant partial pressure of HCl above the electrolyte. The flow system shown in Figure 2.10 allowed blending of HCl and argon in any proportion in order to precisely control the partial pressure of HCl over the molten salt. The outlet bubblers prevented atmospheric contamination of the electrolyte under study and served to maintain a constant total pressure in the cell. Although the relationship between

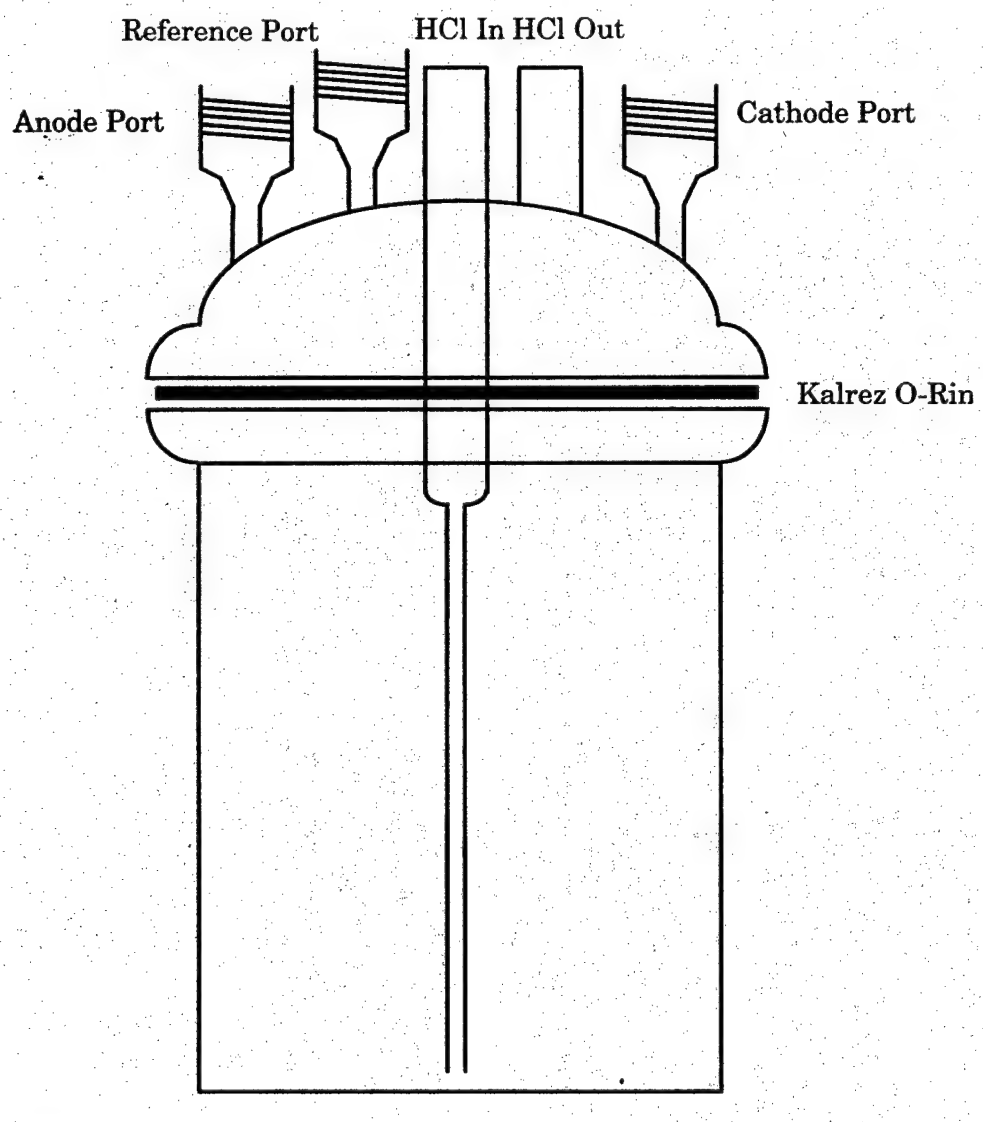

Figure 2.9. Closed Cell Used for HCl addition

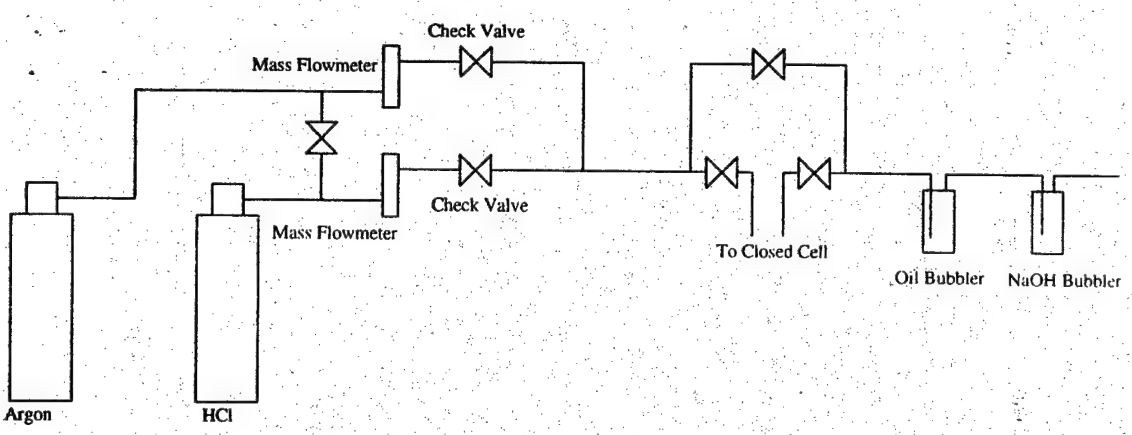

Figure 2.10. Gas Flow System for HCl Addition

dissolved HCl in the molten salt and the partial pressure of HCl above the molten salt was unknown, a Henry's law type behavior was suspected to exist.

Typically, blended HCl and argon would be passed through the electrolyte for 1 hour, after which the cell was sealed to maintain a constant HCl partial pressure. Experiments indicated that the electrochemical properties did not change with longer periods of HCl flow. This suggested that the electrolyte and gas reached equilibrium within 1 hour.

2.5.2 Electrodes

The most practical anode substrate is stainless steel; the stainless steel electrode is pictured in Figure 2.11B. However because stainless steel contains many elements, extraneous electrochemical reactions might be present. For initial experiments, a pure substrate is desirable. Tungsten was inert in the system and a tungsten disk electrode is easily fabricated using borosilicate glass due to their similar thermal expansion coefficients. The tungsten electrode is shown in Figure 2.11A. Stainless steel was also of interest because of its usefulness in practical cells. For studies of the electrode surface using optical microscopy, a flag type electrode constructed from tungsten sheet. This electrode is pictured in Figure 2.11C. The tungsten sheet electrode was modified slightly to minimize edge effects by coating the back and edges of the electrode with epoxy. This configuration is pictured in Figure 2.11D.

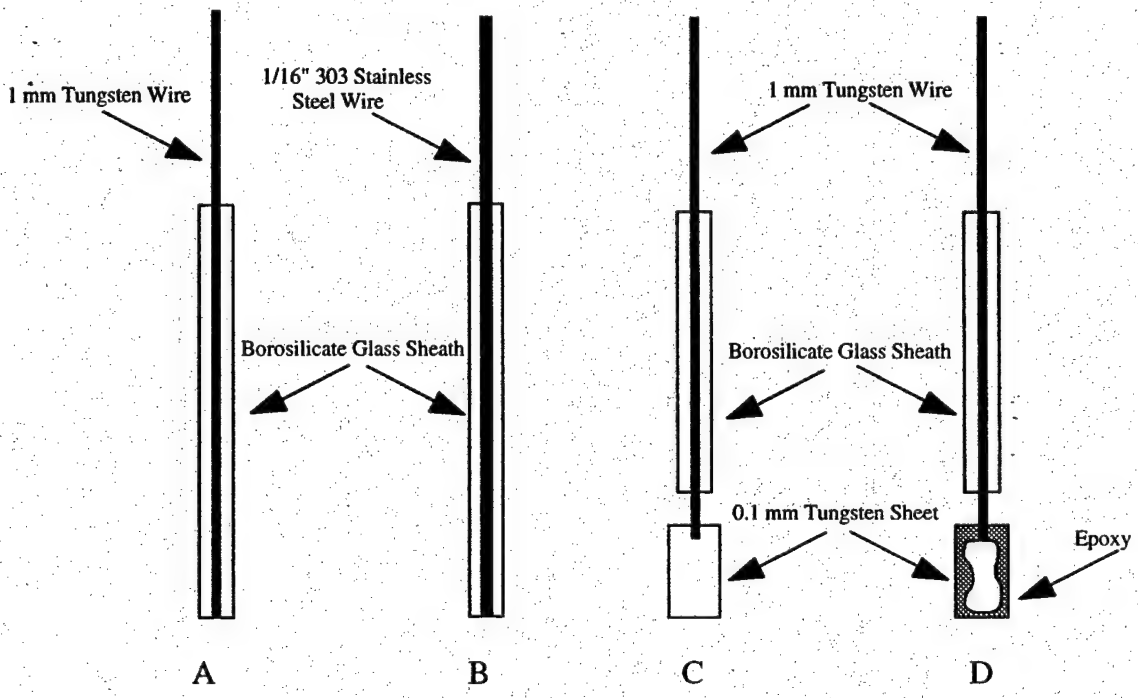

Figure 2.11. Electrodes used in Electrochemical Studies

2.5.3 Techniques

Several electrochemical techniques were used to examine the properties of the room temperature molten salts and their interaction with metallic sodium. These methods included cyclic voltammetry, chronopotentiometry, and chronoamperometry. All electrochemical methods involve the modulation of potential versus time and the recording of the resulting current behavior or the modulation of current versus time and the recording of the resulting potential behavior.

The instrument used for electrochemical analysis was a EG&G Princeton Applied Research Model 273 Potentiostat/Galvanostat interfaced with an IBM compatible PC. A simple schematic of the potentiostat is pictured in Figure 2.12.

2.5.3.1 Cyclic Voltammetry

This potential scan experiment involves the modulation of the potential at the working electrode in a linear fashion. The potential scan is reversed at a switching time, λ. Figure 2.13A illustrates the potential versus time behavior at the working electrode. The resulting current response is recorded. A typical current response for a reversible, diffusion controlled system is shown in Figure 2.13B. Generally, the current is plotted versus potential at the working electrode. Cyclic voltammetry is a popular technique for new systems because it can provide a insight into both the thermodynamics and the kinetics of complex electrochemical reactions.

2.5.3.2 Chronopotentiometry

A useful controlled current method is chronopotentiometry. This method involves modulation of the current driven through the working electrode. Frequently, the current is reversed at some time, λ, through the scan. Figure 2.14A illustrates the behavior of the current with time during chronopotentiometry. This method provided insight into the plating of sodium at constant current. Since the current is precisely controlled, isolation of the plating reaction was more straightforward than with cyclic voltammetry. A typical potential response for chronopotentiometry is shown in Figure 2.14B.

2.5.3.3 Chronoamperometry

The complimentary technique of chronopotentiometry is chronoamperometry. This technique modulates the potential of the working electrode in a stepwise fashion. The potential begins at the open circuit potential, the potential corresponding to zero current flow. At time zero the potential is stepped to a value of interest. At the switching time, λ, the potential is stepped to a second value of interest. This potential versus time behavior is illustrated in Figure 2.15A. The current is recorded versus time; a typical response is shown in Figure 2.15B. This technique is useful when precise control of the electrode potential is necessary. Currents generally vary greatly during the course of the experiment as reactants near the electrodes surface are consumed very quickly immediately following the potential steps generating very high initial currents.

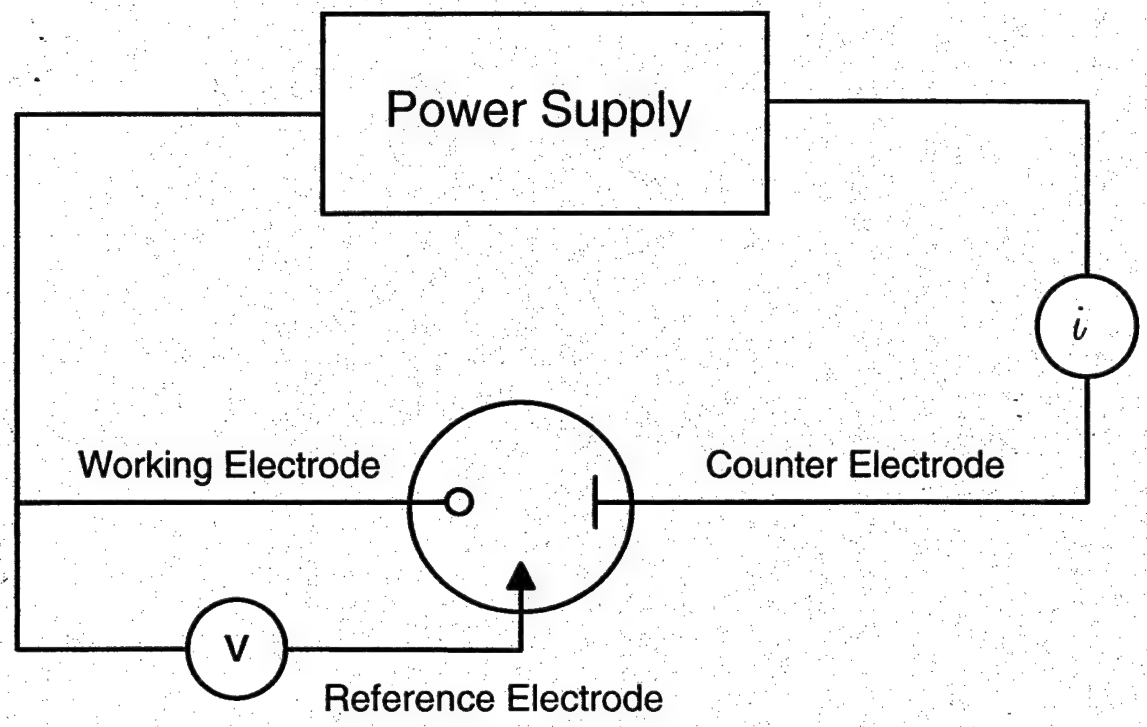

Figure 2.12. Electrochemical Analysis Equipment

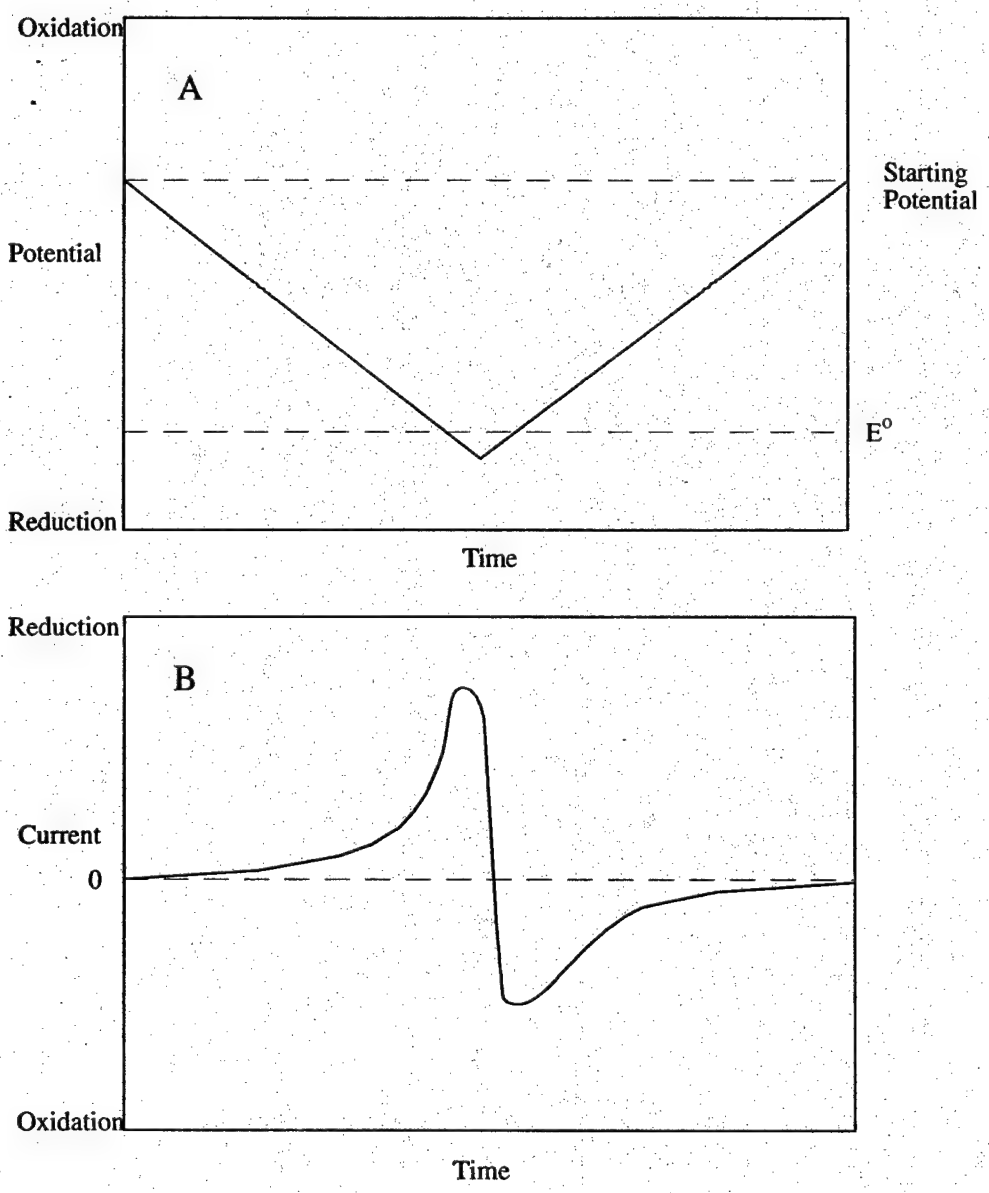

Figure 2.13. Cyclic Voltammetry: Applied voltage waveform (A), Resulting current response(B).

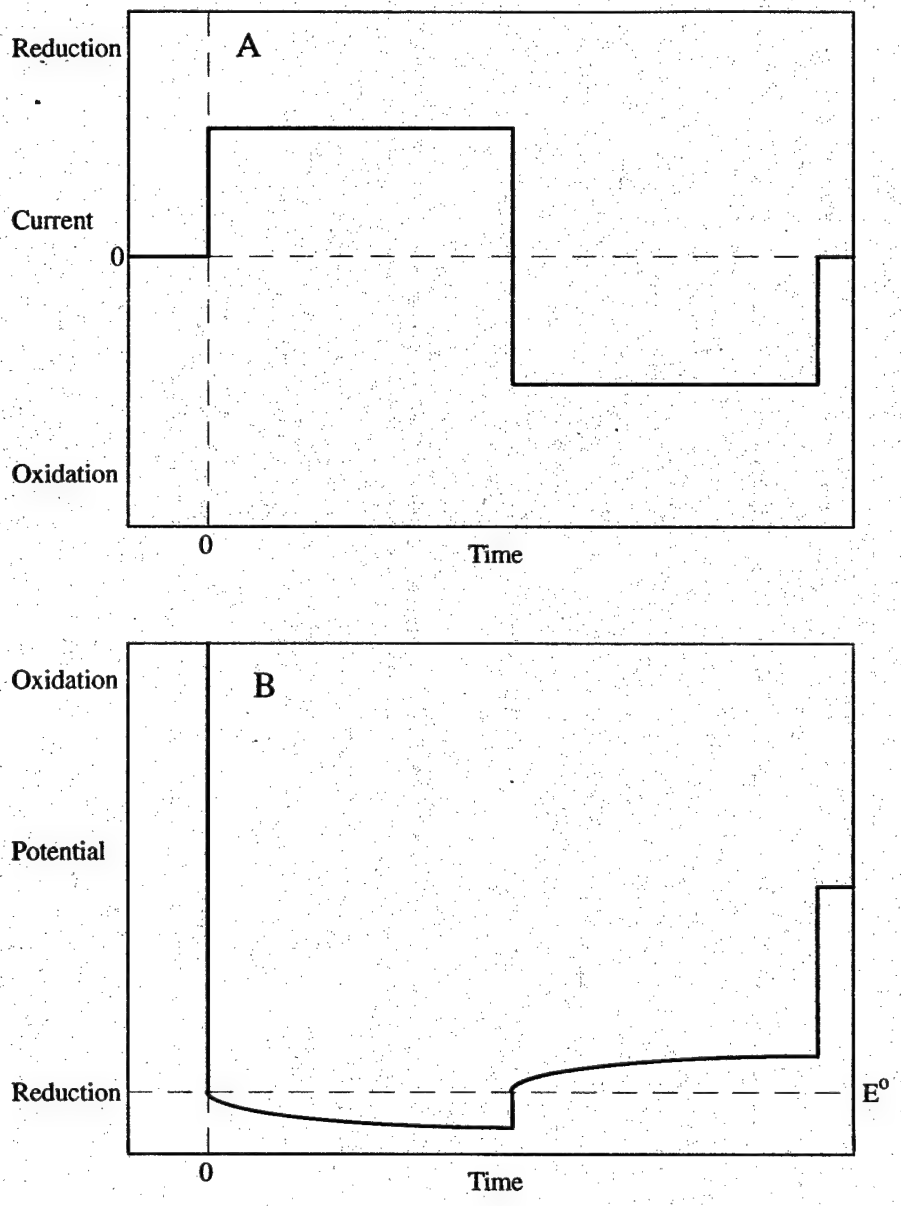

Figure 2.14. Chronopotentiometry: Applied current waveform (A), Resulting potential response (B).

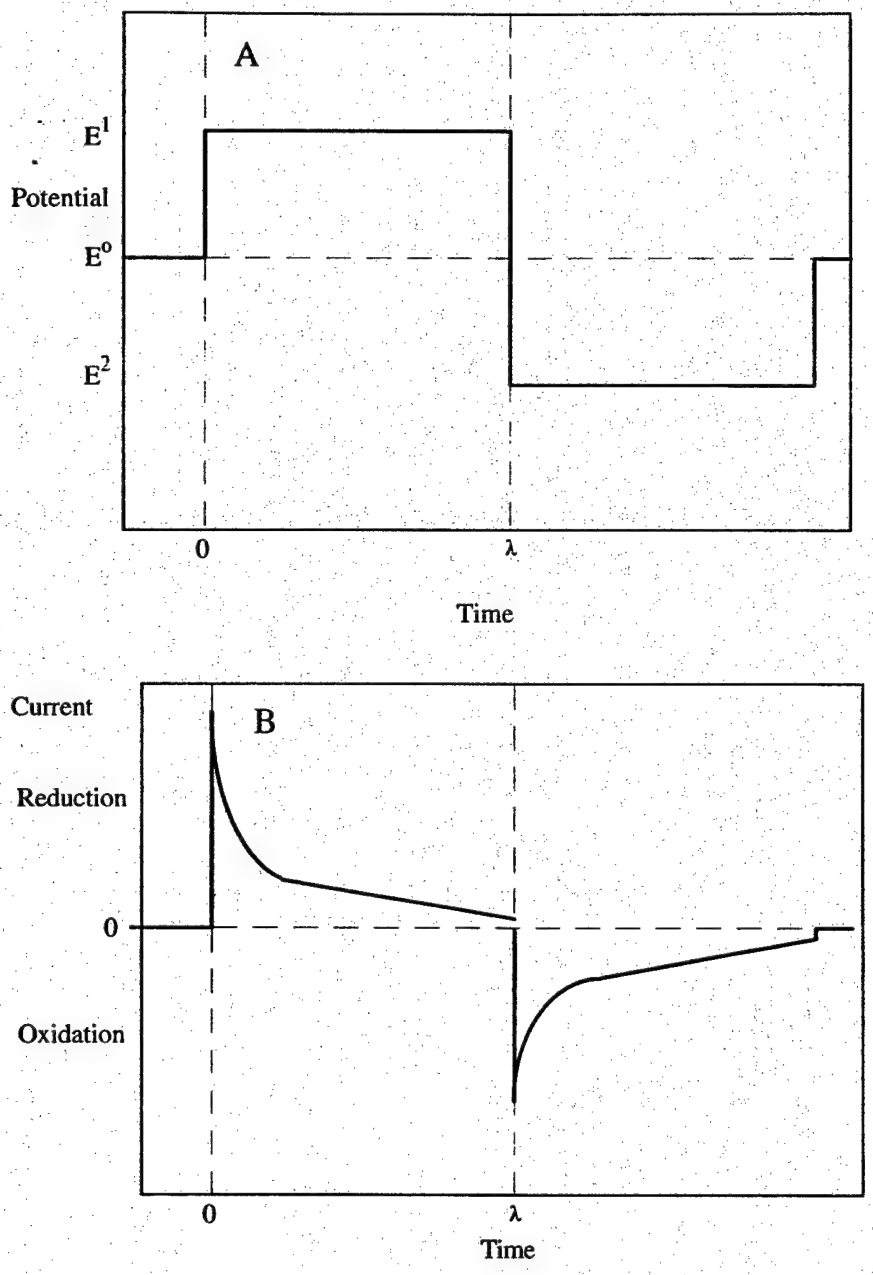

Figure 2.15. Chronoamperometry: Applied voltage waveform (A), Resulting current response(B).

CHAPTER 3

THE MEIC/$AlCl_3$/ NaCl SYSTEM

3.1 Results

The cathodic stability of the neutral, buffered MEIC-$AlCl_3$-NaCl melt and the effect of HCl addition on the deposition and stripping of sodium were studied. Figure 3.1 shows a cyclic voltammogram of the MEIC-$AlCl_3$-NaCl buffered, neutral melt using a 0.78 mm^2 area tungsten disk. The scan was started at 1.5 V and the initial scan direction was toward negative potentials. The scan rate was 100 mV/s. The reduction limit of the untreated melt was approximately -2.1 V, as defined by the potential at which the electrolyte reduction current was 1.5 mA/cm^2. Riechel and Wilkes attribute the cathodic peak at -1.3 V to the reduction of aluminum.[14] The peak current density for the impurities seen between 1.0 and -1.5 V were greater on a platinum electrode than on a tungsten or stainless steel electrode. This observation is in agreement with that of previous workers.[9] The exact nature of these impurities has not been determined.

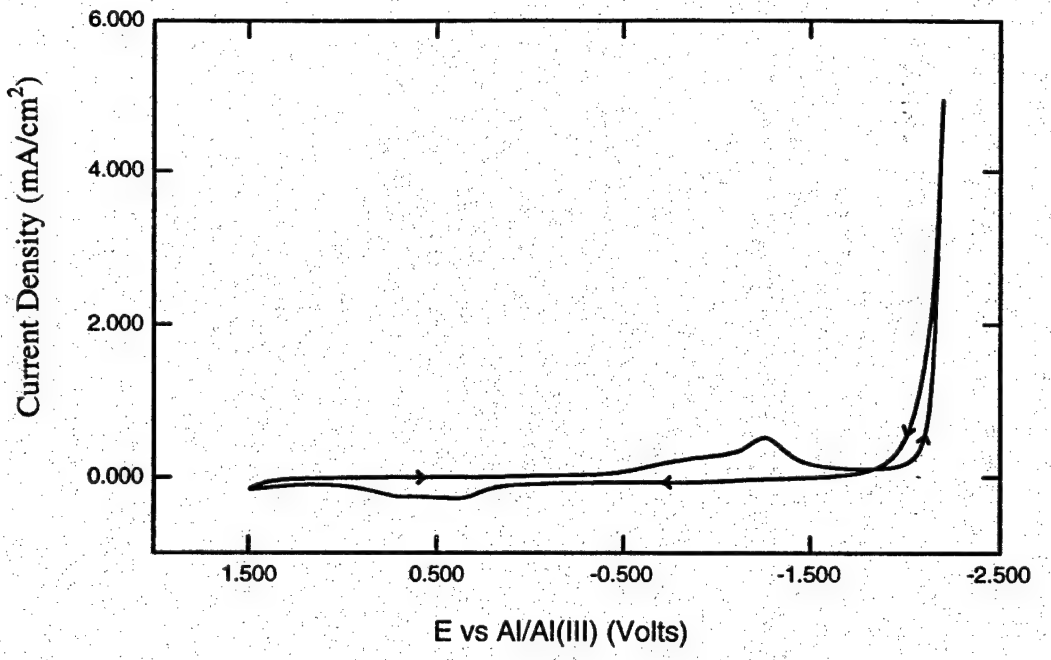

Figure 3.1. Cyclic Voltammogram of the buffered, neutral MEIC melt at tungsten.

It is possible that the cathodic potential range is limited by the reduction of the MEI^+ which may dimerize. It does not appear that Na^+ has been reduced at the negative potential limit on tungsten, because there is no anodic stripping peak observed upon scan reversal at -2.2 V versus the reference. Sodium deposition has previously been observed on a mercury electrode.[11,7] Figure 3.2 shows a cyclic voltammogram for the buffered neutral melt at a 303 stainless steel disk (2.0 mm^2 area). The scan rate was 100 mV/s. The current peaks at 1.0 V and -1.4 V were much smaller at the stainless steel electrode than at tungsten. The cathodic limit of the melt appears to be the same at 303 stainless steel as with tungsten (ca. -2.2 V at 1.5 mA/cm^2).

It has been reported that the addition of protons to the melt extends the cathodic limit of the melt and allows the reduction of Na+. Gaseous HCl and organic acids have previously been used to treat the melt.[15] Smith et al. formed $MEIHCl_2$ which is liquid a room temperature by reacting liquid HCl and solid MEIC.[16] Riechel treated melts by using this liquid HCl source. Riechel, Miedler, and Schumacher demonstrated that a shift in reduction potential of the organic cation occurred only in buffered neutral melts.[17] During this study, a similar effect was observed. The potential required to achieve a current density of ~1.3 mA/cm^2 shifted negative approximately 200 mV with HCl addition to the level needed to observe the sodium couple.

The flow-cell constructed for this study was used to quantify the effect of treatment with HCl. The partial pressure of HCl was varied by diluting a pure HCl stream with an inert gas (nitrogen or argon). The cyclic voltammogram for the neutral,

buffered melt treated with 5.0 torr HCl is shown in Figure 3.3. The shift in the cathodic limit of the melt to more negative values can be seen; however, the deposition of sodium was not observed. The current due to the reduction and oxidation of impurities is smaller. The I-V behavior of the neutral, buffered melt with the partial pressure of HCl maintained at 6.1 torr is shown in Figure 3.4. The sharp rise in the reduction current at approximately -2.3 V again showed the melt is more stable than the unbuffered melt. In Figure 3.4, the cathodic current continued to rise after the sweep reversal at -2.4 V, and a sharp oxidative stripping peak was observed on the positive going scan, which is characteristic of sodium oxidation. The reduction peak was primarily that of sodium reduction. The increase in the reduction current following the scan reversal at -2.4 V was attributed to the overpotential associated with the nucleation of sodium on tungsten. The kinetic details of this process were not investigated. Once sodium was deposited on the surface, the overpotential was reduced and the current rose at the same potential. There was no evidence to suggest the concentration of sodium in at the surface of the electrode was significantly reduced for these experiments using modest currents for short times. At potentials positive of the sodium redox potential (ca. -2.1 V), the electrodeposited sodium was oxidized, resulting in a sharp rise in the anodic current. When the electrodeposited sodium was exhausted, a very sharp drop in the oxidation current was observed. Integration of the reduction and oxidation currents was used to evaluate the coulombic efficiency of the process.

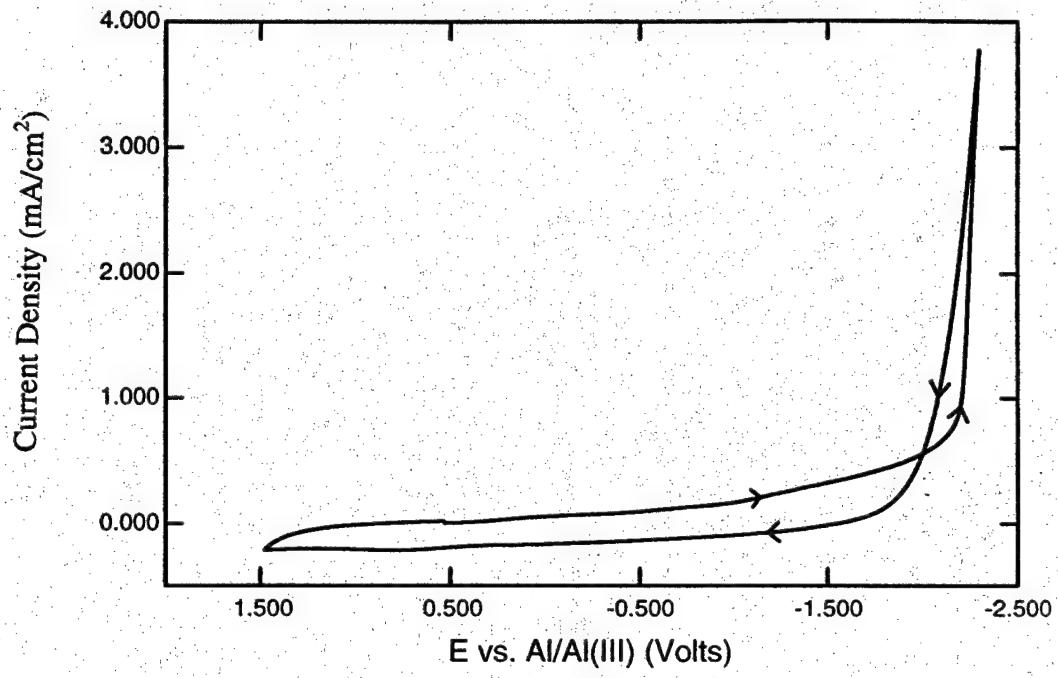

Figure 3.2. Cyclic Voltammogram of neutral, buffered MEIC at 303 stainless steel.

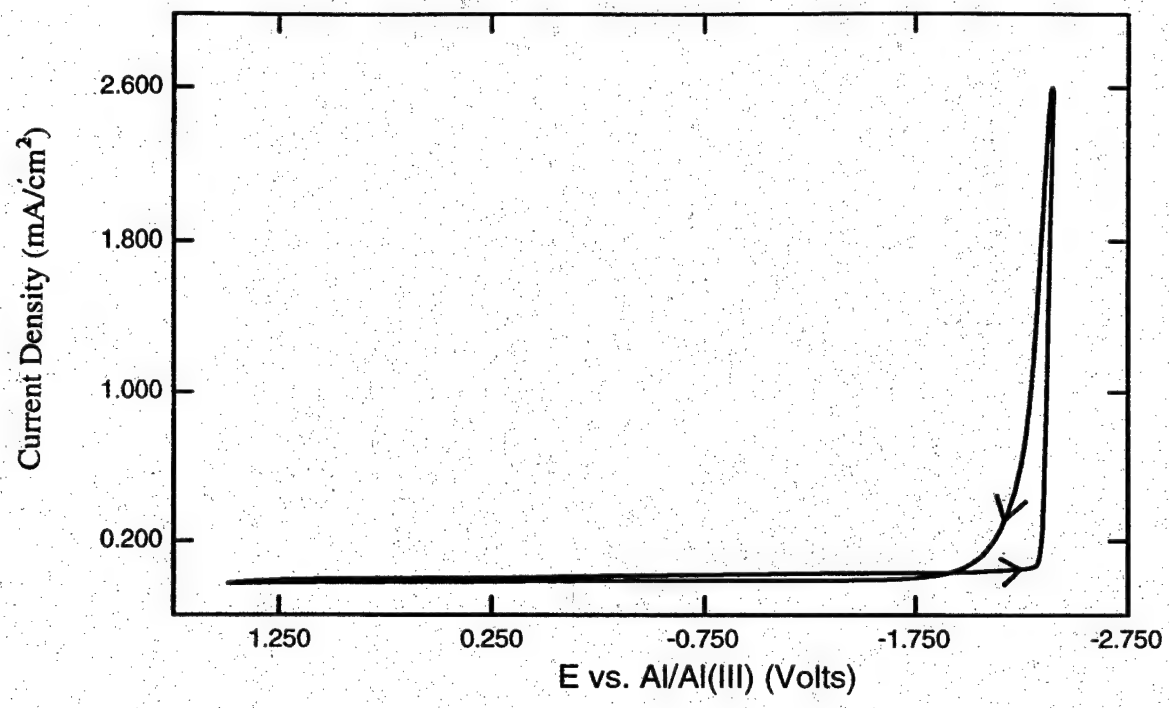

Figure 3.3. Cyclic Voltammogram at tungsten at a neutral, buffered MEIC melt treated with a partial pressure of 5 torr HCl

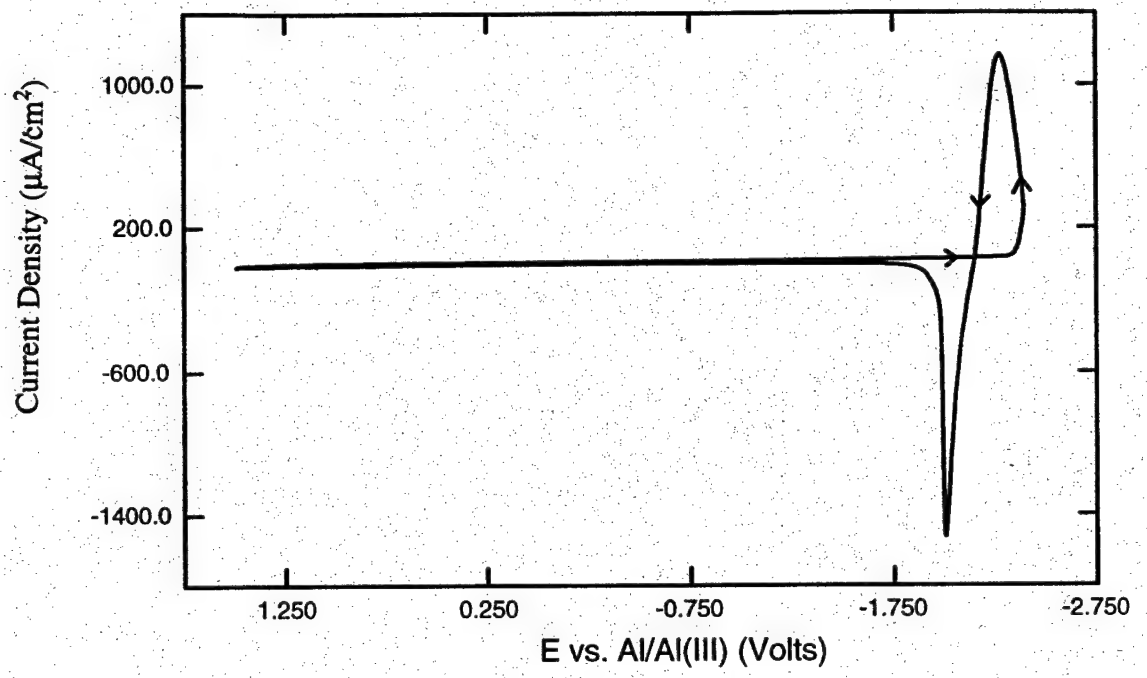

Figure 3.4. Cyclic Voltammogram at tungsten at a neutral, buffered MEIC melt treated with a partial pressure of 6.1 torr HCl

For cyclic voltammetry, the beginning of the reduction process and the end of the oxidation process were chosen based on a significant change in slope of the curve. The end of the reduction process and the beginning of the oxidation process were assumed to occur simultaneously when the current changed from positive to negative. For cyclic voltammetry, the limits of the integration also corresponded to the lowest currents. Thus, the technique used in choosing the limits did not result in a significant error in the total charge passed or the calculated efficiency. For chronopotentiometry, the beginning of the reduction process was arbitrarily chosen as the point at which the potential reached -2.0 volts. The end the reduction process and the beginning of the oxidation process were assumed to occur simultaneously when the current was reversed. The end of the oxidation process was chosen based on a significant change in slope of the potential versus time curve. For chronopotentiometry, the changes in potential associated with the reduction and oxidation processes were usually very dramatic and the potential changed rapidly with time. Coulombic efficiency is defined as the ratio of oxidation charge associated with sodium stripping divided by the reduction charge associated with sodium plating. The coulombic efficiency for the deposition and stripping of sodium in Figure 3.4 is 63%.

The shift in the cathodic stability of the melt with HCl addition was reversible. If the cell was purged with 5 torr HCl following the 6.1 torr experiment, no sodium reduction is observed. The cathodic stability shifted back to -2.1 V from -2.3 V when purged with pure nitrogen.

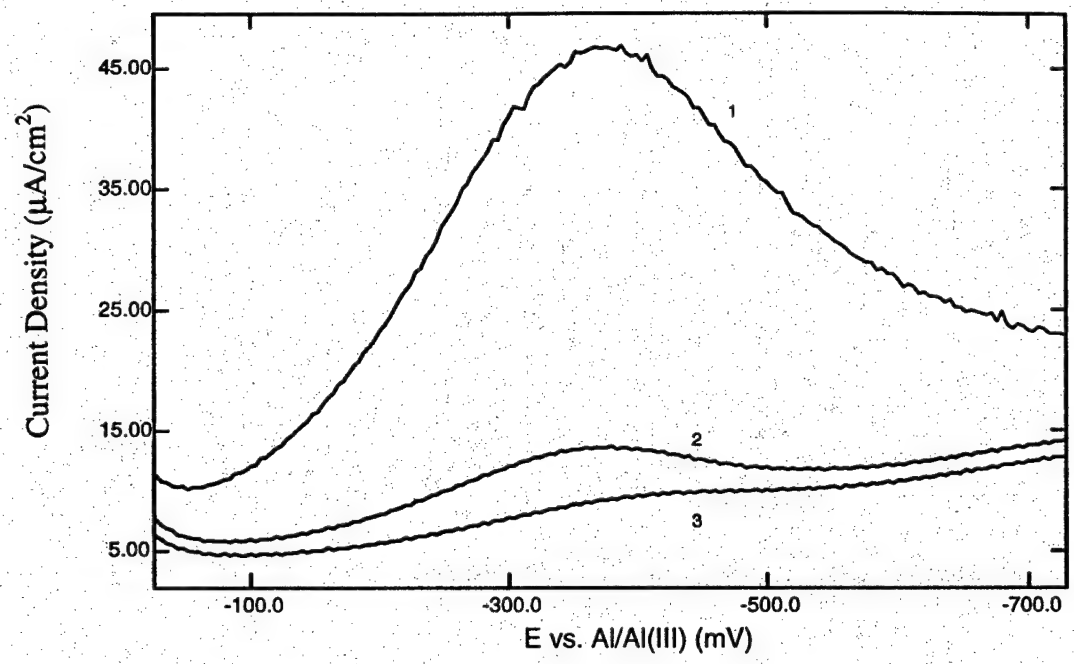

Figure 3.5. The reduction peak observed after the addition of HCl to the buffered, neutral melt (1) and subsequent scans (2,3).

In addition to facilitating the reduction and stripping of sodium, several other I-V effects were observed with the addition of HCl. The impurity peaks observed in Figure 3.3 and Figure 3.4 were significantly smaller. A peak attributed to the reduction of protons due to HCl additions is shown in Figure 3.5 at approximately -0.4 V. The reduction peak decreased with subsequent scans (see scans 1 to 3) and was seen only following HCl treatment. It was eliminated by flowing inert gas through the cell and reducing the HCl concentration. The reduction of protons has been reported in melts under similar conditions.[18] The diminishing magnitude of this peak with successive scans suggested that it may be due to a surface effect. The peak at -0.4 V was also observed when the melt was treated with substituted amine • hydrogen chlorides.[15] As the HCl partial pressure was increased, the reduction current associated with the addition of protons also decreased. This unexpected effect was reproducible and was demonstrated in more detail in the chronopotentiometric experiments. It again suggested that this proton related peak is due to a surface effect, such as changing the chemical composition of an oxide layer on the tungsten surface.

The chemical stability of the sodium in the melt and its coulombic efficiency are very important parameters in the use of this melt and redox couple in a battery application. The coulombic efficiency was investigated as a function of the partial pressure of HCl for the buffered, neutral melt at a tungsten electrode. Figure 3.6, Figure 3.7, and Figure 3.8 show three chronopotentiograms for an untreated melt (Figure 3.6), 5 torr HCl treated melt (Figure 3.7), and 6.1 torr HCl treated melt (Figure 3.8) at a tungsten

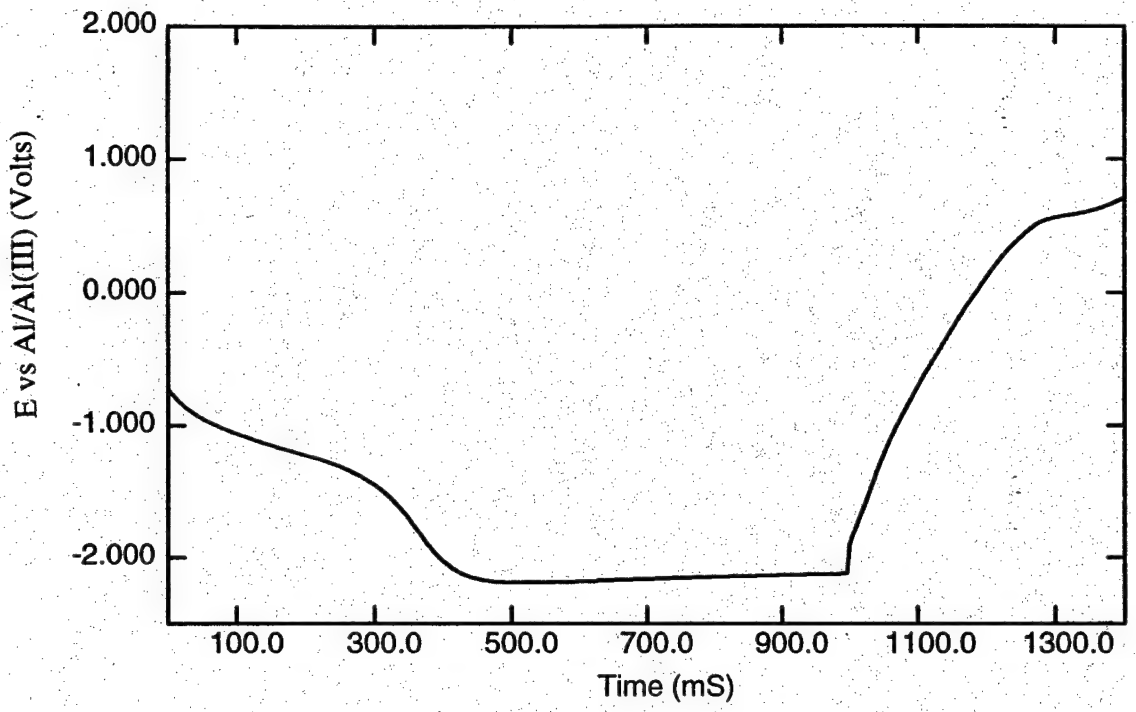

Figure 3.6. Chronopotentiogram for the buffered, neutral MEIC system with no HCl added.

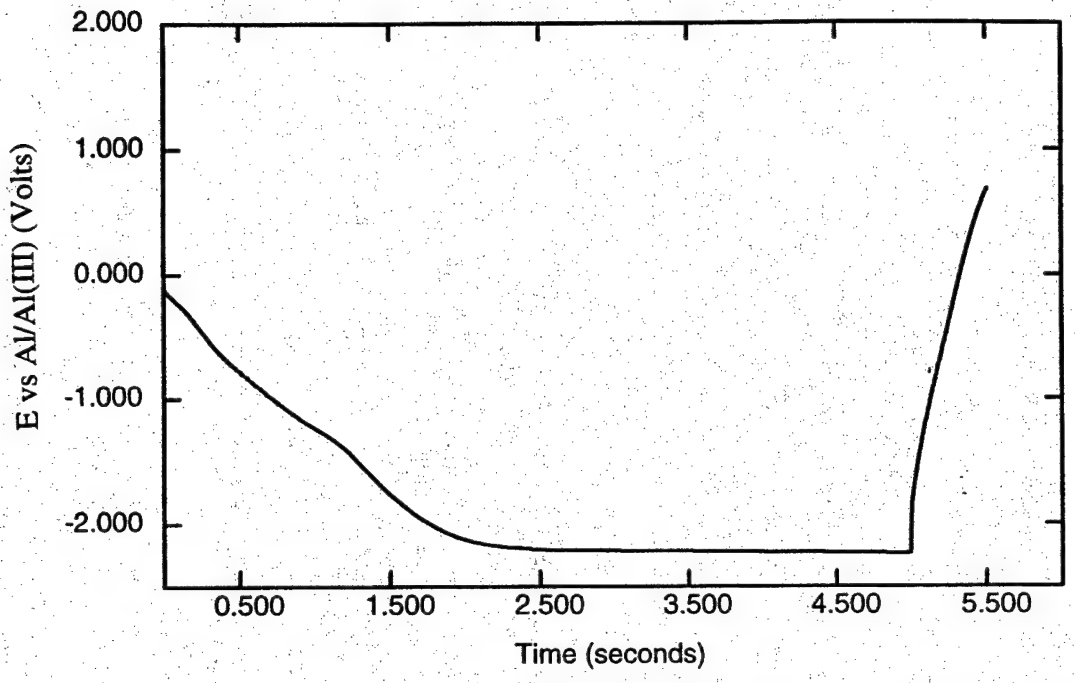

Figure 3.7. Chronopotentiogram for the buffered, neutral MEIC system with HCl added to a partial pressure of 5 torr.

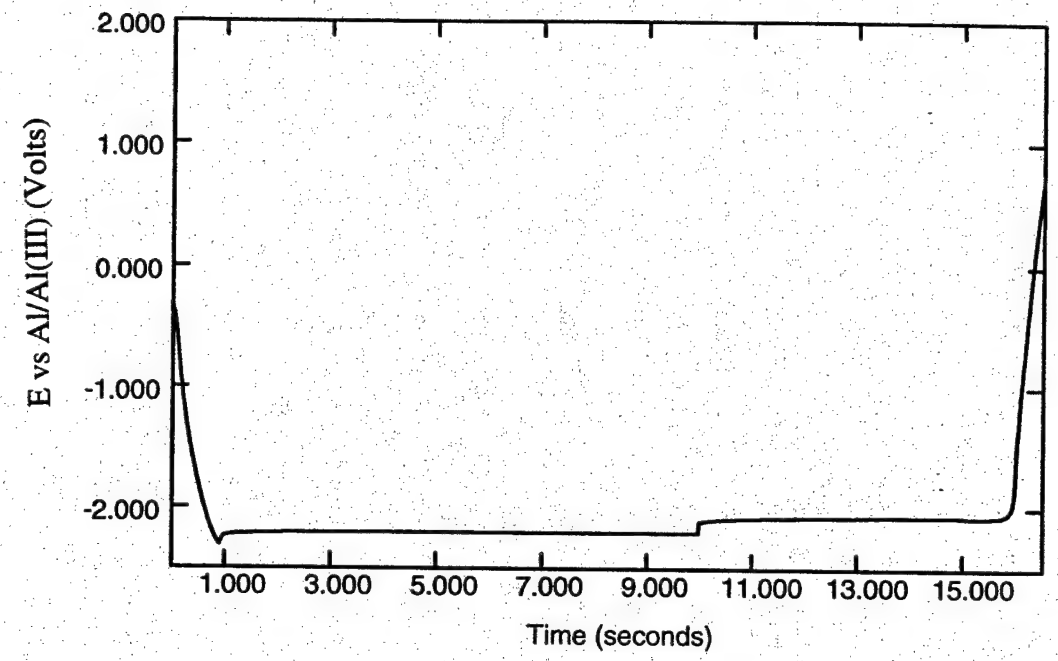

Figure 3.8. **Chronopotentiogram for the buffered, neutral MEIC system with HCl added to a partial pressure of 6.1 torr.**

electrode. The reduction current was 2.56 mA/cm^2; the oxidative current was the same magnitude after current reversal. The current was reversed after 1 s for the untreated melt, Figure 3.6. The proton reduction current at approximately -1.5 V is easily seen, corresponding to the peak seen at -1.5 V in the cyclic voltammogram. Following the consumption of all available reducible species at -1.5 V, a second reduction begins at -2.18 V. After current reversal, the first available oxidation reaction occurs at about 0.6 V. If a reversible sodium couple were present, oxidation of the metallic sodium would have occurred at approximately -2.1 V. The lack of sodium oxidation shows that the reduction at -2.18 V is either MEI^+ or Na^+ that has already reacted with a melt component.

The effect of 5.0 torr HCl on the reduction of sodium is shown in Figure 3.7. The increased stability of the melt and proton reduction peak can be seen. No sodium oxidation was observed upon current reversal. The chronopotentiogram of the neutral, basic melt with 6.1 torr HCl is shown in Figure 3.8. A smaller time for proton related current is seen, followed by a small overpotential for the nucleation of sodium. Once this initial layer has been deposited, the reduction of additional sodium proceeds at a constant potential of -2.20 V. After current reversal at 10 s, the constant current oxidation of sodium is observed at -2.08 V, followed by the oxidation of the melt beginning at approximately 16 s.

The coulombic efficiency of the sodium couple was measured as a function of HCl partial pressure by both cyclic voltammetry and chronopotentiometry, and is plotted in Figure 3.9. The threshold for achieving sodium deposition and stripping was

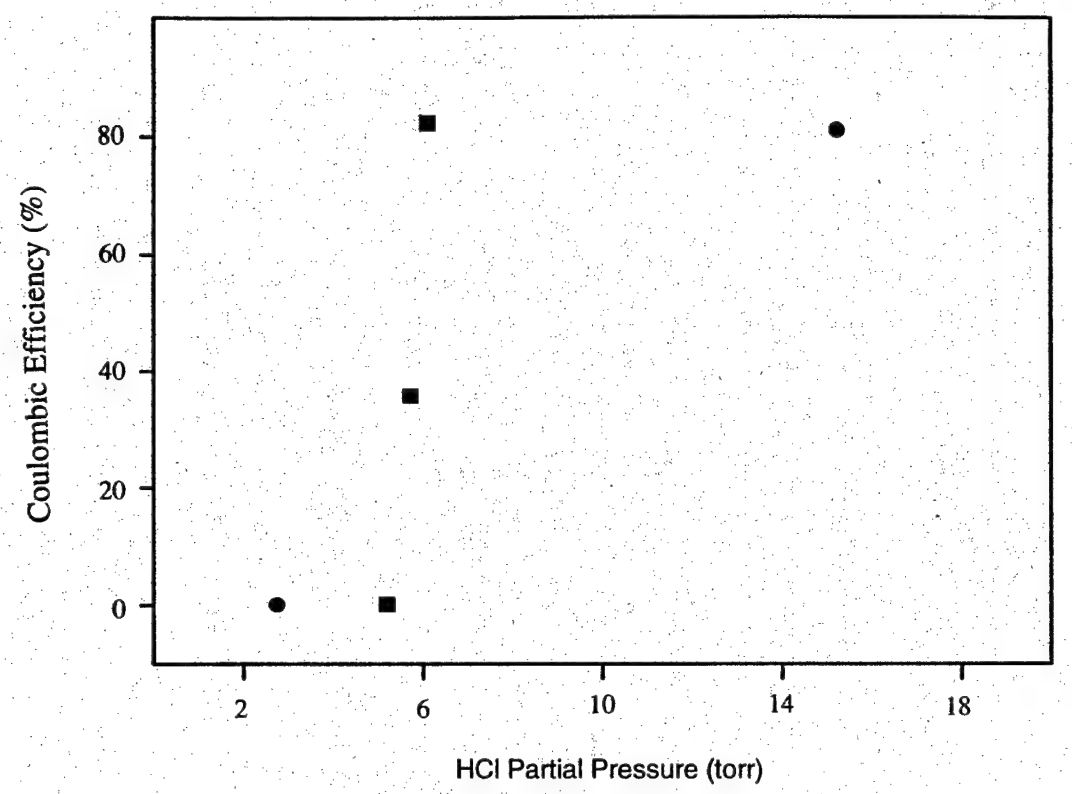

Figure 3.9. Coulombic efficiency from cyclic voltammetry (●) and chronopotentiometry (■) vs. HCl partial pressure.

approximately 6 torr. Below this threshold, no facile sodium couple exists. This threshold effect was reversible. If the HCl partial pressure was decreased below the threshold following treatment of a melt at a partial pressure above the threshold for plating and stripping of sodium, sodium plating is no longer observed. One could repeatably purge the melt to a condition above and below the threshold.

The highest coulombic efficiency obtained for the sodium couple was 94%. This maximum efficiency was obtained at tungsten in a constant current experiment at a current density of 6.4 mA/cm^2 and a plating time of 30 s. A series of chronopotentiometric and cyclic voltammetry experiments involving current density, charging time, and current interrupts were performed to help identify the nature of the parasitic reaction.

The effect of current density on the coulombic efficiency of the sodium couple was examined. Using chronopotentiometry, a series of reduction / oxidation experiments were carried out with current densities ranging from ~0.5 to 7 mA/cm^2. The reduction was performed for 60 s followed immediately by oxidation. The effect of current density on efficiency is shown in Fig 4.6. These results suggested that for relatively short times and moderate current densities, increasing current density increased the efficiency of the couple to a maximum of about 94%.

Two series of constant charge experiments were performed. First, a set of chronopotentiometric experiments were executed while varying the current density and time of reduction in order to reduce the same amount of sodium (51 mC/cm^2).

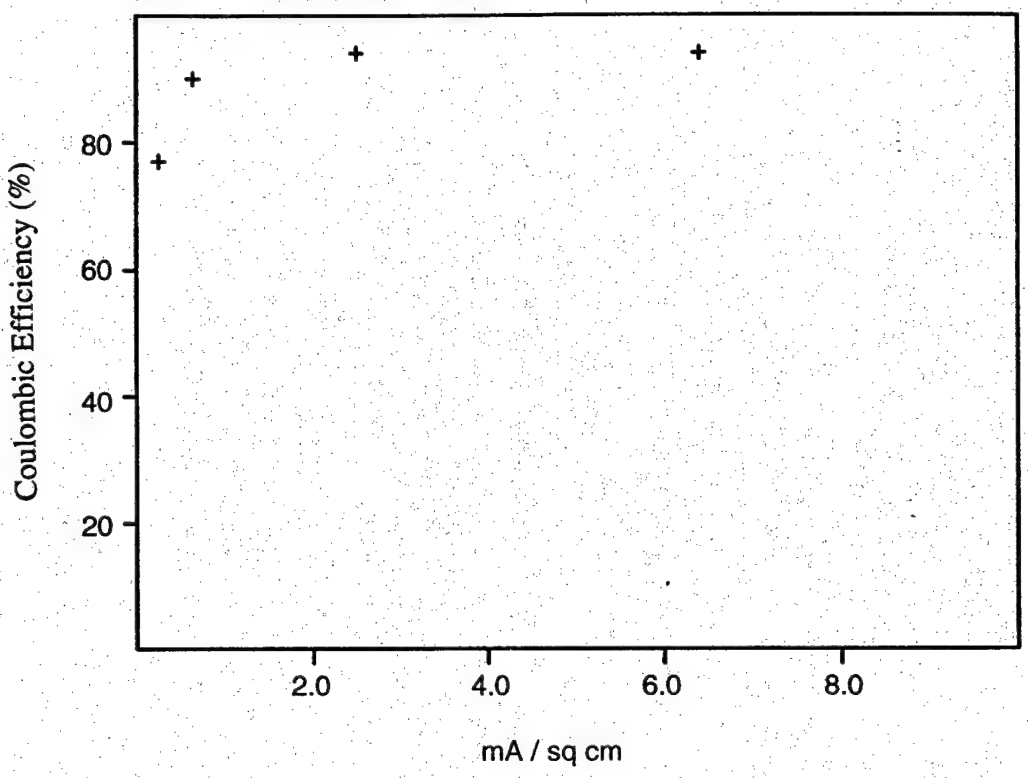

Figure 3.10. Coulombic efficiency vs. current density for plated sodium on tungsten. The chronopotentiometric reduction was performed for 60s for all current densities.

Immediately after reduction of the sodium at tungsten, the current was reversed and the sodium was oxidized. Current densities ranging from 5 to 25 mA/cm^2 were used. Similarly, current densities ranging from 0.5 to ~13 mA/cm^2 for a total charge of 102 mC/cm^2 were used in a second experiment. It should be noted that at low current densities, the electrodeposited sodium was in contact with the melt for long periods of time, whereas at high current density, the electrode potential was at its most negative value. The results are shown in Figure 3.11.

In order to further evaluate the effect of exposure time, an additional series of chronopotentiometric experiments were performed where the reduced sodium was exposed to the melt for nearly a constant time. An open circuit delay was inserted between the constant current reduction and constant current oxidation so that the time between the start of reduction and the start of oxidation was constant. Current densities ranging from ~0.5 to 5 mA/cm^2 were used. The results of a 1.0 mC reduction using this method at stainless steel are shown in Figure 3.12.

Finally, the open circuit stability of reduced sodium in the buffered neutral melt was studied. Sodium was plated on a tungsten electrode at a current density of 15 mA/cm^2 for 30 seconds while stirring. This corresponds to 3.6 mC and ~1300 monolayers of electroplated sodium. The open circuit potential of the electrode was monitored for 3 hours at which time the experiment was terminated. The potential of the reduced sodium stayed approximately constant at about -2.1 volts with respect to the reference.

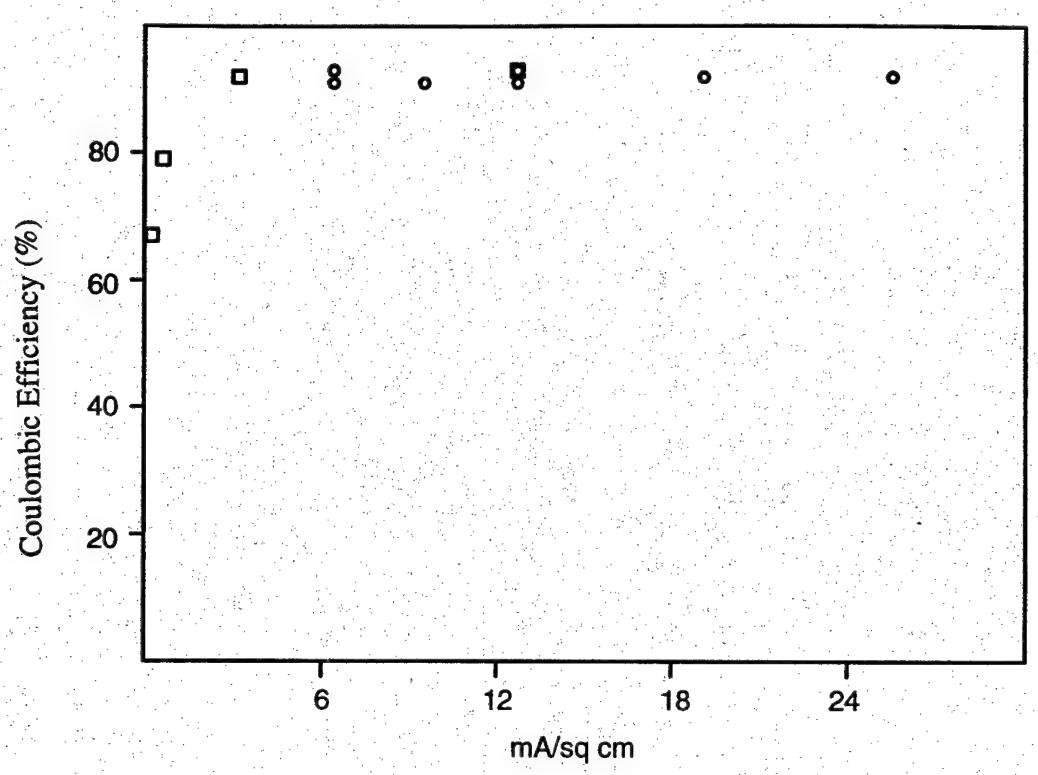

Figure 3.11. Coulombic efficiency versus current density for sodium plated on tungsten using chronopotentiometry. The total reduction charge was (□) 51mC/cm^2 or (○) 102 mC/cm^2.

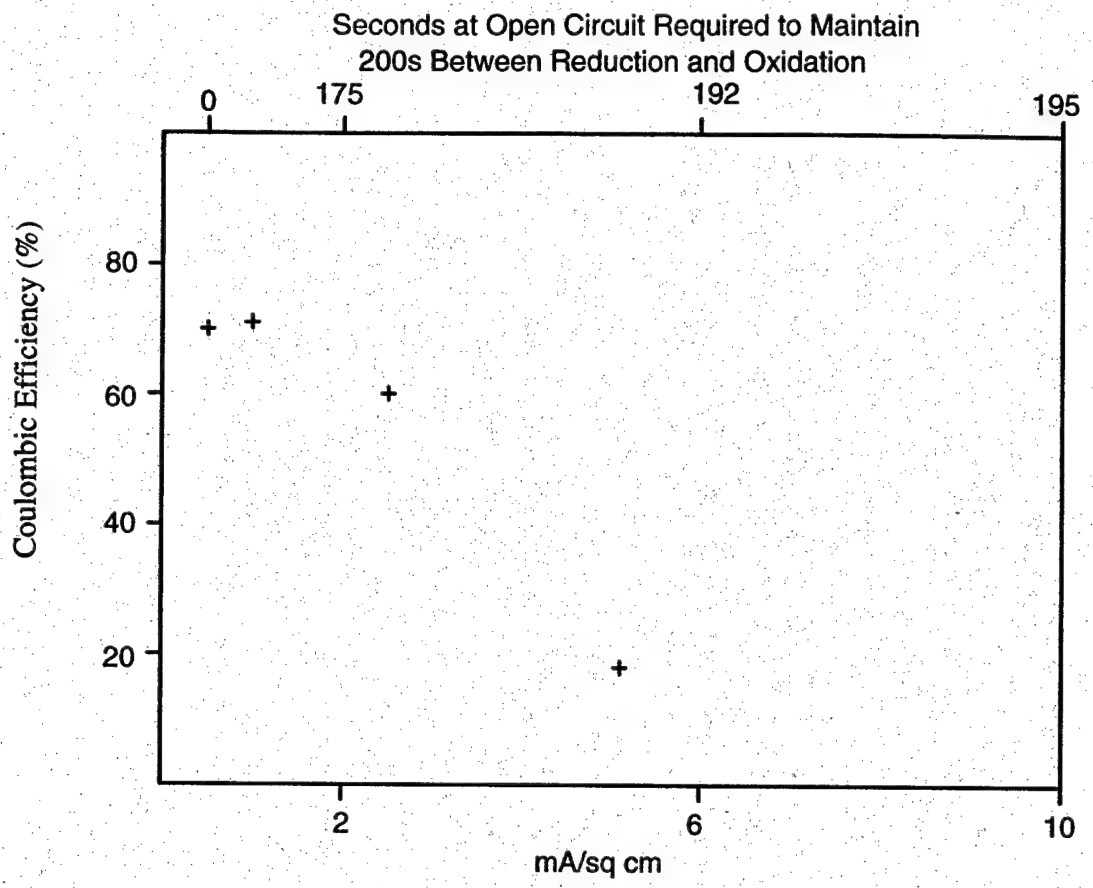

Figure 3.12. Coulombic efficiency versus current density for plated sodium on 303 stainless steel. Time between beginning of reduction and beginning of oxidation is constant and the total reduction charge is 51 mC/cm^2.

3.2 Discussion

Examination of the cathodic limit of the buffered, neutral MEIC system with varying levels of HCl treament showed that HCl extends the reduction limit of the system. There was a threshold partial pressure of HCl which must be reached in order for a facile sodium couple to appear. Riechel's results[9] indicate the concentration of HCl in the melt corresponding to this threshold partial pressure is very low (0.02 mole fraction) compared to the concentration of the organic cation (0.41 mole fraction). Keil showed that HCl combines with free chloride (Cl^-) in melt and that once all the free chloride is consumed, there is marked change in conductivity and HCl partial pressure.[19]

The low concentration of protons compared to that of other species in the molten salt is inconsistent with the notion that the HCl was causing a Nernstian shift of the reduction potential of all MEI^+ present in the melt. One explanation for the observed shift in the cathodic limit of the melt is that MEI^+ was reduced at slightly different potentials depending on its environment. This leads to the following theory: The reduction of MEI^+Cl^- is slightly positive of the reduction of Na^+ and the reduction of $MEI^+AlCl_4^-$ is slightly negative of the reduction of Na^+. Examination of the equilibrium data for the MEIC / $AlCl_3$ system indicated that in the buffered, neutral state some MEI^+Cl^- did exist in the melt at a very low concentration. The addition of HCl to the

melt could titrate the MEI^+Cl^- present to form $MEI^+HCl_2^-$. If the reduction potential for $MEI^+HCl_2^-$ was slightly negative of that for Na^+, then once all the MEI^+Cl^- reacted, a dramatic shift in the cathodic limit of the melt would be observed and a facile sodium couple could be realized. This theory is consistent with the results shown here and with Riechel's observations if the $MEIHCl_2$ he added to his melts contained excess HCl.

The literature suggests that HCl is not irreversibly bound to MEIC in the $MEIHCl_2$ complex.[18] This is consistent with the observation that the effect caused by HCl addition to the MEIC system can be reversed by purging with an inert gas. Additional HCl, above that which is needed to complex MEI^+Cl^-, may be observed in portions of the electrochemical window far removed from the cathodic limit. This work showed a reduction process occurring near -0.4 V immediately following HCl treatment. This was consistent with other researchers' findings.[9] This work also showed that a facile sodium couple can exist even when the reduction process near -0.4 V was not present. This observation is explained by the previously stated theory if sufficient HCl was present to complex all MEI^+Cl^- available, but no excess HCl was present to be reduced at -0.4 V.

Having established a reasonable explanation for the effect of HCl on the melt, there remains the question of why the sodium couple less than 100% efficient. Three mechanisms for decreased efficiency have been observed. The first involves reduction processes that occur at potentials positive of the sodium couple. These reactions consumed electrons that might otherwise be used for sodium ion reduction. If the species involved in these reactions diffused to the electrode surface in sufficient amounts, they

could consume current even when the electrode was at the potential for sodium reduction (~2.1 V). If these reactions were reversible, the corresponding oxidations would have occured positive of the sodium couple and would result in an apparently inefficient sodium couple. One such reduction was the one observed at -0.4 V and associated with the addition of HCl to the melt. The low coulombic efficiency at lower current densities or long exposure times can easily be seen in Figure 3.12.

The second mechanism for decreased efficiency of the sodium couple involved the overpotential at the cathode during sodium reduction. Overpotential due to nucleation of sodium at tungsten was observed. In HCl treated melts, the potential for reduction of MEI+ was shifted slightly negative of the potential for reduction of sodium. Any overpotential for the reduction of sodium could cause the potential of the cathode to shift into the region where reduction of the melt occurs. This additional reduction current was difficult to distinguish from the reduction current associated with sodium reduction and resulted in an apparently inefficient sodium couple. This effect has been observed in chronopotentiometric experiments at higher current densities.

The final mechanism for decreased efficiency of the sodium couple was a direct chemical reaction of sodium with the melt components. In this case, sodium was successfully reduced, but before it could be electrochemical oxidized, it reacted chemically with the melt. This resulted in an inefficient sodium couple. This mechanism was supported by experiments that had an open circuit delay inserted between reduction and oxidation. Efficiency decreased as open circuit time increased. The long open circuit

stability of reduced sodium in contact with the melt suggested that this chemical process proceeds at a slow rate or a rate that diminishes with time. This was perhaps due to a thin, semi-passive film that forms on contact between the sodium and the melt.

3.3 Conclusions

Gaseous HCl, added to buffered, neutral melts of MEIC and $AlCl_3$ had a quantitative effect on the coulombic efficiency of the sodium couple. This effect was only observed after the partial pressure of HCl reaches a threshold of about 6 torr. This phenomena can be described by three mechanisms. The results suggest all three are occurring and subsequently preventing the formation of a completely efficient sodium couple. These mechanisms are: parasitic reduction of impurities below the sodium reduction potential, co-reduction of sodium and of the MEI^+ cation at potentials negative of the sodium couple, and direct chemical reaction of the melt with the electrodeposited sodium. An understanding of these mechanisms is necessary in order to successfully utilize the MEIC / $AlCl_3$ room temperature molten salt system as an electrolyte for the sodium / iron(II) chloride cell.

CHAPTER 4

THE DMPIC/$AlCl_3$/NaCl SYSTEM

4.1 Results

Cyclic voltammetry was performed on a basic (N=0.48) DMPIC/$AlCl_3$ melt in the absence of Na^+ to examine the melt window. This unbuffered melt is primarily composed of $AlCl_4^-$ with a small amount of Cl^-. Figure 4.1 shows the current-voltage (I-V) behavior using a tungsten working electrode at a scan rate of 100 mV/s. The initial, negative-going scan was started at -0.30 V, and scan reversal took place at -2.3 V versus the Al/$Al_2Cl_7^-$ (N=0.6) reference. A small increase in current was observed both at -1.0 V and -1.5 V; a large increase in current was observed at -2.3 V. This current was due to the reduction of the melt components, which includes the reduction of the $DMPI^+$ cation. The deposition of aluminum, which was thermodynamically possible by reducing $Al_2Cl_7^-$, was not observed because of the low equilibrium concentration of $Al_2Cl_7^-$ in basic melts,

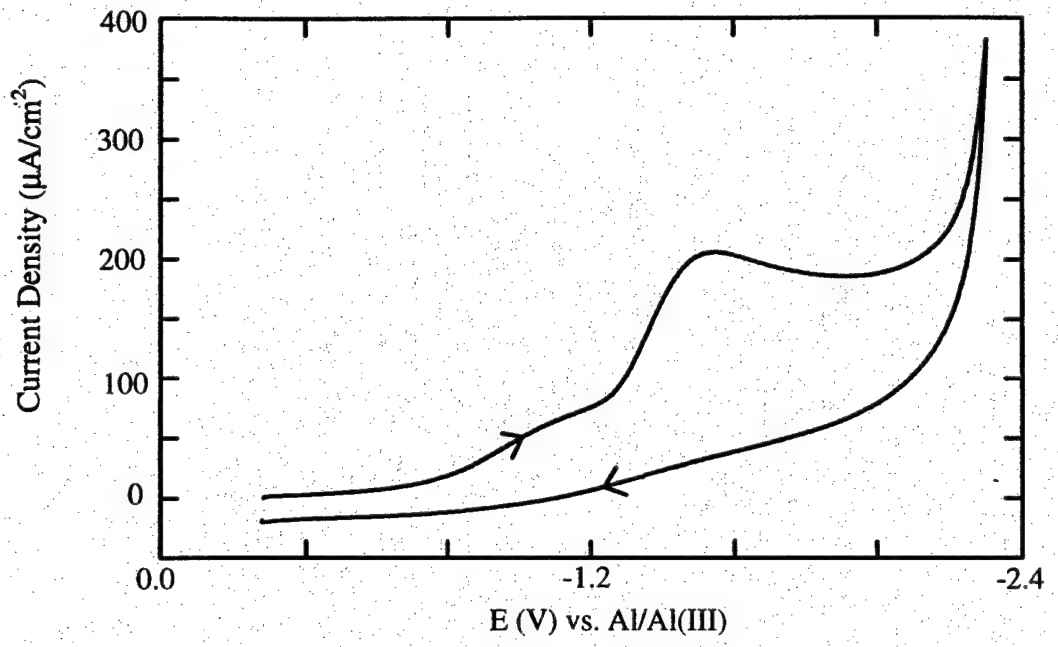

Figure 4.1. **Cyclic voltammogram (u=100 mV/s) of basic DMPIC (N=0.45) electrolyte at tungsten.**

and the slow equilibrium between $Al_2Cl_7^-$ and $AlCl_4^-$. The negative potential limit was very similar to the reduction limit reported in a previous paper.[20] However, in contrast with the previous report of Gifford and Palmisano,[10] the negative potential limit of the triakyl substituted DMPIC molten salt was found to be about the same as the dialkyl substituted MEIC system, and not 0.3 V to 0.5 V more negative. Previous results[21] show the reduction limit of the basic MEIC system is also close to -2.3 V, so that the increased stability in the reduction limit of the DMPIC melt is much less dramatic than those values previously published.[10] The reduction waves at approximately -1.0 V and -1.5 V were similar to those previously reported. These were attributed to impurities in the organic chloride, possibly from starting material or atmospheric contamination, which were not removed during the purification process. The magnitude of the reduction current for the impurities reported by Gifford et al.[10] was slightly different than those shown in Figure 4.1 because higher scan rates were used in this work (five times faster).

The focus of this study was to examine the stability of the neutral, buffered DMPIC melt with respect to the deposition of sodium, and contrast it with the previous results for the MEIC melt. The basic DMPIC melt was made acidic (N=0.52) by the addition of $AlCl_3$ and then made neutral by the addition of NaCl, as described previously. A CV for this melt is shown in Figure 4.2; the working electrode was a tungsten disk and the scan rate was 100 mV/s. The reduction and oxidation limits of the acidic melt were approximately the same as those reported by Gifford et al.[10] The shapes of the curves

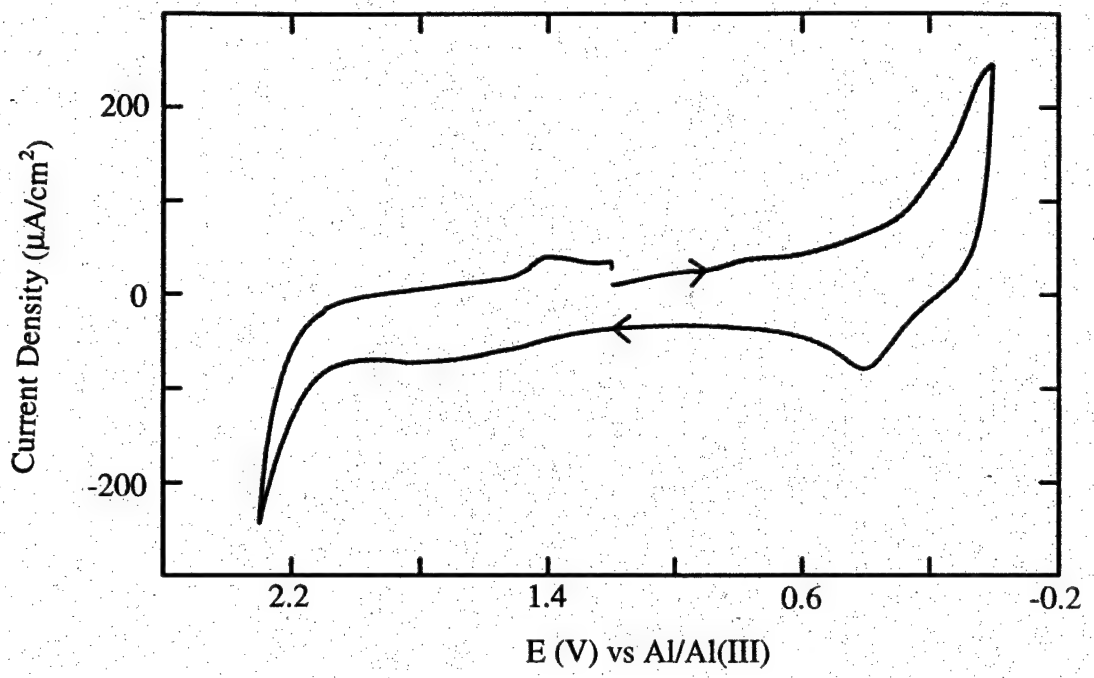

Figure 4.2 **Cyclic voltammogram (u=100 mV/s) of acidic DMPIC (N=0.55) electrolyte at tungsten.**

were similar; however, the potential limits were not as extreme in this work so that smaller currents were observed. Compared to the MEIC melts of the analogous composition and acidity (neutral melt), the cathodic limit for the DMPIC system was very similar; at the positive potential limit, chlorine gas is produced. One important difference between the MEIC and DMPIC melts was the observation of a small anodic current on the positive-going scan, following the reduction process at the negative potential limit. This effect was however, very short lived and was only observed on the first scan or two after the melt was freshly made, or was left exposed to the dry box for extended periods of time. The appearance of this effect was coincident with the absorption of impurities like water emphasizing that this may be the production and reoxidation of hydrogen.

The effect of hydrogen chloride gas on the stability of the buffered, neutral DMPIC/$AlCl_3$/NaCl melt was examined. Previously, it has been shown that the plating and stripping of sodium at a solid electrode was not possible for the MEIC system without an additive, such as HCl.[9] The critical partial pressure of HCl necessary to observe this beneficial effect for the MEIC system was about 790 Pa (6 Torr). The coulombic efficiency for the plating and stripping of sodium was investigated as a function of the partial pressure of HCl over the range from 0 to 50 kPa. The investigation at very low partial pressures was more complicated than for MEIC melts because of the slow equilibrium between the DMPIC melt and the gaseous HCl. The DMPIC melt also had lower conductivity and higher viscosity than the MEIC melt. The coulombic

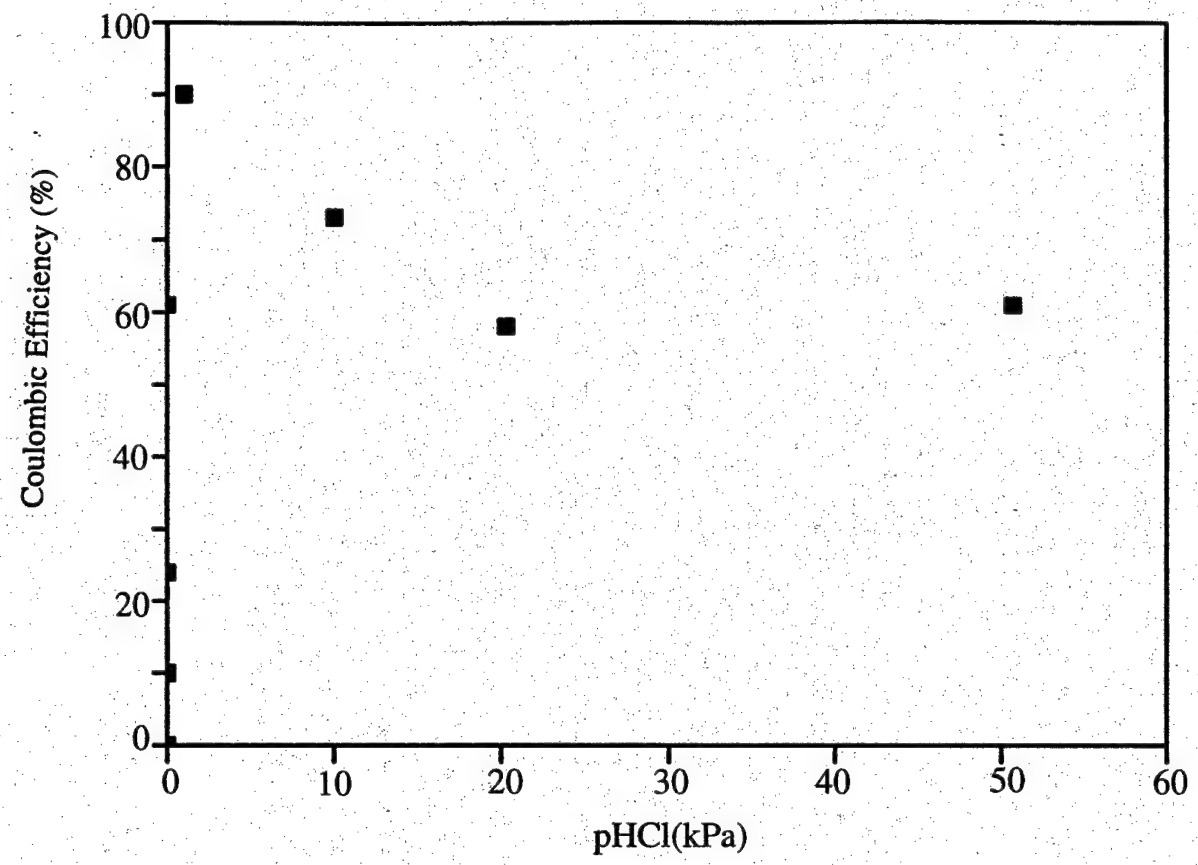

Figure 4.3. **Coulombic efficiency of sodium plating and stripping calculated from cyclic voltammograms for DMPIC electrolyte at tungsten versus HCl partial pressure.**

efficiency (the ratio of the charge passed during oxidation of sodium to the charge passed during the deposition of sodium) of the MEIC melt was highest at room temperature after bubbling the melt with a gas whose HCl partial pressure was 1 kPa. The coulombic efficiency for the MEIC melt was just over 90% and lasted for several days. Figure 4.3 shows the coulombic efficiencies, measured using cyclic voltammetry, for the buffered, neutral DMPIC melt versus partial pressure of HCl. This behavior is similar to that observed in the MEIC system in that high efficiencies could be obtained; however, 100% efficiency has not been demonstrated. Within experimental error, these results were not as favorable as those for the MEIC melt, contrary to pervious reports.[9,10] In an effort to compare quantitatively the negative potential limits of the DMPIC and MEIC melts as functions of HCl, the reduction limits, arbitrarily defined as the potentials corresponding to a cathodic current density of 1 mA/cm^2, were measured. The electrode potentials at 1 mA/cm^2 as a function of HCl partial pressure are shown in Figure 4.4 for MEIC and DMPIC melts. The MEIC melt shows a more distinct transition from a region of insufficient HCl concentration to a region of adequate HCl than the DMPIC melt.

The higher viscosity, and hence slower mass transport properties, of the DMPIC melt as compared to the MEIC melt was an undesirable attribute. However, the more sluggish equilibrium of the DMPIC melt is advantageous because the positive attributes of the HCl addition lasted longer than with the MEIC melt, although it made this study more complicated. For example, the coulombic efficiency, as measured from the CVs, versus time after HCl addition is plotted in Figure 4.5. The beneficial effect of HCl

addition in the DMPIC melt lasted more than 100 days whereas the effect of HCl on the MEIC melt lasted only a few days even under the best conditions; i.e. treated and sealed in a closed vessel.

The slow chemical equilibrium of HCl with the melt made the study at low HCl partial pressures particularly difficult. The coulombic efficiency at zero HCl partial pressure (achieved by extensive purging with Ar) was, with a few exceptions, zero. Generally, it would require days, with intermittent purging, to return the melt to its original, HCl free state. Thus, the threshold partial pressure of HCl required to observe a reversible sodium couple in the buffered, neutral DMPIC melt was semiquantitatively evaluated. The threshold to achieve sodium plating/stripping is lower for DMPIC than for the MEIC melt. The lowest HCl partial pressure found to induce the sodium plating/stripping couple was 1.0 kPa. However, we have found that sodium cannot be plated from an HCl-free melt, contrary to previous reports.[20] This discrepancy is not as controversial as it may appear. It was found that sodium could be plated and then stripped from freshly prepared DMPIC melts, which had never been exposed to HCl. Sodium could also be plated from melts which had been exposed to the dry box atmosphere for long periods of time (e.g. months). In both of the above mentioned cases, impurities (e.g. H_2O) were responsible for the momentary ability to plate sodium. The coulombic efficiency for these melts ranged from 0% to 75%. The ability to plate sodium without intentional HCl addition faded after a short time. For example, Figure 4.6 shows

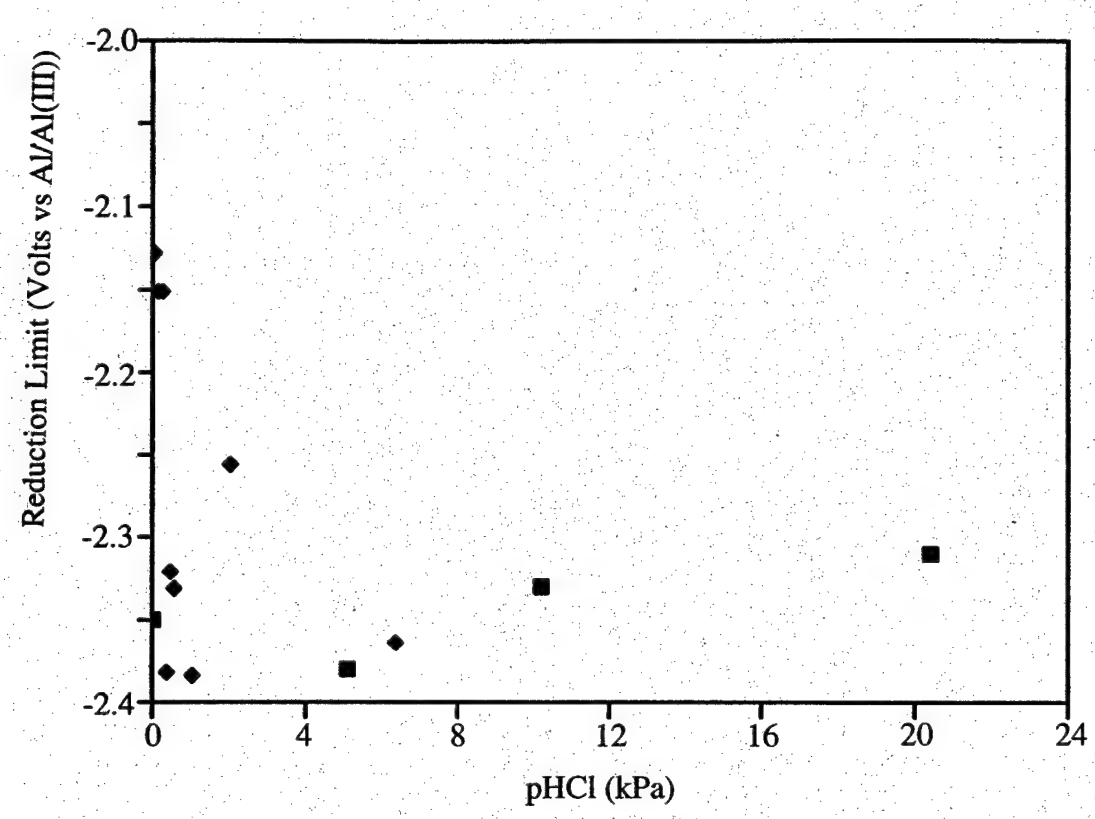

Figure 4.4. Cathodic potential corresponding to a reduction current density of 1 mA/cm2 for both DMPIC(n) and MEIC(u) electrolytes versus HCl partial pressure.

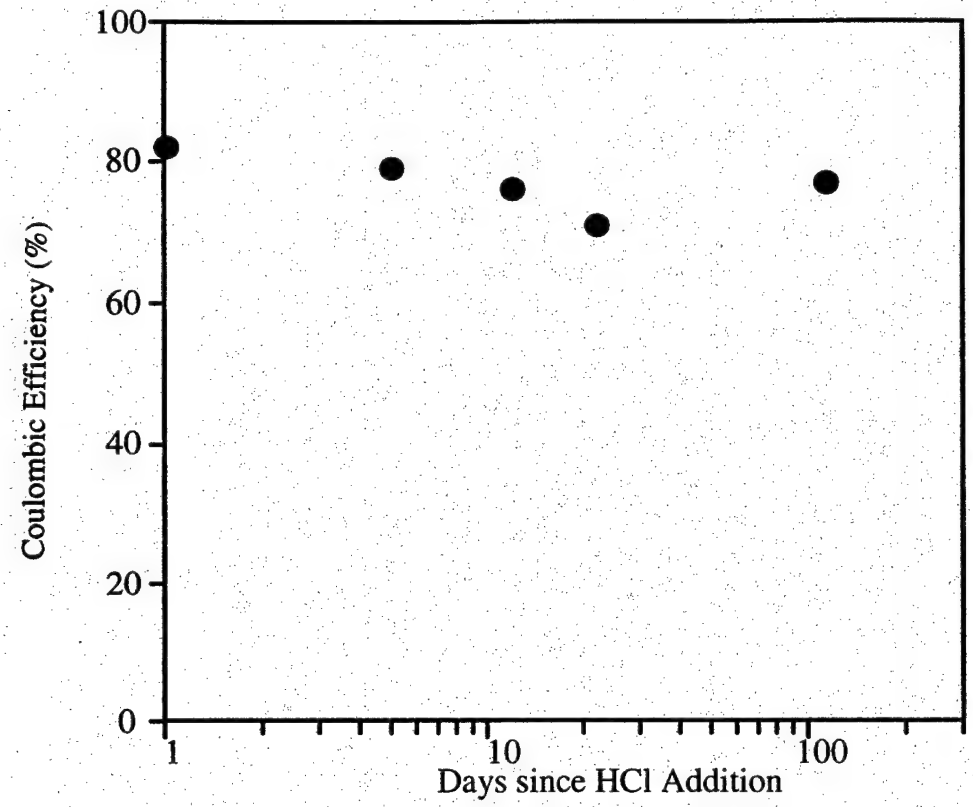

Figure 4.5 **Coulombic efficiency of sodium plating and stripping calculated from cyclic voltammograms for DMPIC electrolyte at tungsten versus time since HCl addition.**

the sodium plating/stripping couple in a freshly prepared DMPIC melt before direct HCl addition. The shape of the CV is similar to those in the MEIC melt, where there is an overpotential for sodium plating onto the tungsten electrode. After the deposition of sodium is initiated, and the scan direction is reversed, the current continues to rise because the overpotential on sodium is not as great as on tungsten. The starting materials were prepared in a manner similar to MEIC melts examined previously; yet, the MEIC melts did not exhibit the ability to plate sodium from an untreated melt. The coulombic efficiency in Figure 4.6 was 49%. The effect disappeared after approximately two days of electrochemical analysis.

These results suggest that this vagarious behavior was not due to an increased stability of DMPIC, as compared to MEIC, but rather was due to the introduction of trace amounts of water from either the starting materials, or from the dry box atmosphere, which was 2 to 10 ppm water vapor. Contamination of the melt components can generate HCl and mimic the effect of HCl addition. Water present in the sodium chloride, the organic chloride, or introduced by absorption from the atmosphere can react with the aluminum chloride upon mixing to form HCl. Water can react with aluminum chloride in the molten salt system to form HCl.

$$3H_2O + AlCl_3 \rightarrow 3HCl + Al(OH)_3 \qquad (3)$$

$$Al(OH)_3 + AlCl_3 \rightarrow 3HCl + Al_2O_3. \qquad (4)$$

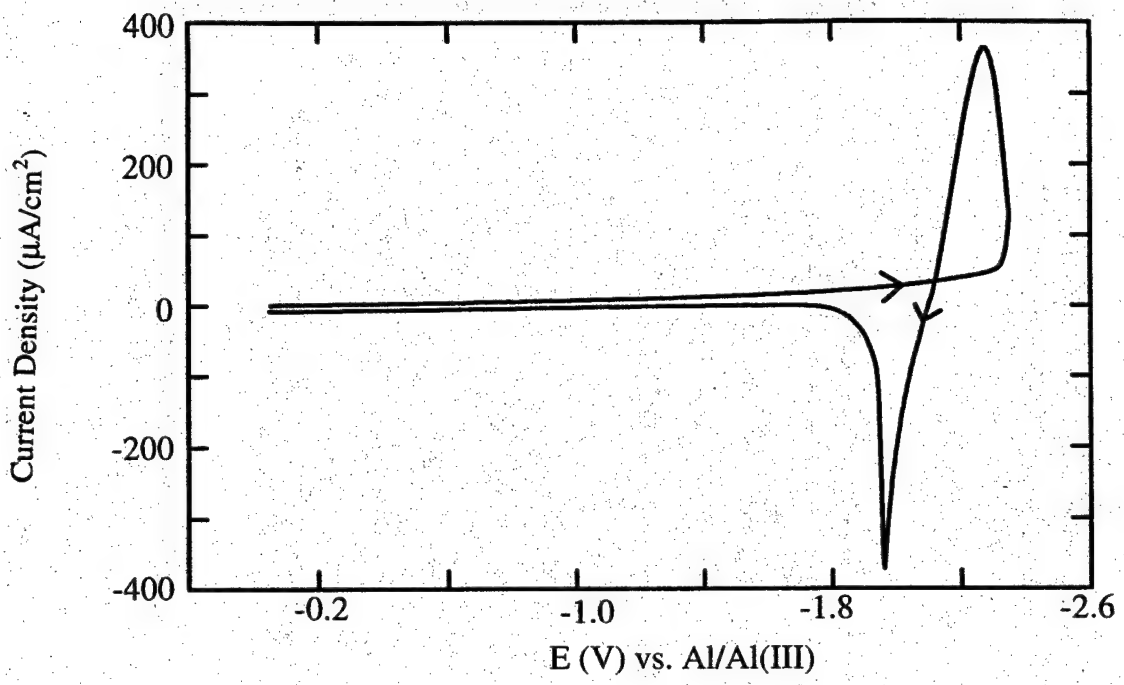

Figure 4.6 **Cyclic voltammogram (u=100 mV/s) of buffered, neutral DMPIC electrolyte at tungsten prior to HCl addition.**

The amount of water needed to generate enough HCl was considered. The effect of water contamination was examined by adding a controlled amount of water to the buffered, neutral DMPIC melt which did not exhibit the sodium couple prior to water addition. The freshly prepared melt had not been treated with gaseous HCl, but had demonstrated a short-lived sodium couple when first analyzed. The addition of 2.1 mmol water resulted in the plating and stripping of sodium with a coulombic efficiency of 76%. A CV (scan rate of 100 mV/s) demonstrating the sodium couple at tungsten following water addition is shown in Figure 4.7.

The effect of temperature on the plating/stripping of sodium is important in understanding (i) the reactions and (ii) the operating parameters of the propose battery. The electrochemical behavior of the buffered, neutral DMPIC melt was examined at approximately 60°C. Higher current densities and higher coulombic efficiencies were observed. A maximum efficiency of 93% on tungsten was obtained for the DMPIC system treated with HCl (partial pressure of HCl was 1 kPa in Ar) then heated to 60°C, as shown in Figure 4.8. A similar effect resulted when the 60°C melt was treated with water rather than HCl. At elevated temperatures, the melts lost the effect gained from HCl or water addition more quickly than the room temperature melts. The current densities observed at 60°C were about ten times higher than those at room temperature and were adequate for high power density battery applications.

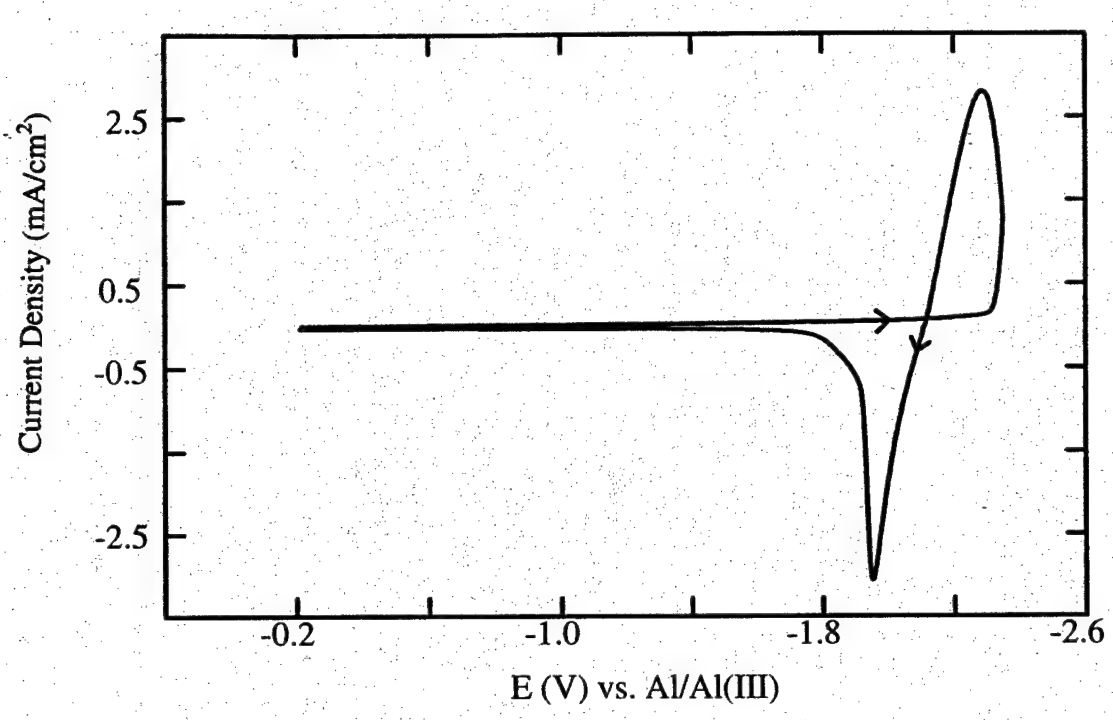

Figure 4.7 **Cyclic voltammogram (u=100 mV/s) of buffered, neutral DMPIC electrolyte at tungsten following water addition.**

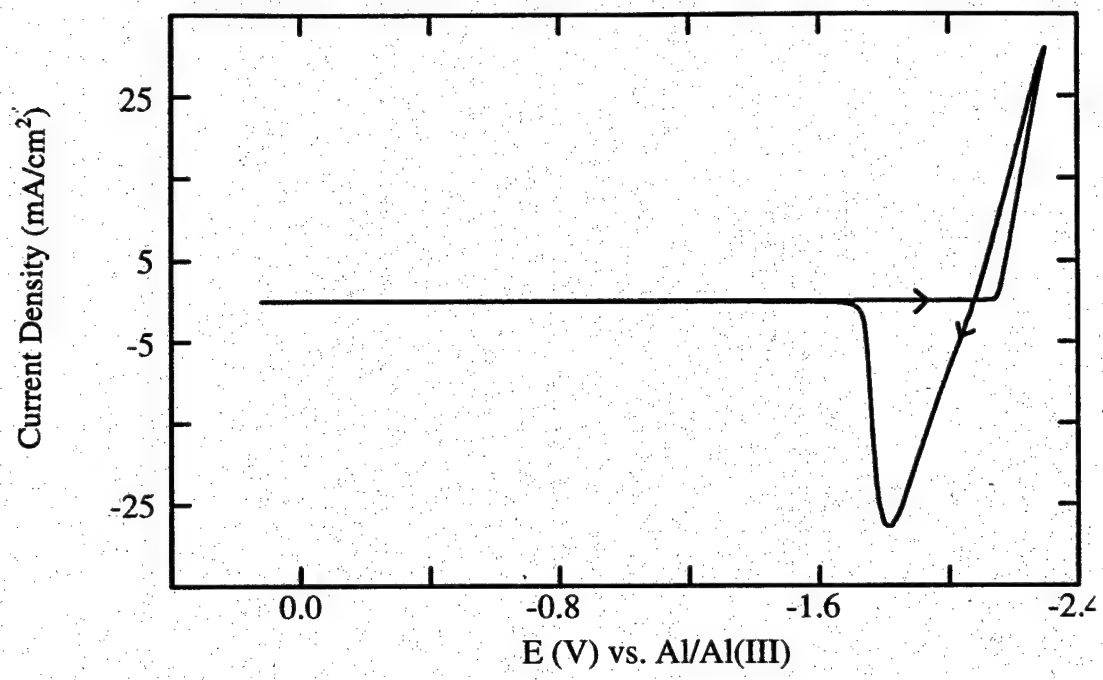

Figure 4.8 **Cyclic voltammogram (u=100 mV/s) of buffered, neutral DMPIC electrolyte at tungsten at elevated temperature (~60°C). 93% coulombic efficiency.**

4.2 Discussion

The stability, and coulombic reversibility of the anode is a critical issue in the development of an ambient temperature battery based on the aluminum chloride melt. Previous work has indicated that the DMPIC melt possesses a wider electrochemical window than the MEIC system.[10] While this work showed similar results for the acidic and basic melts, the reduction limit was not improved to the extent that sodium plating and stripping could be observed without additives in the buffered, neutral DMPIC melt. The equilibrium with HCl was sufficiently slow so that once HCl was absorbed, the beneficial effects would persist for months. This slow uptake and discharge of HCl, enabled trace amounts of water or other impurities, which can react with the melt to form HCl, to act as additives enabling the deposition and stripping of sodium. This may account for the previous observations of sodium plating and stripping from a fresh melt without any intentional proton source.[20] The effectiveness of water as a proton source was verified by the observation of a sodium couple following the addition of water to a recently prepared DMPIC melt. The beneficial effect of trace amounts of water, is potentially useful in battery applications. The formation of aluminum oxide as a result of the trace amounts of water, did not seem to have any significant negative effects.

The reduction of imidazolium most likely leads to the formation of a neutral radical which could dimerize, particularly at the 2 position on the imidazolium ring. The

rationale for investigating DMPIC was that by substituting a methyl for the hydrogen at the 2 position of the imidazolium ring (MEIC), the rate of dimerization would be decreased by steric hindrance. However, this appears not to be the case. Once the radical has been formed, dimerization (or other reactions, such as electroreduction) will occur at a fast rate in comparison to the preceding reactions. Thus, sterically hindering the dimerization was not accomplished with the methyl groups, or is not a prudent path to increasing the stability of the melt.

The observation of a sodium couple in a melt that was never intentionally exposed to water or HCl suggests the threshold amount of HCl needed to enable the sodium couple was lower than for the MEIC system. The slow discharge of HCl made quantification of the HCl threshold very difficult. However, the slow discharge is advantageous for battery operation. The data indicates that a partial pressure of 1 kPa HCl is sufficient to activate the sodium couple with a coulombic efficiency of 80% to 90%.

Purging the HCl was accelerated by heating the molten salt, supporting the concept that the kinetics of HCl dissolution in the DMPIC system were slow at room temperature. Higher partial pressures of HCl did not appear to have an additional benefit. The exact role of HCl in stabilizing the melt components against reduction, and the exact quantity of HCl absorbed have not been established.

Heating the molten salt appeared to have several beneficial effects. First, the conductivity of the system increased. The result of increased conductivity was higher

diffusivities and peak currents during cyclic voltammetry. This would be expected to directly lead to higher power densities for battery applications. A second effect of higher temperature was an increase in the coulombic efficiency of the sodium couple. The efficiency of the sodium couple appeared to increase by approximately 10 to 15% (under otherwise similar conditions) when the temperature was increased from 22°C to 60°C. The increased conductivity and kinetics of the melt were most likely the cause of this increase in efficiency because the rate of sodium deposition increases at the same potential.

The absence of any report of 100% coulombic efficiency is particularly troublesome. One explanation is that in addition to melt reduction at the most negative potentials, there are parasitic reactions, such as hydrogen ion reduction, at more modest potentials, which consume some of the cathodic current and/or sodium. If the kinetics of this reaction increased more slowly with temperature than the kinetics of sodium deposition, or the reaction was mass transport limited, the increase in the rate of sodium consumption would be less than the increase in sodium production, leading to a slightly higher efficiency, but still short of 100%. Thus, a larger fraction of the electrodeposited sodium would be available for oxidation. Such a parasitic reaction (e.g. hydrogen gas production) would also lead to the result that additional HCl, beyond that need to shift the melt window, would not be a benefit.

4.3 Conclusion

Significant differences existed between room temperature molten salts containing two similar organic chlorides (MEIC and DMPIC). The addition of a methyl group at the 2 position of the imidazolium ring and the substitution of a propyl group for the ethyl group clearly altered the transport properties of the DMPIC melts. These changes are increased viscosity, decreased conductivity, and slower equilibrium with gaseous HCl. While these changes in transport properties impact the electrochemical behavior of the DMPIC system, evidence does not support the conclusion that the changes in the substituents significant alter the thermodynamics of the system. Change in the rate of HCl (arising from melt impurities) off-gassing due to a difference in the transport properties could account for other researchers' observations that sodium plating and stripping is possible without melt additives. Although a very strong positive effect of temperature was found, the DMPIC system does not appear capable of sustaining a more efficient sodium couple than the MEIC system and its decreased conductivity makes it less attractive for use as a battery electrolyte.

CHAPTER 5

THE MPIC/$AlCl_3$/NaCl SYSTEM

5.1 Results

Basic (N=0.45) and acidic (N=0.55) melts of MPIC and aluminum chloride were prepared in order to examine the oxidation and reduction limits of the room temperature molten salt system. The mole fraction of aluminum chloride is designated by N. Melts with N greater than 0.5 are referred to as acidic due to the presence of the Lewis acidic species, $Al_2Cl_7^-$. Melts with N less than 0.5 are referred to as basic due to the presence of the Lewis basic species, Cl^-. Two cyclic voltammograms on tungsten (scan rate = 100 mV/s) are shown in Figure 5.1. illustrating the reduction and oxidation limits of the MPIC system. As with similar alkylimidazolium chloride molten salt systems, the negative potential limit of the basic melt was determined by the reduction of the imidazolium cation. The cathodic limit for the MPIC system was approximately -2.2 V versus the aluminum reference. Within experimental error, this was nearly the same as the MEIC system and slightly (50-100 mV) narrower than the DMPIC system. The

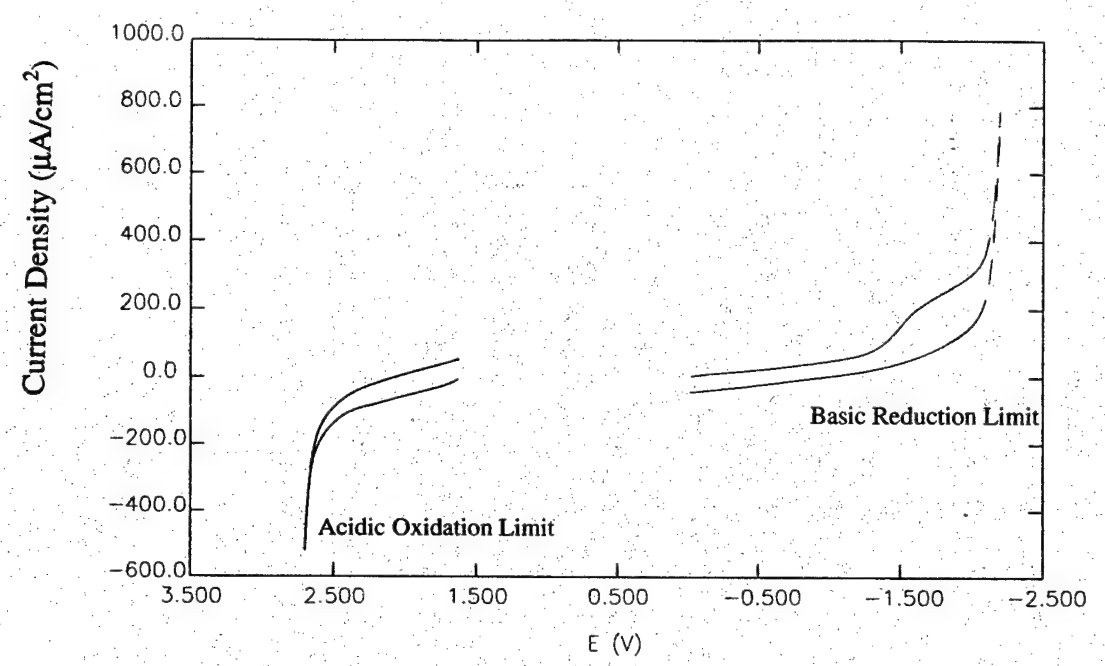

Figure 5.1. Reduction and oxidation limits of the acidic (N=0.55) and basic (N=0.45) MPIC/$AlCl_3$ system.

positive potential limit in the acidic melt is determined by the oxidation of the Lewis acidic $Al_2Cl_7^-$ species. The oxidation limit for the acidic MPIC system was approximately 2.7 V. This is slightly more positive than the limits reported for the MEIC and DMPIC melts under similar conditions.

The range of potentials for which sodium can be plated and the coulombic efficiency of the sodium couple is of paramount importance. Three mechanisms have been proposed for decreased coulombic efficiency.[21] These include a predeposition parasitic reaction, reduction of the organic cation, and chemical reaction between the deposited sodium and the melt. At the most negative potentials, the reduction of the imidazolium cation can occur. At potentials positive of the sodium couple, solvated species can be reduced. Thus the coulombic efficiency of sodium is less than 100% at low currents (more positive potentials) and high currents (more negative potentials). Of the three electrolytes studied, the MPIC system appears to exhibit the largest potential range over which sodium can be reduced. Figure 5.2 illustrates this phenomena. In Figure 5.2, coulombic efficiency is plotted versus switching potential for the MEIC, DMPIC, and MPIC. The coulombic efficiency is defined as the ratio of oxidation current to reduction current and was measured by integrating cyclic voltammograms. In order to separate the three effects, the potential of the electrode was swept negatively and reversed (switched) and several different potentials. As the switching potentials grew increasingly negative, the coulombic efficiency of the couple passed through a maximum. This magnitude of maximum coulombic efficiency was limited by the most insidious of the

three effects, the direct reaction of the melt with the metallic sodium. The MPIC system appeared to have a wide region where the dominant mechanism for decreased coulombic efficiency was the reaction of the electrolyte with the freshly plated sodium. The experiments shown in Figure 5.2 were not the "record best" efficiencies, but rather a self-consistent set of data for quantitative comparison.

In order to approximate the rate of the reaction between the molten salt electrolyte and the plated sodium, a series of experiments were devised to measure the self discharge rate of a sodium anode. A fixed amount of sodium was plated with constant current and left in contact with electrolyte for times ranging from 0 to 3 hours. The electrolyte was a buffered, neutral MPIC melt treated with an HCl / Ar gas mixture where the partial pressure of HCl was 1 kPa HCl. Following the open circuit period, the sodium was stripped from the substrate using constant current oxidation. The amount of charge lost due to chemical reaction was calculated by subtracting the zero delay charge loss from the charge lost during the each open circuit period. The amount of charge lost due to self discharge was plotted versus the length of the open circuit period. The amount of charge lost due to this "self discharge" was plotted versus the length of the open circuit period in Figure 5.3 The slope of the line passing through the points gives a rate of self discharge of 22 $\mu A/cm^2$.

The surface of a tungsten electrode was examined using optical microscopy to help identify the nature of the parasitic reactions. Following treatment of the molten salt with 1 kPa HCl, the cell was positioned so that the electrode surface could be viewed

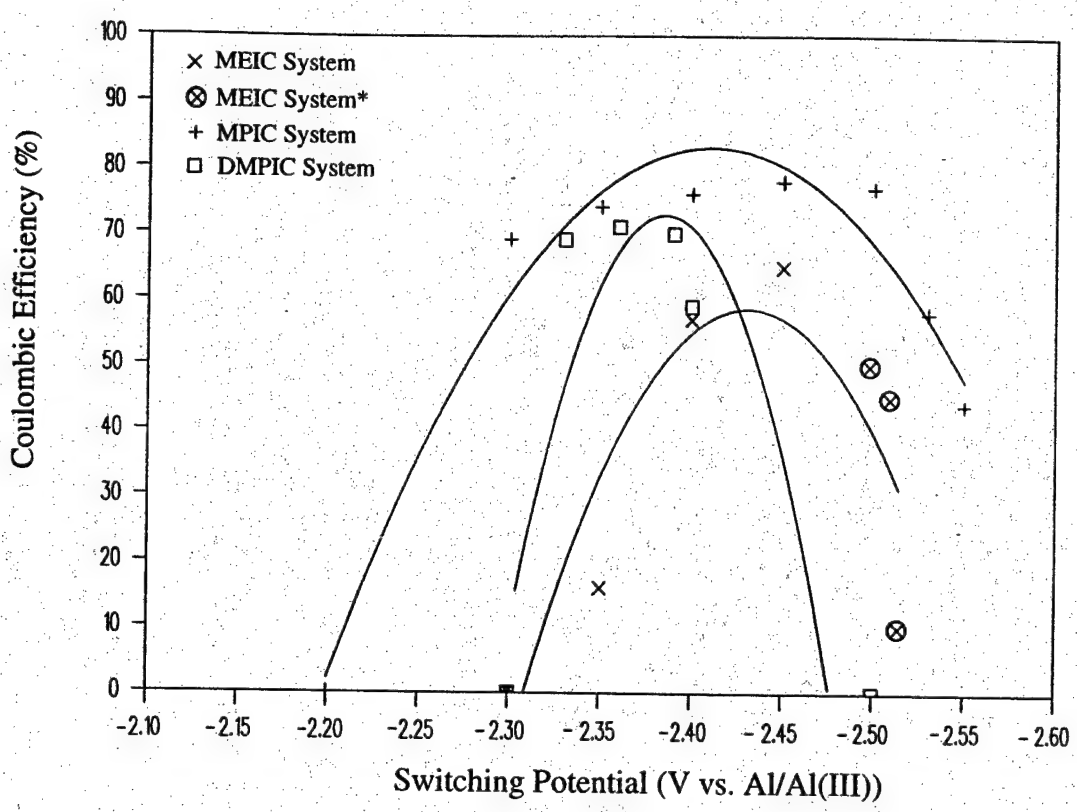

Figure 5.2. Range of potentials which allow reversible sodium plating and stripping for three room temperature molten salt systems.

* Estimated from the data of Riechel and Wilkes.

through the side of the electrochemical cell and through the dry box window. Magnifications ranging from 10X to 30X were used to observe the electrode during the reduction and oxidation cycles. Gas evolution was observed during the cathodic sweep beginning at approximately -0.2 V with respect to the aluminum reference. The production of gas continued during the plating of sodium and its subsequent oxidation. The gaseous product was apparently the result of the HCl treatment. Melts extensively purged with argon did not exhibit gas evolution. The gas evolved was probably hydrogen and was observed with and without sodium deposition. Gas evolution occurred predominantly at the edges of the electrode and a few specific points on the electrode surface. In an effort to eliminate surface defects on the electrode, it was heat treated at 1000°C for 2 hours. The heat treated electrode did not exhibit markedly different gas production than untreated electrodes; however, the heat treatment did darken the electrode and made the bubbles much easier to observe. The electrode was further modified by coating the back and edges with epoxy. The coated electrode exhibited gas evolution from regions where sodium preferentially plated.

Optical microscopy also provided some insight into the nature of sodium deposition on tungsten. Sodium had a tendency to plate in a very non-uniform manner. During repeated plating and stripping, sodium was deposited on the same regions of the electrode. During the plating process, sodium grew outward from the regions of preferential deposition. This observation fits well with the previously observed nucleation overpotential for sodium deposition on tungsten. The regions of preferential

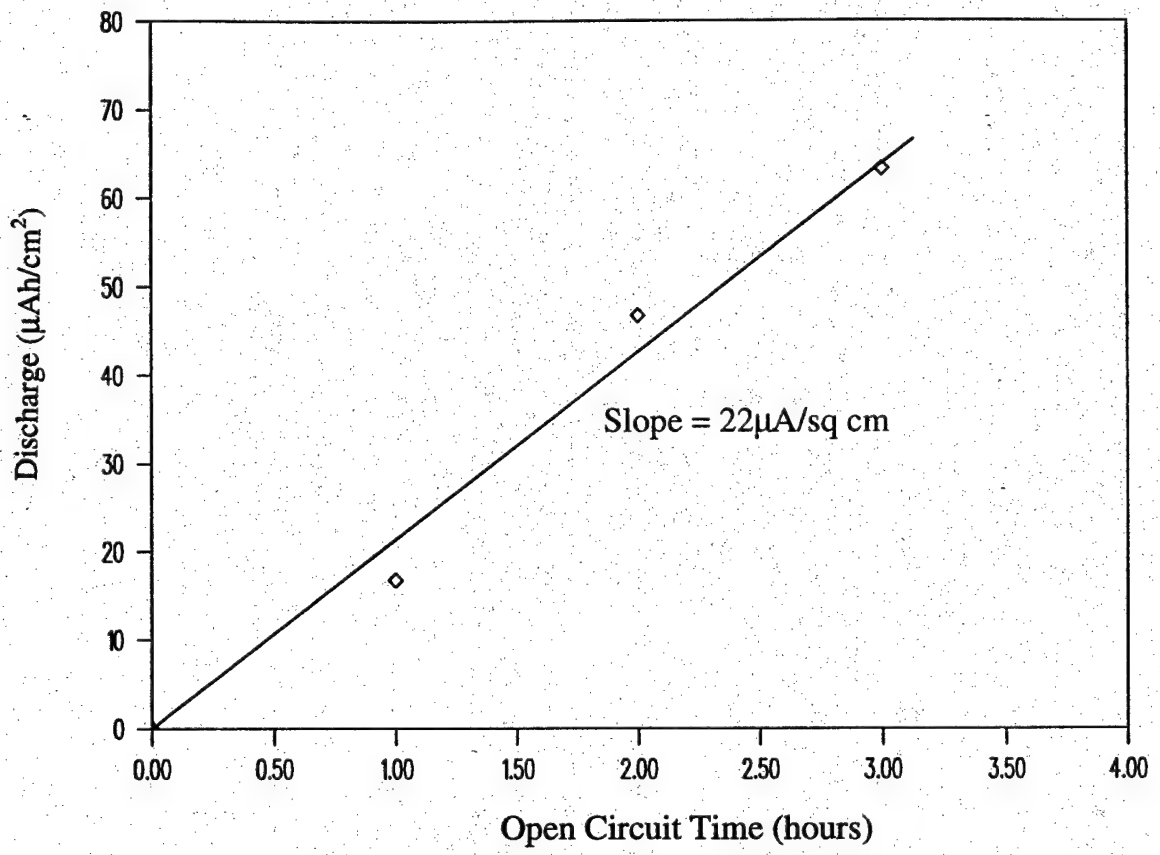

Figure 5.3. Self discharge of a sodium plated tungsten electrode in the buffered, neutral MPIC system.

deposition are regions of lower overpotential. Once sodium has been deposited, additional sodium easily plates on the fresh sodium surface. A cyclic voltammogram illustrating this phenomena is show in Figure 5.4 As the electrode approaches the potential required for sodium deposition, the current increases. The reduction current continues to increase following sweep reversal because the reduction potential on tungsten has been overcome by coating with sodium. Current densities reported here were based on the entire tungsten surface area, which clearly underestimates the actual current density.

Additional observation of the electrode surface during plating and open circuit periods revealed the formation of a dark film in the regions of sodium deposition. This film appeared to be the product of a reaction between the sodium and the MPIC electrolyte. During oxidation, sodium not coated with this film disappeared from the electrode (was oxidized), while the darkened regions remained intact throughout the oxidation. A similar film formation was observed on the surface of solid sodium exposed to the MPIC electrolyte.

To examine the effect of HCl addition on the reaction between the solid sodium and the MPIC electrolyte, a study of sodium open circuit potential versus HCl partial pressure was initiated. A solid sodium electrode was introduced into a buffered, neutral MPIC melt previously treated with 1 kPa HCl. Over the course of approximately 4 hours the HCl partial pressure of the flowing gas was modulated while the potential of the sodium electrode versus an aluminum reference was recorded. It was of interest to see if

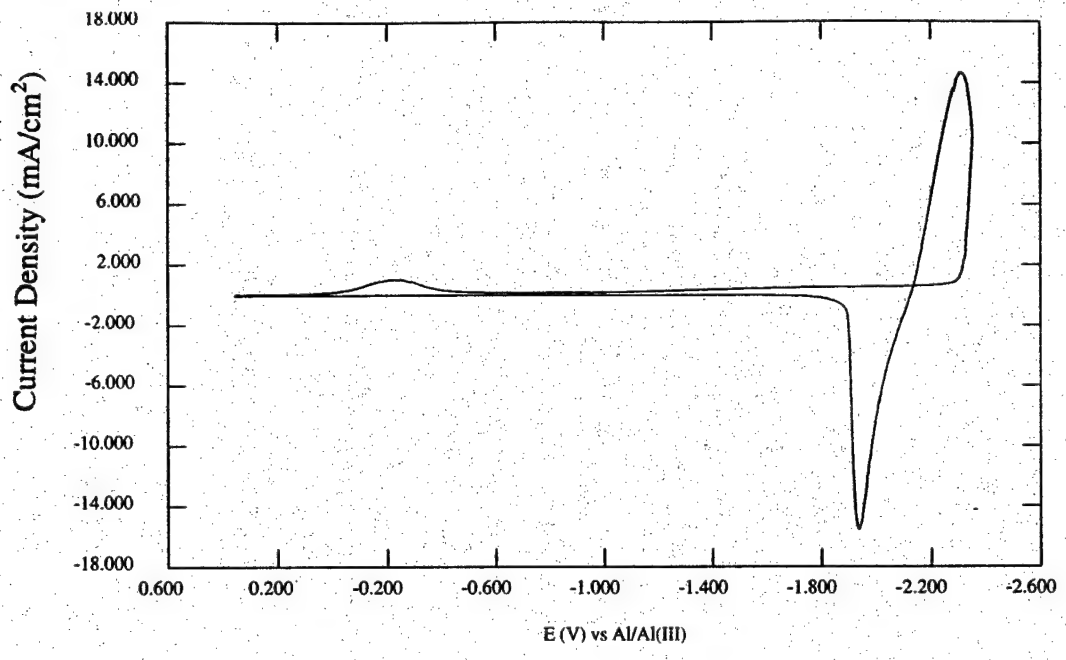

Figure 5.4. CV (v = 100mV/s) on tungsten of the buffered, neutral MPIC system.

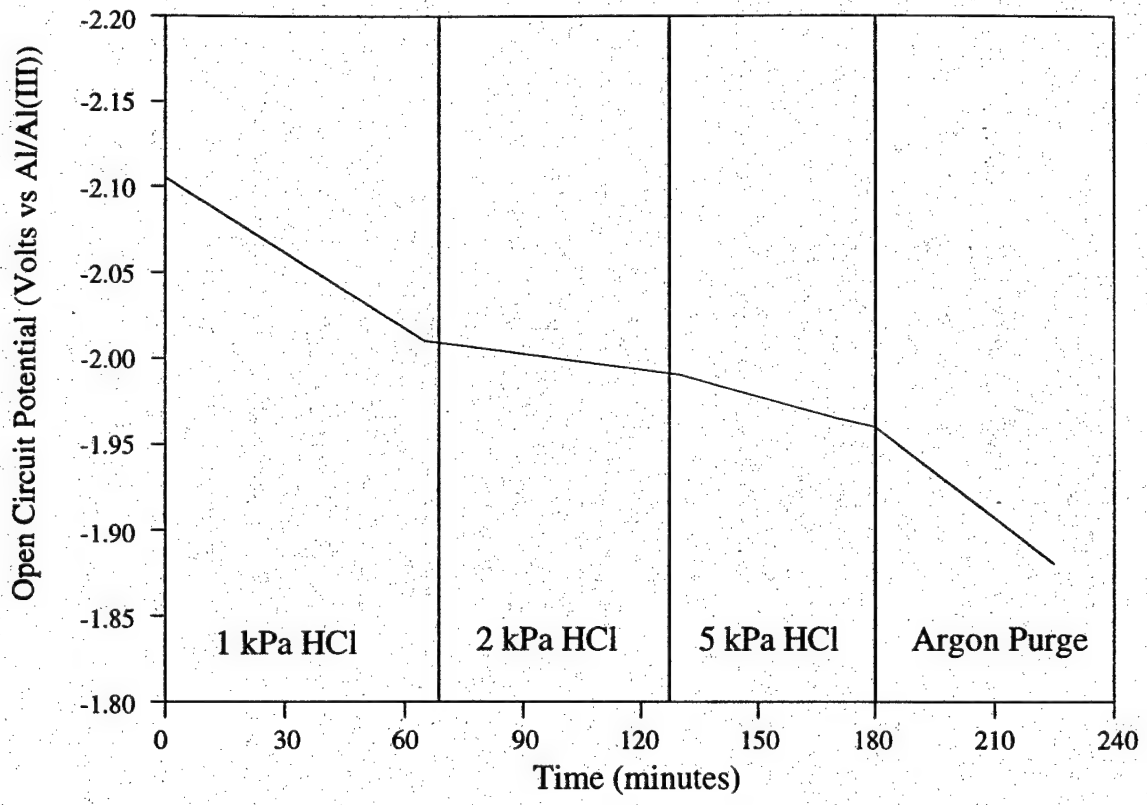

Figure 5.5. Sodium open circuit potential versus time for changing hydrogen chloride partial pressure.

hydrogen chloride has a Nerstian effect on the oxidation potential of the sodium or the reduction potential of the organic cation. If the open circuit potential of sodium is affected in a Nerstian manner, the potential of the solid sodium electrode should shift logarithmically with an increase or decrease in HCl partial pressure. The results are shown in Figure 5.5. The potential of the sodium electrode became less negative for the entire experiment, regardless of HCl partial pressure. This result suggested that the beneficial effect of HCl is not a simple Nerstian one and that the effect of HCl on the reduction potential of sodium was minor compared to its effect on the reduction potential of the organic cation.

Recent reports have indicated that thionyl chloride ($SOCl_2$) has a beneficial effect on the plating and stripping of sodium in the MEIC system. A melt that was previously treated with HCl, but failed to exhibit a reversible sodium couple was treated with $SOCl_2$. Prior to $SOCl_2$ addition, visual observation revealed gas evolution associated with cathodic current. Following the addition of $SOCl_2$ (~0.5 wt%), a reversible sodium couple was observed without gas evolution. Additionally, $SOCl_2$ facilitated a sodium couple which had a higher coulombic efficiency than HCl treated melts. Figure 5.6 shows a cyclic voltammogram on tungsten at a scan rate of 100 mV/s for the $SOCl_2$ treated system. This CV includes a 30 s potentiostatic delay at -2.5 V. The cathodic charge was estimated to be 170 mC/cm^2 and the anodic charge was estimated to be 154 mC/cm^2. The resulting coulombic efficiency was 91 %. A chronopotentiogram is shown in Figure 5.7. The tungsten substrate was held at -2.6 for one second to eliminate

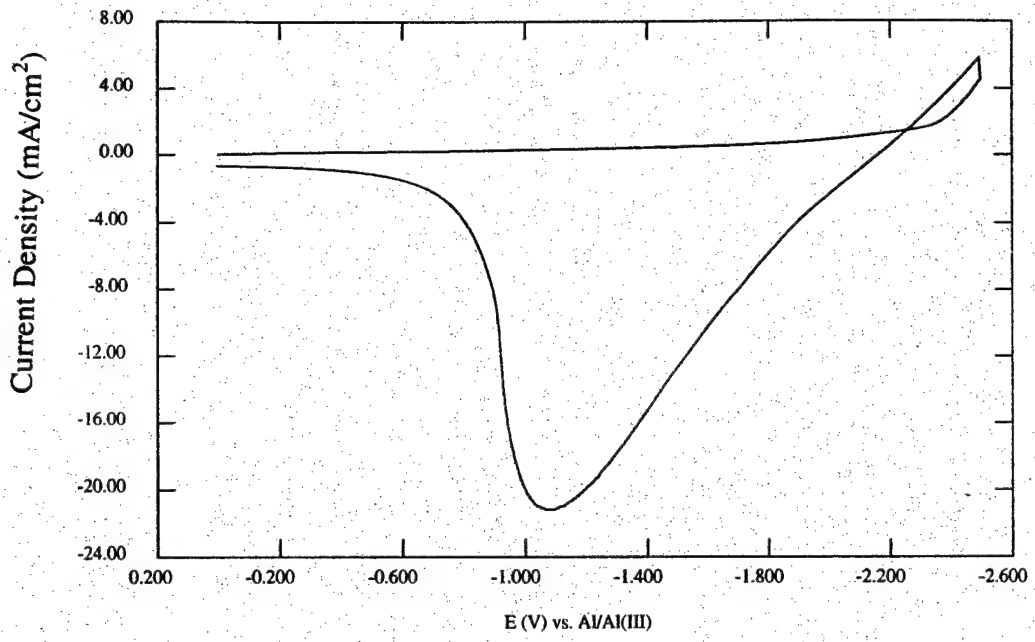

Figure 5.6. Cyclic voltammogram (v=100mV/s) on tungsten for buffered, neutral MPIC system treated with SOCl2. Scan includes a 30 second hold at -2.5 V.

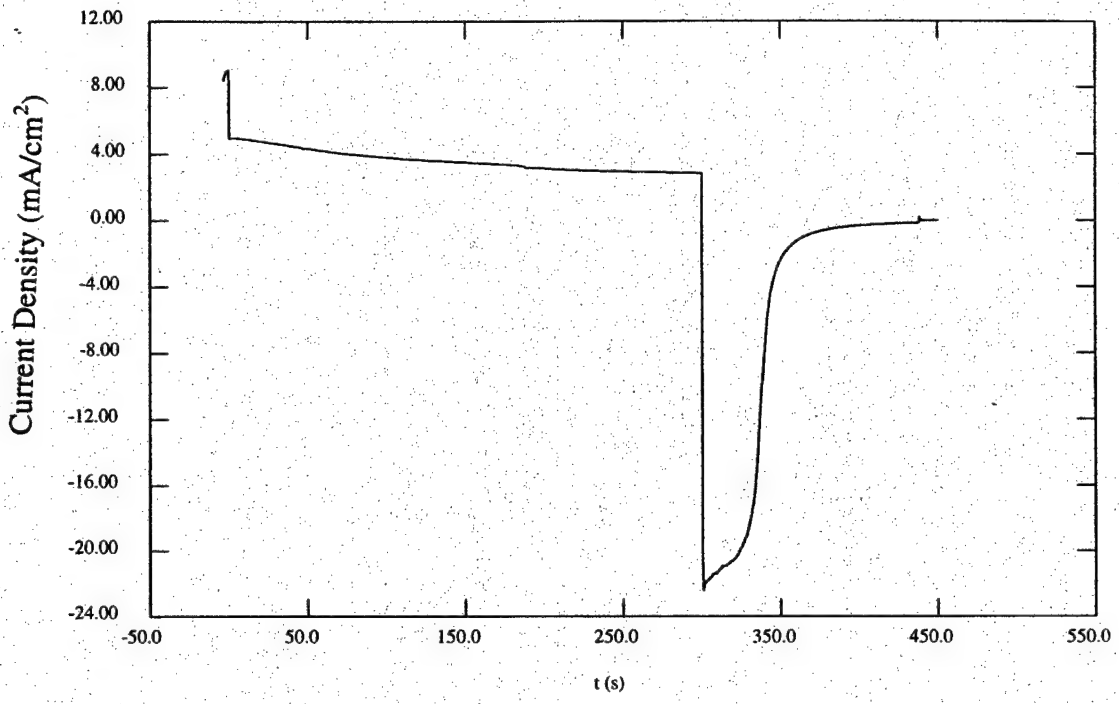

Figure 5.7. Chronoamperogram on tungsten for the buffered, neutral MPIC system treated with $SOCl_2$. Reduction at -2.4 V. Oxidation at -1.0 V.

the sodium nucleation overpotential. This treatment was followed by the constant potential plating of sodium at -2.4 V for 300s. Sodium oxidation immediately followed at a potential of -1.0 V. The coulombic efficiency of this experiment was 75%.

5.2 Discussion

The electrochemical windows of the basic (N=0.45) and the acidic (N=0.55) MPIC melts did not differ greatly from previously studied room temperature molten salts. The behavior of the buffered, neutral system did exhibit a subtle difference in the form of a slightly wider plateau of increased coulombic efficiency. We suggest this difference is due to the more negative reduction potential of the MPIC cation. The slight change in reduction potential occurs with MPIC as compared to MEIC because the propyl group is less electron-withdrawing than the ethyl group. The methyl group at the #2 position of DMPIC, which is the site where dimerization probably occurs, provides less steric hindrance than anticipated. This allows a more distinct separation of the three mechanisms for decreased coulombic efficiency for MPIC and isolates the direct reaction of sodium with the molten salt electrolyte.

Careful examination of this process allowed an estimation of the rate of self discharge reaction with the melt. The direct reaction of the sodium with the buffered, neutral MPIC melt appears to proceed at a rate of approximately 22 $\mu A/cm^2$, an acceptably low level.

Optical microscopy also provided insight into the decreased efficiency of the sodium anode. The evolution of gas was clearly associated with the treatment of the molten salt system with HCl gas. The observation of a facile sodium couple without gas evolution along with the observation of gas evolution without a sodium couple suggests that protons are available for reduction, which may be independent of the beneficial action of the HCl. The HCl appeared to associate with the imidazolium cation, thus changing its reduction potential to more negative values; this resulted in the observation of a facile sodium couple. Hydrogen may also be a product of the reduction of the organic cation; this would account for the observation of gas evolution when the level of HCl in the melt is insufficient to allow reversible plating and stripping of sodium.

Study of the open circuit potential of sodium versus HCl partial pressure reinforced the hypothesis that HCl acts on the organic cation and did not directly affect the sodium deposition potential. Optical microscopy also verified the previous electrochemical observation of a nucleation overpotential associated with the deposition of sodium on a tungsten substrate. The tendency of sodium to plate repeatedly on specific regions of the tungsten substrate indicated that these regions have a surface structure which creates a slightly lower overpotential for deposition than the surrounding area. The growth of metallic sodium outward from these regions during extended deposition indicates that additional sodium is more easily plated on sodium than the tungsten substrate.

Thionyl chloride appears to have an effect on the room temperature molten system similar to that of associated HCl. Treatment of the MPIC system with $SOCl_2$ resulted in a slightly more efficient sodium couple with no gas evolution. HCl and $SOCl_2$ are both Lewis acids and may alter the reduction potential of MPIC not completely complexed by $AlCl_3$.

5.3 Conclusions

Molten salt electrolytes comprised of mixtures of MPIC and aluminum chloride appeared to be slightly more stable than similar mixtures of MEIC or DMPIC and aluminum chloride. This additional stability was the result of the electron-donating nature of the larger propyl group, on the MPIC structure, as compared to the ethyl group, in MEIC. MPIC appears more stable than the similar DMPIC, possibly due to additional strain on the imidazolium ring structure resulting from the third substituent group in the DMPIC structure. Gas evolution is the product of parasitic reactions at potentials positive of the sodium couple resulting in a lower coulombic efficiency for sodium. The largest coulombic efficiency was observed when no gas evolution took place. Thionyl chloride provides the same beneficial effect of HCl without creating the parasitic current resulting in higher coulombic efficiency for the $SOCl_2$ treated system.

Chapter 6

COMPARISON OF ELECTROLYTES

Examination of the series of room temperature molten salts prepared from aluminum chloride and three different organic chlorides led to an understanding of the physical and electrochemical properties of these mixtures. Studying three distinct organic cations facilitated a better understanding of the general properties of this class of room temperature molten salts and highlighted the differences in electrolytes formed from each organic chloride. These results included the examination of the transport and thermodynamic properties of each candidate electrolytes. Of specific interest was the impact these properties had on the electrochemical window of each system. Additionally, the effect of several melt additives which permit sodium plating and stripping was examined to determine which combination yield the best electrolyte / anode combination. The study of these melt additives focused on the mechanisms for reduced coulombic efficiency and the impact melt additives have on these undesirable reactions.

6.1 Transport Properties

The room temperature molten salts exhibited significant differences in transport properties such as viscosity and conductivity. The greatest difference was for the 1,2-dimethyl-3-propylimidazolium chloride system. This system had a noticeably higher viscosity than either of the diaklyimidazolium chloride systems. Associated with this higher viscosity was a lower conductivity and slower equilibrium with hydrogen chloride and other melt additives used to facilitate alkali metal plating.

6.2 Electrochemical Window

All three room temperature molten salt systems examined had a large range of electrochemical inactivity. This electrochemical window was limited on the positive side by oxidation of $AlCl_4^-$ for all three systems and occured at ~2.6 V versus an aluminum reference. More significant differences were expected for the negative limit which was controlled by the reduction of the organic cation. However, results from this work failed to reveal meaningful differences in the reduction potentials of the organic cations in basic or buffered neutral melts. The systems did exhibit different responses to several melt additives.

6.3 Melt Additives

The observations regarding HCl addition and $SOCl_2$ addition can be used to draw some conclusions about this beneficial effect. Initial reports in the literature describing the beneficial effect of HCl attributed the change in organic cation reduction potential to the presence of protons in the form of HCl. The discovery that $SOCl_2$ can function similar to HCl suggested the effect was not due to the presence of protons. Both HCl and $SOCl_2$ have a similar effect, suggesting the cause of this change in electrolyte behavior is a result of the Lewis acid nature of the additive. The low concentrations of the additives suggest the additives are acting on a species in the melt which is also present in low concentrations. Evidence indicates the species in the electrolyte that interferes with the alkali metal couple, in the case of the MEIC system, is unassociated MEI^+Cl^-. In a buffered neutral melt, most MEIC is associated with $AlCl_3$ to form $MEI^+AlCl_4^-$. The equilibrium of this reaction can leave a low concentration of the organic chloride unassociated. This unassociated organic chloride is a Lewis base and apparently interferes with alkali metal deposition and oxidation. The Lewis acid additives associate with the free organic chloride and push its reduction potential sufficiently negative so that it does not interfere with the alkali metal couples. One disadvantage of these melt additives is that when unassociated additive is present, a result of slower reaction kinetics or excess additive addition, they can be reduced contributing to low coulombic efficiencies. A good example if this was seen when melts a treated with high (>50 torr)

levels of HCl. Initially, HCl combines with free organic chloride, but at high partial pressures, some additional HCl is dissolved in the melt. This excess HCl is subsequently reduced at potentials positive of the alkali metal couple resulting in reduction current that cannot be easily distinguished from alkali metal reduction and results in lower coulombic efficiencies.

While the melt additives studied allowed the observation of the alkali metal couple, the coulombic efficiency of the couple did not exceed 90% routinely. The maximum coulombic efficiency observed for the molten salt electrolytes was 94%. This apparent limit on the attainable current efficiencies led to an examination of the mechanisms for reduced efficiency in hopes of designing a system that can routinely obtain current efficiencies of 100%. Three mechanisms were identified which appear to the limit the current efficiency of the alkali metal couple.

6.4 Mechanisms for Reduced Coulombic Efficiency

The first mechanism involves the reduction of species dissolved in electrolyte at potentials positive of the alkali metal reduction potential. Impurities or contamination in the melt are sources of such species. Melt additives have also been observed to produce such parasitic reduction currents. These reactions lower coulombic efficiency by generating reduction current that cannot be recovered during the oxidation of the freshly

plated alkali metal. This effect can be minimized by reducing melt impurities and using the precise amount of melt additive needed to react with unassociated organic chloride.

The second mechanism is the co-reduction of alkali metal cations and organic cations. This phenomena is observed when the electrolyte has insufficient HCl or $SOCl_2$ and the unassociated organic chloride is available. The free organic chloride was irreversibly reduced at potentials very near the alkali metal plating potential. The reduction of the organic chloride resulted in reduction current which cannot be recovered during alkali metal oxidation. If the reduction potential is allowed to stray several hundred millivolts negative of the alkali metal plating potential, reduction of other organic species can take place also creating irreversible reduction current. Reduction of the organic chloride species can be minimized by removing any available unassociated organic chloride and carefully controlling the alkali metal reduction potential. Treatment of the melt with HCl or $SOCl_2$ was one method to effectively remove this undesirable form of organic chloride.

The third mechanism for reduced coulombic efficiency was the direct reaction of sodium with the electrolyte. This reaction was observed with optical microscopy in the MPIC system. Freshly deposited sodium was observed to darken slightly as the metal was exposed to the electrolyte during open circuit. This darkening was non-uniform and the product appeared to interfere with the controlled oxidation of the sodium during the application of anodic current. The product of the reaction was not readily apparent but the brownish film is consistent with a product other researchers have ascribed to

polymerization of the organic species. A clearer understanding of this undesirable reaction is necessary in order to make changes in the melt chemistry and eliminate this pathway for reduce coulombic efficiency. Changes in melt chemistry include the exploration of slightly different imidazolium salts or the use of more effective melt additives.

This work has led to a greater understanding of the thermodynamic and transport properties of room temperature molten salts produced from combination of imidazolium chlorides and aluminum chloride. These properties are critical to the evaluation of this class of mixtures as electrolytes for a high energy density battery utilizing an alkali metal anode and a metal chloride cathode. Of the imidazolium chlorides studied, 1-methyl-3-propylimidazolium chloride demonstrates the most promising combination of desirable thermodynamic properties and fast transport properties. Further investigation of melt additives is necessary to design a system that is 100% coulombic efficient.

CHAPTER 7

IMPLICATIONS FOR FUTURE WORK

With the preceding results and conclusions in hand, the state of this technology can be evaluated. Of specific interest are the additional hurdles that must be overcome in order to construct a viable commercial battery. Each major component of the battery: electrolyte, anode, and cathode, is evaluated separately. Based on these findings a more rigorous analysis of a hypothetical cell is possible. Table 7.1 shows the parameters of such a cell. The results fall short of the long term USABC targets described previously, mainly due to the low solubility of sodium chloride in the electrolyte. This results in a cell with a very large ratio of electrolyte to active material.

7.1 Electrolyte

Room temperature molten salts, specifically those prepared from alkylimidazolium chlorides, aluminum chloride, and sodium chlorides, have been studied because they possess a set of thermodynamic and transport properties which are necessary for a room temperature sodium / metal chloride battery. These properties include a wide electrochemical window, a reasonable conductivity, and the ability to dissolve sodium chloride. Additionally, the electrolyte responds favorably to increases in temperature.

7.1.1 Electrochemical Window

All three electrolyte systems studied possess an extraordinarily wide electrochemical window, exceeding 4 V. This is one of the most appealing properties of this class of room temperature molten salts. Further study of the electrochemical window of these or similar melts is only necessary as it pertains to the reduction limit of the electrolyte. This region is of interest because the potential of the sodium couple is near the reduction potential of the electrolyte.

7.1.2 Conductivity

The conductivity of the electrolyte is important because it directly impacts the voltage drop in the cell during discharge. This voltage drop is proportional to the current passed through the cell and results in energy lost in the form of heat. Conductivities observed during this work for both the MEIC and MPIC systems agree with the value reported in the literature of 3.25×10^{-2} S/cm. Based on a hypothetical cell with operating parameters as shown in Table 7.1, the voltage drop would be 100 mV. This is a very tolerable figure, but clearly any increase in electrolyte conductivity would be beneficial.

Table 7.1. Specifications of a theoretical Na / $MeCl_2$ cell.

	Theoretical Na/$MeCl_2$ Cell
Specific Energy (Wh/kg)*	77
Energy Density (Wh/L)*	104
Specific Power (W/kg)*	77
Power Density (W/L)*	104
Life Cycles	<40
Maximum Current Density (mA/cm^2)	15
Charge Density (mAh/cm^2)	15
Electrode Spacing (mm)	2
Electrolyte Volume (cm^3/cm^2)	0.2
Terminal Voltage (V)	2.3

* Based on electrolyte and active material

Future work to increase the conductivity of the molten salt systems should focus on alternative organic chlorides.

7.1.3 Dissolved Sodium Chloride

Sodium chloride is dissolved in the electrolyte via the buffering of a Lewis acidic melt. Results from this work suggest that the maximum solubility of sodium chloride is ~10 mole%. This results in a maximum concentration of sodium cations of 6.6×10^{-4} moles/g of electrolyte in a buffered neutral melt. For the cell described in Table 7.1, complete utilization of the dissolved sodium and results in a charge density of 7 mAh/cm^2. With the buffering reaction, some initially undissolved sodium can be dissolved during the reduction of the sodium cations. A reasonable assumption would be that equivalent amounts of dissolved and undissolved sodium chloride could be utilized. This would result in a charge density of 15 mAh/cm^2. This work did not extensively study the thermodynamics and kinetics of melt buffering and several questions remain regarding this process.

7.1.4 Temperature

Increased temperature has a favorable effect on the properties of these room temperature molten salt electrolytes. The most significant improvement was seen for the conductivity of the DMPIC system. Currents during cyclic voltammetry experiments increased two-fold for a 40°C increase in temperature. More modest increases in

conductivity for the other two systems were observed. Slight increases in current efficiency were also observed, probably closely related to the increases in conductivity. The effects of temperature are still largely unexplored and could be the subject of future investigation.

7.2 Anode

This work yielded many insights into the nature of the sodium anode and the effects of several melt additives. Maximum practical current density, self discharge rate, and coulombic efficiency of the sodium electrode were carefully examined

7.2.1 Current density

Results of this work indicate a superficial current density of 15 mA/cm^2 can be achieved with a sodium electrode using the studied room temperature molten salt electrolytes. Optical microscopy revealed that sodium deposition occurs on less that 50% of a tungsten substrate. Even higher current densities may be achieved with a properly treated substrate by increasing the utilized electrode area. Investigation of the overpotential for sodium deposition and methods to achieve a more uniform coating could be the subjects of future work.

7.2.2 Self discharge

The rate of self discharge was calculated to be 22 $\mu A/cm^2$ for the MPIC system. This parameter impacts the decrease in cell capacity for a charged cell. For the cell described in Table 7.1, the translates into an initial loss of capacity of 4% per day. Further investigation of this phenomena is warranted. The rate of self discharge was determined for relatively short times (hours). This rate may decrease as the reaction proceeds. No loss of electroactive material was observed for the cell in the discharged state.

7.2.3 Coulombic efficiency

The maximum observed coulombic efficiency observed for both the MEIC and MPIC systems was 94%. This directly affects the cycle life of a full cell. For the cell described in Table 7.1, this coulombic efficiency results in a cycle life of less than 40 cycles at which point the cell has lost 90% of its original capacity. This remains one of the key weaknesses of the sodium anode. Although this work has provided many new insights into the mechanisms for reduced coulombic efficiency, future work could build on these results in hopes of producing a more viable sodium electrode.

7.3 Cathode

This work does not address the properties of the metal chloride cathode. Future work could examine the feasibility of an iron(II) chloride or nickel(II) chloride cathode. Additionally, other metal chlorides could be investigated in an effort to find a cathode which utilizes more of the available electrochemical window. Issues to be resolved include stability of the metal chloride cathode, coulombic efficiency, and cycle life.

Appendix A

THE MEIC/$AlCl_3$/LiCl SYSTEM

Initial attempts to plate and strip an alkali metal from room temperature melts were made using lithium chloride. Lithium has the advantage over sodium of light weight and slightly higher voltage. However, it stability is more questionable and its supply uncertain.

A.1 The Buffering Capacity of Lithium Chloride

Room temperature chloroaluminate melts may be buffered with alkali metal chlorides. The following reactions are shown for lithium chloride.

$$LiCl + Al_2Cl_7^- \leftrightarrow Li^+ + 2\ AlCl_4^- \qquad (1)$$

$$Li^+ + Cl^- \leftrightarrow LiCl \qquad (2)$$

The equilibrium for (2) lies far to the right. In contrast, reaction (1) does not always go to completion. Melts exhibit a maximum buffering capacity. There exists some maximum concentration of Li^+ which a melt can attain. Once this concentration is reached, reaction 1 ceases and $Al_2Cl_7^-$ is left unreacted. This limits the amount of LiCl which may be dissolved in a melt.

Trifluoroacetic acid was used a melt additive to promote lithium reduction and oxidation. Trifluoroacetic acid (99%, Aldrich) was purified by refluxing over P_2O_5 for approximately three hours under a nitrogen atmosphere. The distillate was collected slowly with constant reflux. Approximately half the bottoms was distilled to the receiving flask. The flask was removed under a nitrogen purge and capped with a ground glass stopper. The product was frozen with a dry ice acetone mixture and transferred to the dry box. A MEIC / trifluoroacetic acid mixture was prepared by adding 14.0 g MEIC to 10.8 g F_3CCOOH. The MEIC dissolved slowly into the F_3CCOOH with constant stirring. The resulting liquid was clear and colorless. The stoichiometry of the resulting solution was 0.9959 moles of F_3CCOOH per mole of MEIC.

This limited buffering capacity was studied in two melts. Each melt was prepared in the same manner. An acidic (N=0.55) melt was prepared and a 20% excess of LiCl was added. Both melts were allowed to stir for over a week. Cl^- was added to each melt until $Al_2Cl_7^-$ reduction was not observed. Cl^- was added to one melt as MEICl / F_3CCOOH (1:0.9959). Cl^- was added to the second melt in the form of MEICl / $AlCl_3$

(N=0.31). Solid MEICl was not used because it dissolves more slowly in nearly neutral melts. The other sources of Cl^- are liquid and dissolve more readily. Cl^- reacts with $Al_2Cl_7^-$ as follows.

$$Cl^- + Al_2Cl_7^- \leftrightarrow 2\ AlCl_4^-$$

With both Li^+ and $Al_2Cl_7^-$ available, additional Cl^- appears to react preferentially with $Al_2Cl_7^-$. This may be a kinetic phenomena. Once all $Al_2Cl_7^-$ is exhausted, Cl^- reacts with Li^+ and LiCl is precipitated.

After each buffered melt was prepared, cyclic voltammetry showed the reduction of $Al_2Cl_7^-$ and the subsequent oxidation of Al. Figure A.1 shows a cyclic voltammogram of the lithium buffered, neutral system. A large reduction peak (I) associated with the addition of protons in the form of MEIC/F_3CCOOH was observed near 0 V. The $Al_2Cl_7^-$ reduction peak (II) was observed at -1.0 V. A related oxidation current, the oxidation of Al (V), was observed at -0.25 V. Other notable features of Figure A.1 are the rapid increase of reduction current (III) associated with the irreversible reduction of the organic cation and the peak current (IV) observed at scan reversal. Figure A.2 shows similar $Al_2Cl_7^-$ reduction current (I) and the Aloxidation current (IV) for the lithium buffered, neutral melt that was treated with basic (N-0.33) MEIC/$AlCl_3$.

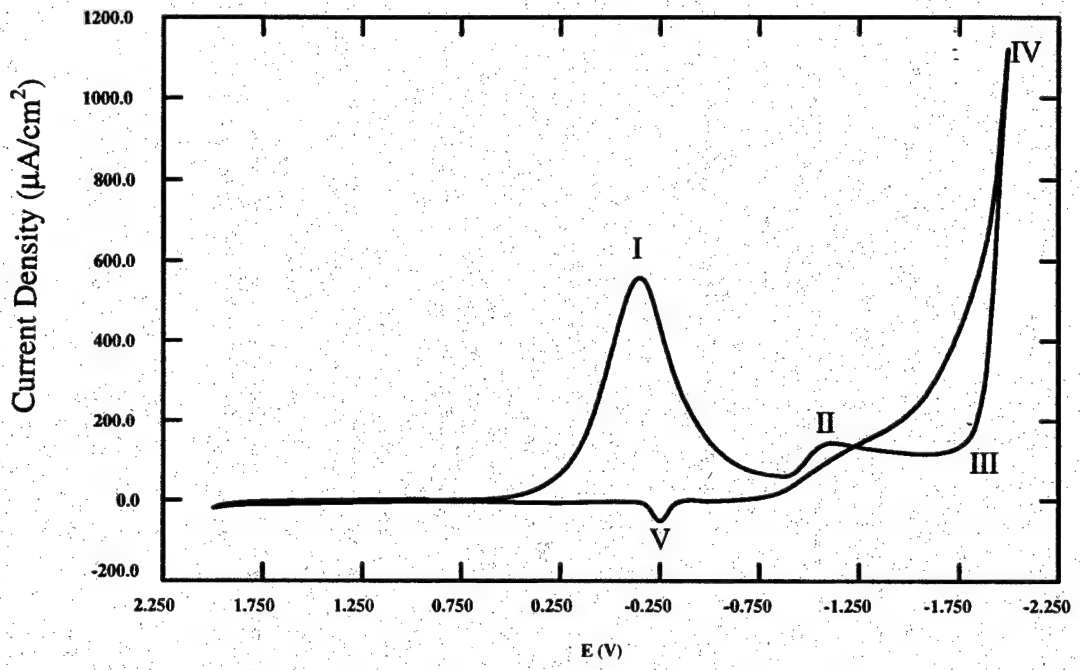

Figure A.1. **The reduction of $Al_2Cl_7^-$(II) and oxidation of Al(V) in melt A prior to the addition of the last aliquot of MEICl/F_3CCOOH to the lithium chloride buffered, MEIC system.**

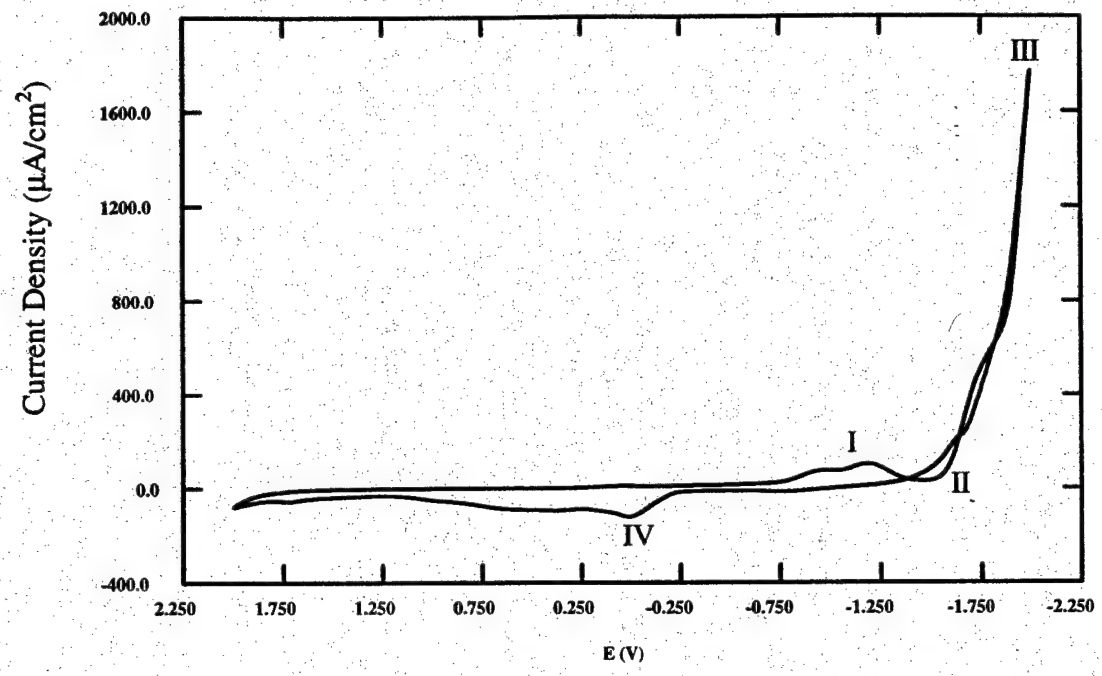

Figure A.2. **The reduction of $Al_2Cl_7^-$(I) and oxidation of Al(IV) in melt B prior to the addition of the last aliquot of MEICl/$AlCl_3$ to the lithium chloride buffered, MEIC system.**

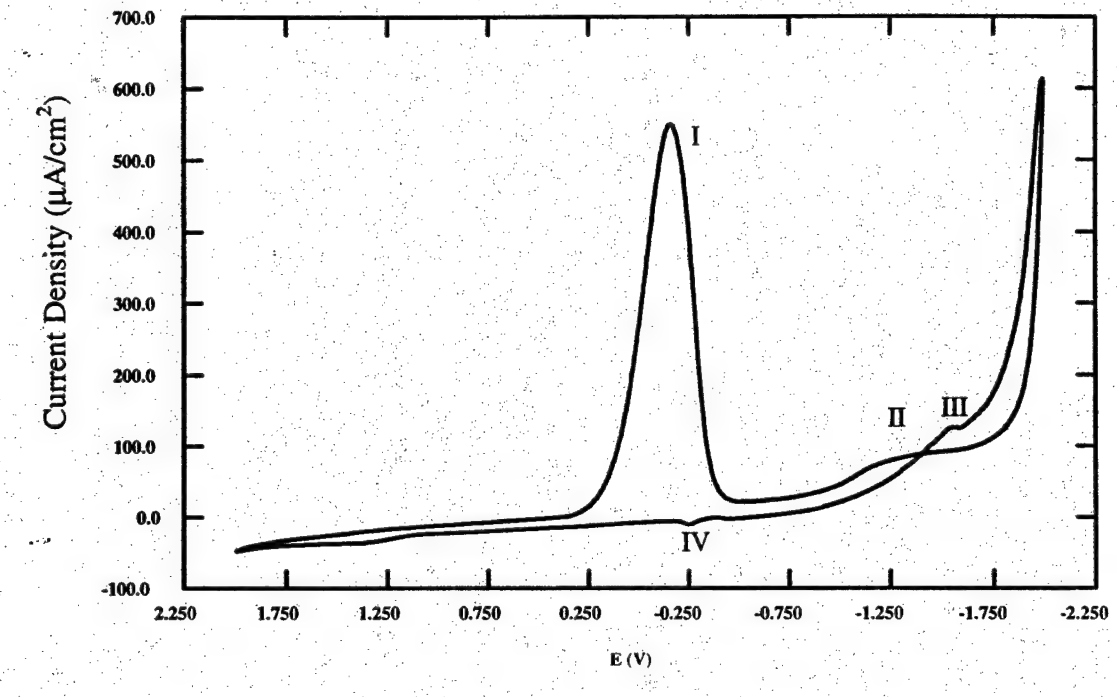

Figure A.3. **The absence of $Al_2Cl_7^-$ reduction in melt A after the addition of the last aliquot of MEICl/F_3CCOOH to the lithium chloride buffered, MEIC system.**

The onset of irreversible reduction of the organic cation (II) and the peak current at scan reversal (III) was also observed. Cl^- was added to each melt in small aliquots and a CV was performed after each addition. When the CV indicated the absence of $Al_2Cl_7^-$ reduction and Al oxidation, the residual Li^+ was calculated. The cyclic voltammogram for the MEIC/F_3CCOOH treated system after consumption of all excess $Al_2Cl_7^-$ is shown in Figure A.3. The magnitude of the current associated with MEIC/F_3CCOOH addition (I) is unchanged, but the magnitude of the currents associated with $Al_2Cl_7^-$ reduction (II) and Al oxidation (III) is greatly diminished. A similar CV for the melt treated with basic MEIC/$AlCl_3$ is shown in Figure A.4. The currents due to $Al_2Cl_7^-$ reduction (I) and Al oxidation (III) are completely eliminated and a slight oxidation current (II), presumably due to Li oxidation, is observed.

The resulting Li^+ concentration was calculated by assuming that each mole of chloride source, MEIC/F_3CCOOH or basic MEIC/$AlCl_3$, reacted with a mole of excess $Al_2Cl_7^-$. By carefully recording the amount of each chloride source added, the amount of excess or unbuffered $Al_2Cl_7^-$ was determined. Table A.1 contains the relevant numerical results.

The data suggest that a maximum solubility of Li^+ exists at about $6x10^{-4}$ moles per gram of melt. This means that the most acidic melt that could be buffered is one that

is 0.54 mole fraction $AlCl_3$ (N=0.54). The data do, however, quantify the observation that LiCl cannot completely buffer some acidic melts.

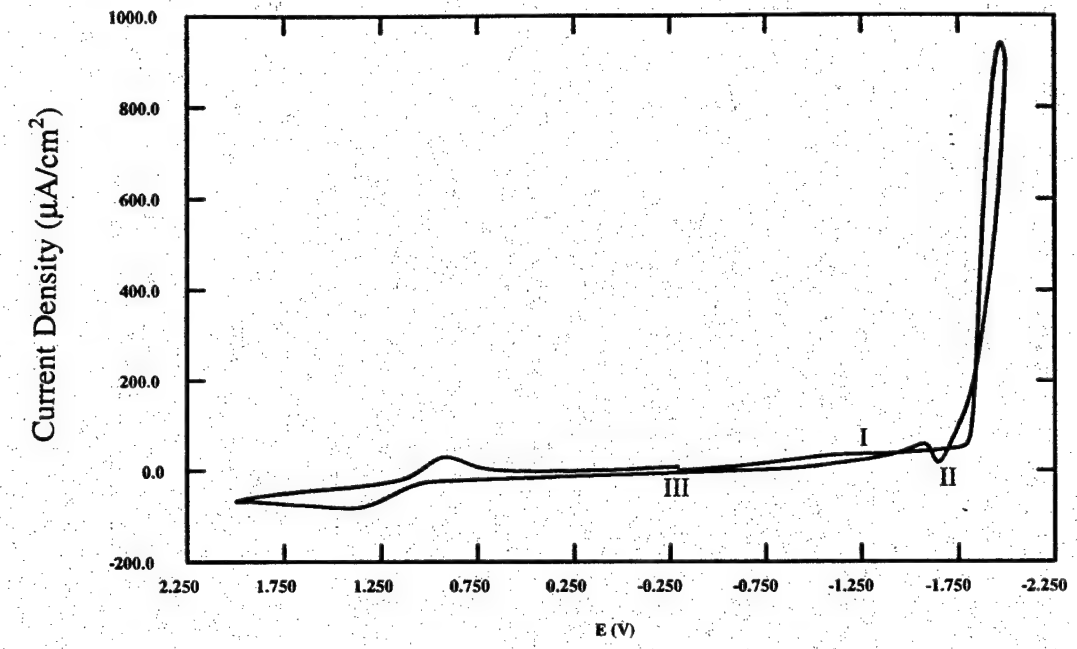

Figure A.4. **The absence of $Al_2Cl_7^-$ reduction in melt B after the addition of the last aliquot of MEICl/$AlCl_3$ to the lithium chloride buffered, MEIC system.**

Table A.1. Determination maximum Li+ concentration

	Melt A	Melt B
Quantity of Melt (N=0.55)	28.95g	46.07g
Moles of $Al_2Cl_7^-$ before Buffering	2.08×10^{-2}	3.31×10^{-2}
Moles of LiCl Added	2.49×10^{-2}	3.97×10^{-2}
Amount of MEICl/F_3CCOOH added	0.81g	
Amount of MEICl/$AlCl_3$ (N=0.31)		1.96g
Moles of Cl- needed to consume Unbuffered $Al_2Cl_7^-$	3.12×10^{-3}	5.23×10^{-3}
Moles of residual Li^+	1.77×10^{-2}	2.79×10^{-2}
Concentration of residual Li^+ (Moles Li^+/g of melt)	6.11×10^{-4}	6.05×10^{-4}

A.2 Impact of Proton Concentration of Coulombic Efficiency

It has been observed that the presence of protons in room temperature chloroaluminate melts extends the electrochemical window by making the reduction limit more negative. This extension allows the reduction of sodium and lithium within the melt window. It has also been observed that the effect of the added protons diminishes over time. The phenomena is apparently caused by the loss of protons from the melt, presumably as HCl gas. The effectiveness of proton additions can also be diminished by performing reduction at a potential somewhat negative of that of the alkali metal reduction / oxidation couple. This may be caused by fouling of the electrode. These two effects are difficult to separate when working with an open cell. The loss of protons due to outgassing seems to take place continuously and many experiments of interest, cyclic voltammetry for example, are performed while gradually making the reduction limit more negative.

A set of experiments was performed to examine this phenomena, one using cyclic voltammetry (CV), the other using chronoamperometry (CA). The experiments were performed by adding an aliquot of proton source ($MEIHCl_2$) to a buffered, neutral melt and repeating, at regular intervals, either a CV or CA scan using a tungsten electrode. The melt was prepared by buffering an acidic (N=0.55) melt with LiCl. The buffering was incomplete, thus, the melt was returned to neutrality by addition of MEICl / $AlCl_3$

(N=0.31). Many additions of protons were made to the melt before the experiments were performed.

The first experiment was performed using CV. The melt indicated an insufficient proton concentration (no lithium reduction/oxidation couple). A single addition of $MEIHCl_2$ was made and CV's performed at ten minute intervals. After 80 minutes, the efficiency dropped from 90.4% to 85.6%. At this time the cell was capped and left stirring overnight. The next day (15 hours later) the CV's were continued at ten minute intervals. These results are shown in Figure A.5. The first scan of the series is shown in Figure A.6. Figure A.7 shows the effect of insufficient HCl, irreversible reduction of the organic cation.

The second experiment was performed using CA. Before the experiment, the melt showed insufficient proton concentration, i.e. no lithium oxidation was observed. A single addition of $MEIHCl_2$ was made and CA's performed at ten minute intervals. The efficiencies increased to a maximum of 86.7% then decreased. The change in CA efficiency versus time is shown in Figure A.8. The most efficient CA (86.7 %) is shown in Figure A.9.

Both of the previous experiments had essentially no time delay between reduction of Li and its oxidation. Because the stability of Li metal in contact with the melt is of great interest, an additional experiment was performed. A set of CA's were performed while varying the time between the reduction and oxidation during which the cell is

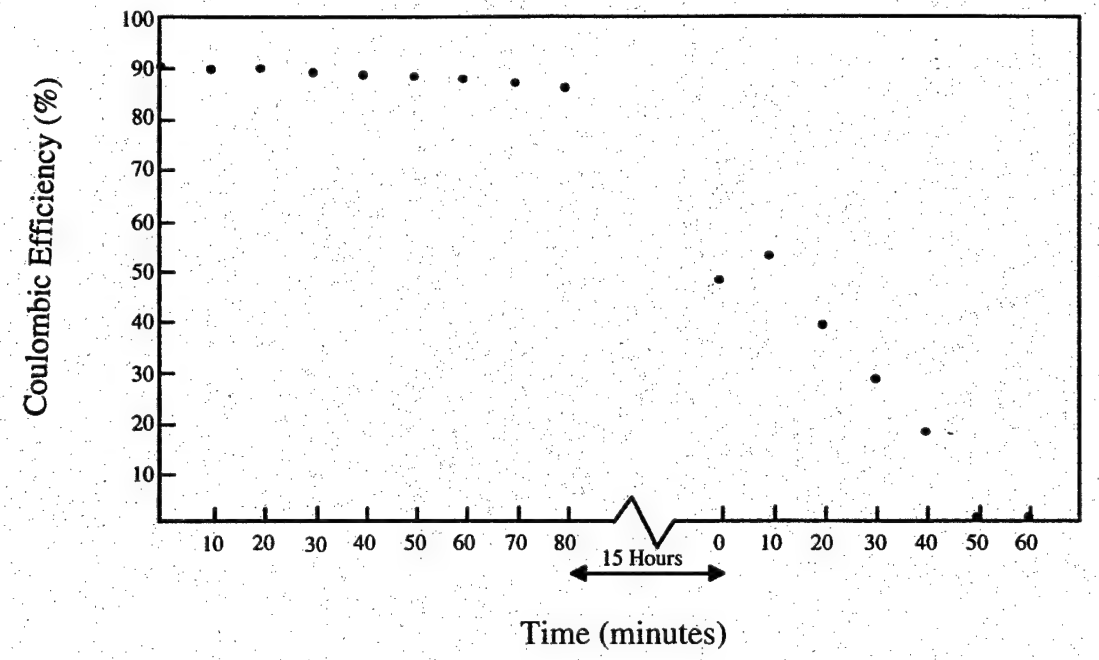

Figure A.5. The loss in reduction-oxidation efficiency versus time. for CV experiments on the lithium chloride buffered, MEIC system

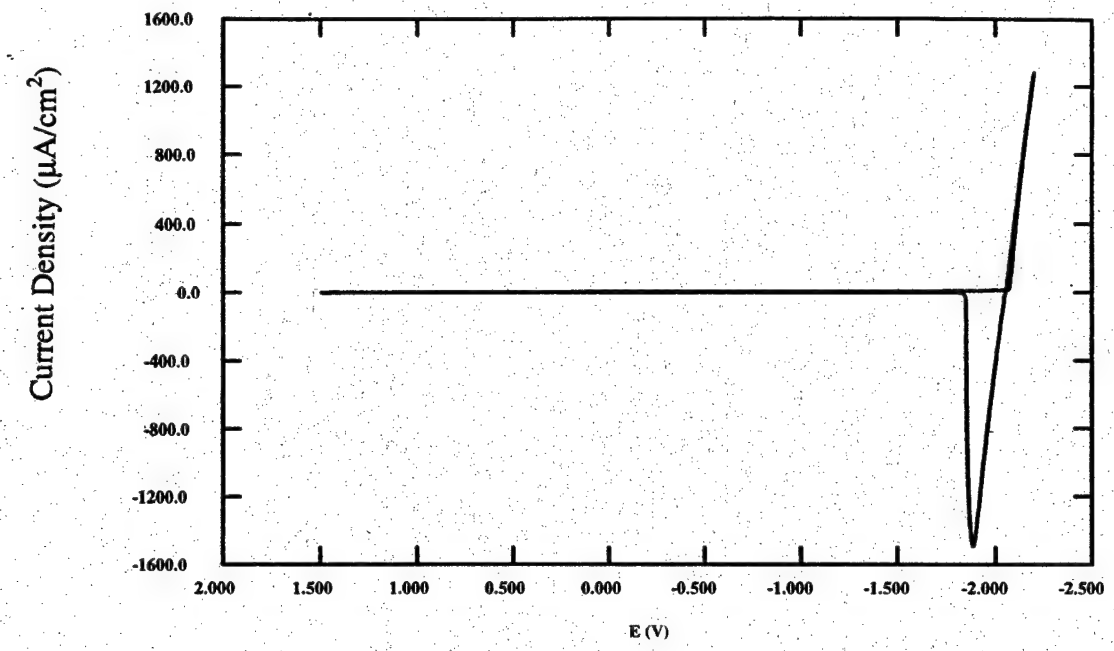

Figure A.6. First CV after proton addition to a lithium chloride buffered, MEIC melt (90.4% efficient).

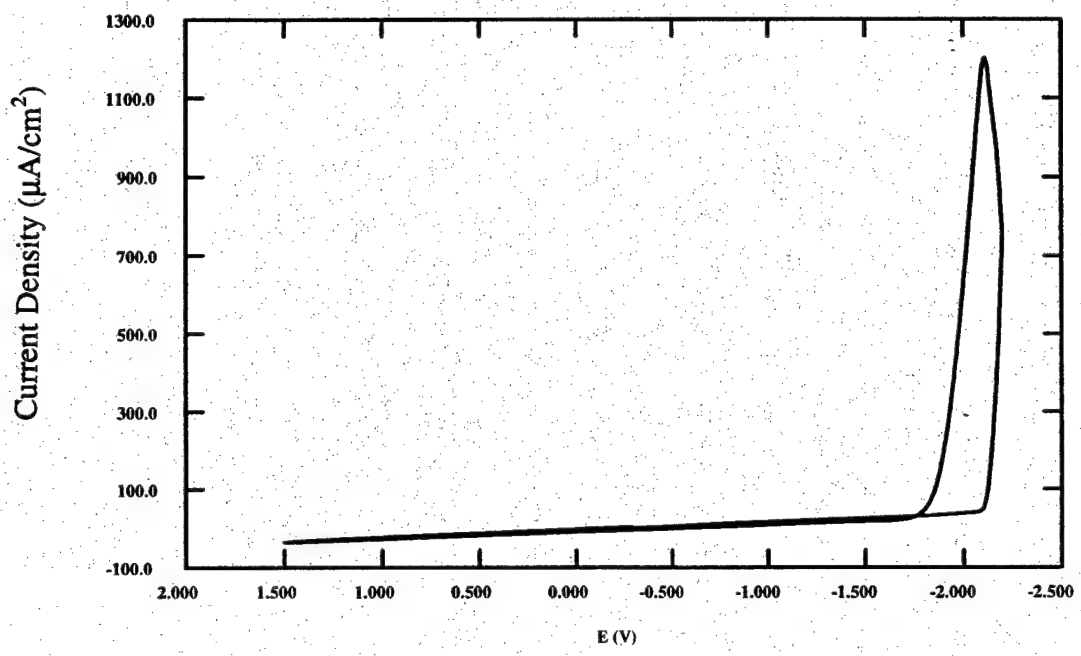

Figure A.7. CV showing the result of insufficient proton concentration for the lithium buffered MEIC system.

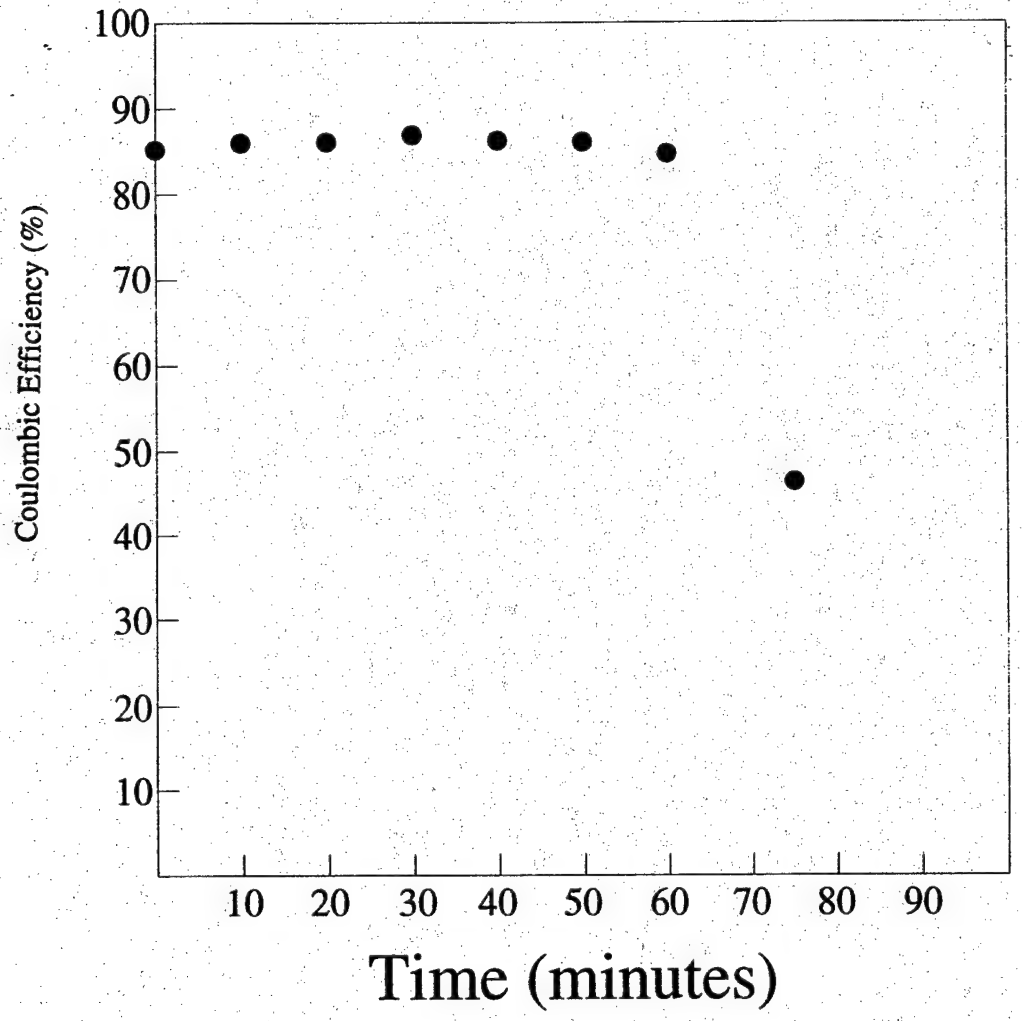

Figure A.8. The loss in reduction-oxidation efficiency versus time for CA experiments on the lithium chloride buffered MEIC system.

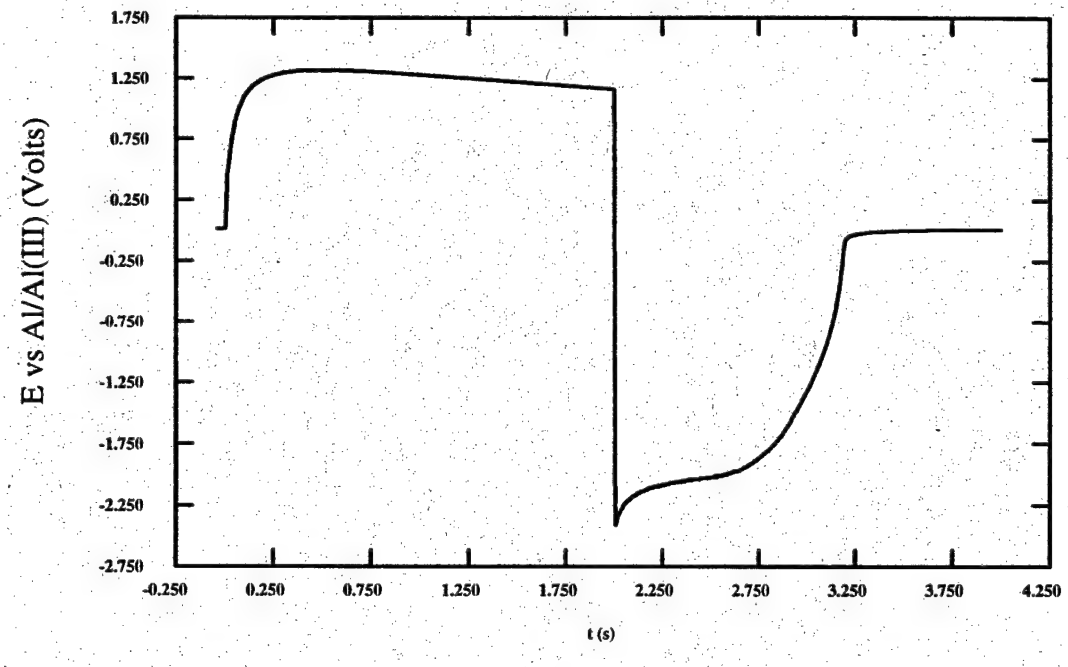

Figure A.9. The most efficient (87%) CA observed for the lithium buffered MEIC system.

Table A.2. Summary of chronoamperometry experiments with open circuit period in lithium buffered system.

Experiment Number	Open Circuit Period (s)	Coulombic Efficiency (%)
1	0	76
2	6.8	23
3	0	55
4	53	0

disconnected and zero current is passed. This was done by starting a CA scan and disabling the cell by pressing the "Cell Enable" button for the amount of time desired for the delay. The efficiencies dropped to zero for long delays. A summary of these results is shown in Table A.2. Following the last scan a brown coating was observed on the electrode.

A.3 Trifluoroacetic Acid as a Proton Source

A popular proton source for room temperature molten salts is $MEIHCl_2$. This species is formed by the reaction of gaseous HCl and solid MEIC to form a liquid at room temperature. The stoichiometry of this liquid can range from 0.8 to 1.4 moles of HCl per mole of MEIC. Unfortunately, melts treated with this proton source have been observed to outgas HCl and thus lose the beneficial effect of HCl addition. In an effort to find a proton source that did not outgas, a neutral buffered melt was protonated with a trifluoroacetic acid / MEIC solution and the electrochemistry observed.

A neutral buffered melt was prepared by first preparing a neutral melt (N=0.50) by combining stoichiometric quantities of $AlCl_3$ and MEIC. This neutral melt was treated to remove protonic impurities by addition of ethylaluminumdichloride ($C_2H_5AlCl_2$, Aldrich). $C_2H_5AlCl_2$ reacts with protonics impurities in the form of HCl as follows:

$$C_2H_5AlCl_2 + HCl \rightarrow C_2H_6 + AlCl_3.$$

Next, the melt was made acidic (N=0.55) by addition of $AlCl_3$. The melt was then buffered by addition of a 20% excess of the stoichiometric amount of LiCl needed to react with the $Al_2Cl_7^-$ present in the melt. The melt was allowed to stir for more than a week. The reduction of excess $C_2H_5AlCl_2$ was observed at tungsten and corrected by the addition of a small amount (1 drop) of $MEIHCl_2$. The LiCl did not appear to buffer the melt completely. Reduction of $Al_2Cl_7^-$ at tungsten and subsequent oxidation of Al (shown in Figure A.10.) persisted even after 17 days of stirring.

MEIC / F_3CCOOH was added to the melt in small aliquots. A tungsten working electrode was used for all experiments. After the first addition, proton reduction was observed. This reduction took the form of a very large peak centered at ~0.12V. The $Al_2Cl_7^-$ reduction and Al oxidation was observed until the apparent Li^+ concentration had been reduced to approximately 8.3 mole%. Clearly, all the lithium chloride did not neutralize the available $Al_2Cl_7^-$. Thus, the MEIC that was added to the melt as MEIC / F_3CCOOH reacted with the $Al_2Cl_7^-$ and made the melt less acidic. Once the additional MEIC begins to react with the dissolved Li to form LiCl, the melt is truly buffered.

A Li reduction / oxidation couple appeared after two additional aliquots of MEIC / F_3CCOOH were added (shown in Figure A.11.). This CV exhibited an interesting feature. The lithium oxidation (I) is superimposed on a background reduction (II). The sum of these two currents results in an oxidation peak that is shifted towards positive currents. The actual concentration of protonic species could not be determined. The

proton concentration appeared to change with time as it does when protons are added as $MEIHCl_2$. A Li couple that appeared reversible was not observed until the Li^+ concentration had been reduced to 6.3 mole%. This couple (shown Figure A.12.) showed an efficiency of 67.2%. The appearance of the lithium couple after repeated additions of MEIC / F_3CCOOH suggest two different explanations for this effect. While the F_3CCOOH concentration is increasing with repeated additions, the apparent Li^+ concentration is decreasing as MEIC reacts to neutralize excess $Al_2Cl_7^-$ or replace dissolved Li^+. The threshold concentration of F_3CCOOH may be reached with the initial MEIC / F_3CCOOH additions, wile subsequent additions are necessary to achieve melt neutrality.

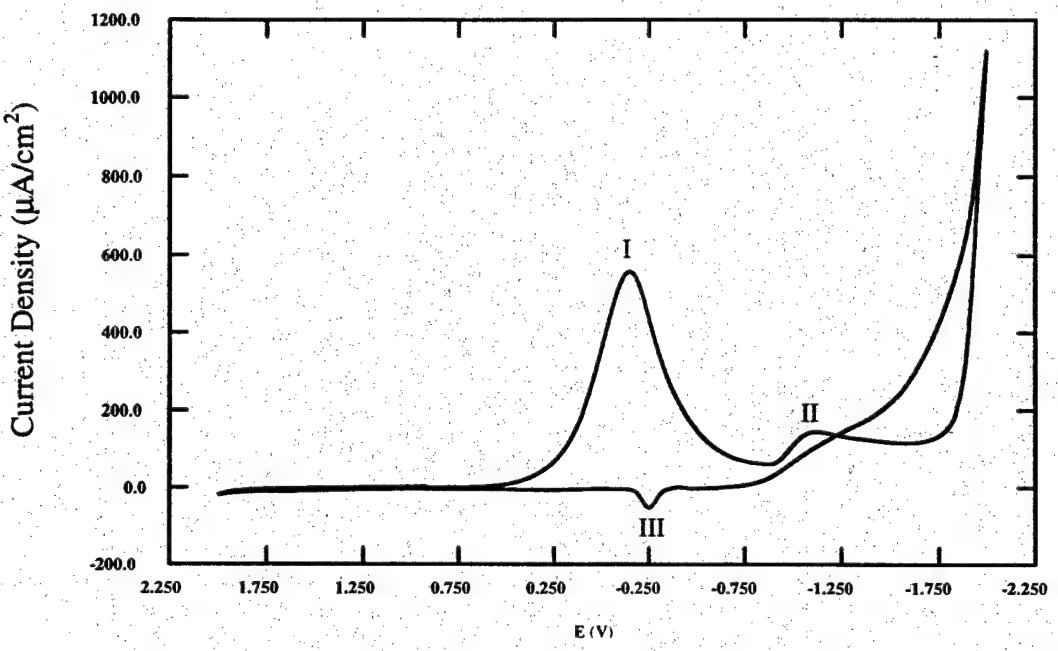

Figure A.10. Lithium chloride buffered, MEIC melt exhibiting Al_2Cl_7- reduction (II) and Al oxidation (III) typical of incompletely buffered systems.

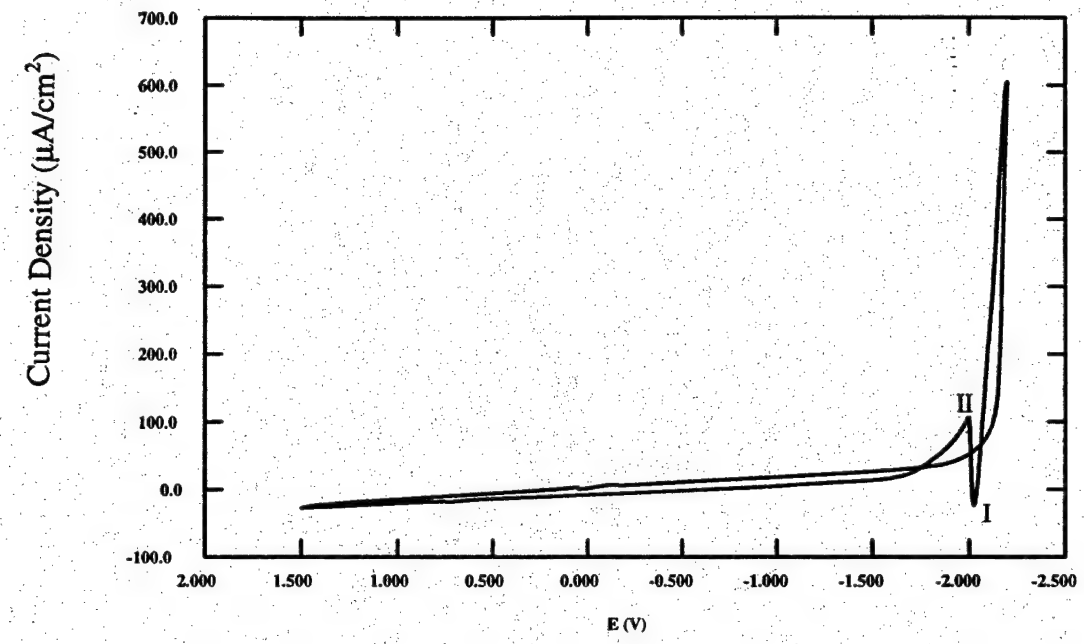

Figure A.11. Li+ reduction and Li oxidation (I) superimposed on a reduction process (II) for a lihtium chloride buffered, MEIC melt treated with CF_3COOH.

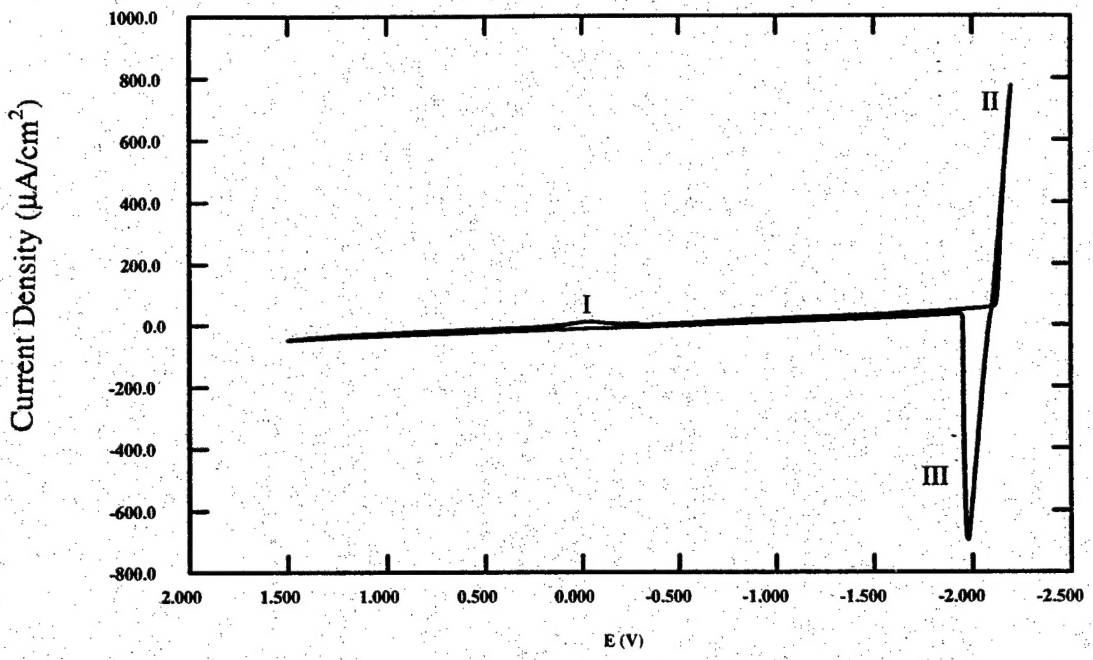

Figure A.12. Reversible Li+ reduction (II) and Li oxidation (III) with a lithium chloride buffered, MEIC melt. The reduction current (I) associated with CF_3COOH is also visible.

REFERENCES

1. B.D. McNicol and D.A.J. Rand, eds.,*Power Sources for Electric Vehicles*, Elsevier, Amsterdam (1984).

2. M.J. Riezenman, *IEEE Spectrum.* **29**, 97 (1992).

3. R.J. Bones, J. Coetzer, R.C. Galloway, and D.A. Teagle, *J. Electrochem. Soc.* 134, 2379 (1987).

4. T.J. Melton, J. Joyce, J.T. Maloy, J.A. Boon, and J.S. Wilkes, *J. Electrochem. Soc.* 137, 3865 (1990).

5. R.J. Gale and R.A. Osteryoung, *J. Electrochem. Soc.* **127**, 2167 (1980).

6. R.T. Carlin and R.A. Osteryoung, *J. Electroanal. Chem.* **252**, 81 (1988).

7. C.L. Yu, J.Winnick, and P.A. Kohl, *J. Electrochem. Soc.* **138**, 339 (1991).

8. R.T. Carlin, J. Fuller, J.S. Wilkes, "Alkali Metal Reductions at Tungsten and Mercury Film Electrodes in Buffered Neutral Aluminum Chloride: 1-Methyl-3-Ethylimidazolium Chloride Molten Salts," FJSRL-TR-90-0003, Frank J. Seiler Research Laboratory, USAF Academy, August 1990.

9. T.L. Riechel and J.S. Wilkes, *J. Electrochem. Soc.* **139**, 977 (1992)

10. P.R. Gifford and J.B. Palmisano, *J. Electrochem. Soc.* **134**, 610 (1987).

11. C. Scordilis-Kelley and R.T. Carlin, *J. Electrochem. Soc.* **140**, 1606 (1993).

12. A.J. Bard, *Electrochemical Methods*, John Wiley and Sons, New York, 1980.

13. *Aluminum Chloride*, Chankya Misra, **Encyclopedia of Chemical Technology**, John Wiley and Sons, New York, (1992).

14. T.L. Riechel and J.S. Wilkes, *J. Electrochem. Soc.* **140**, 3104 (1993).

15. B. J. Piersma, *Proceedings of the Ninth International Symposium on Molten Salts*; The Electrochemical Society: Pennington, NJ, **94-13** (1994).

16. G. P. Smith, A. S. Dworkin, R. M. Pagni, and S. P. Zingg, *J. Am. Chem. Soc.*, **111**, 525 (1989).

17. T.L. Riechel, M.J. Miedler, and E.R. Schumacher, *Proceedings of the Ninth International Symposium on Molten Salts*; The Electrochemical Society: Pennington, NJ, **94-13** (1994).

18. T. A. Zawodzinski and R. A. Osteryoung, *Inorg. Chem.*, **27**, 4383 (1987).

19. R. G. Keil, *An Electrochemical and Spectroscopic Study of Electrode Processes*, WRDC-TR-89-2065, Wright Research and Development Center, Wright-Patterson Air Force Base, OH.

20. C. Scordilis-Kelley, J. Fuller, R. T. Carlin, and J. S. Wilkes, *J. Electrochem. Soc.*, **140**, 1606 (1993).

21. G. E. Gray, J. Winnick, and P. A. Kohl, *J. Electrochem. Soc.*, **142**, 3636 (1995).

VITA

Gary Edward Gray was born June 30, 1969, in Atlanta, GA, to Cleve E. Gray and Carolyn S. Salemi. He graduated from Pebblebrook High School, in Mableton, GA in June 1987. He attended the Georgia Institute of Technology in Atlanta, GA, and received his Bachelor's degree in Chemical Engineering in 1991. Following graduation, he entered the graduate program in Chemical Engineering at the Georgia Institute of Technology. He was married to Laura Elise Shaeffer on June 20, 1992.